Creep Rupture of Steels for Nuclear Reactor Applications

Raymond Douglas Nicholson

Thesis presented to the University of Aston in Birmingham for the degree of Doctor of Philosophy.

November, 1975

SUMMARY

The creep rupture properties of nuclear fuel cladding materials (AISI type 316, M316 and 20Cr/25Ni/Nb stainless steels) have been investigated. The effects of environments relevant to nuclear reactor applications (i.e. fission product attack and neutron irradiation) on the creep rupture properties are also considered.

The validity of various criteria controlling creep crack growth from defects in AISI type 316 stainless steel has been examined. It is found that crack growth rates correlated well with the nett section stress in the temperature range 600 to 850°C. Certain minimum displacements must be achieved for crack initiation and propagation and the possibility of using a strain-based criterion such as crack opening displacement or the angle between fracture surfaces is developed and such a criterion is found to have advantages. Other macroscopic aspects (e.g. creep stress distributions ahead of notches) and microscopic aspects of crack initiation and propagation have also been considered.

A new method of measuring creep crack growth particularly suitable for use in hazardous or closely controlled reactive environments has been developed. This method has been used to study the creep rupture properties of M316 steel in iodine vapour, air and vacuum at 650°C and 750°C. Iodine vapour causes extensive intergranular surface nucleated cracking and a selective corrosion process is thought to occur. The environment is found to have much more effect on crack initiation than propagation. Environmental effects become less marked as the time of test is reduced.

The effect of neutron irradiation on the creep rupture properties of primary recrystallised 20Cr/25Ni/Nb steel at 750°C. has

been found to be negligible. It is thought that a combination of a uniform boron distribution and small grain size causes sufficiently low helium bubble concentrations on the grain boundaries to have negligible effects on the creep rupture properties.

CONTENTS

CHAPTER 1.

GENERAL INTRODUCTION

A brief summary of the economics of nuclear power stations and present reactors operating in the United Kingdom is given. The Advanced Gas Cooled Reactor (A.G.R.) and the Prototype Fast Reactor (P.F.R.) are described and the relevance of the work presented in this thesis to these reactor systems is mentioned.

1.1. Nuclear Power in the United Kingdom.

In recent years, people have become increasingly aware of the need for reliable, economic sources of energy which are also capable of long-term exploitation. Of the present available energy sources, nuclear power most closely satisfies these requirements. Accordingly, increased ordering of nuclear power stations is expected over the next decade. The rate of ordering will depend upon the relative economics of nuclear stations and fossil fuelled stations and also the total requirements of new electrical generating capacity.

A nuclear power station costs perhaps 25 - 30% more to build than a coal-fired plant of equivalent output, but the cost of the nuclear fuel is about a quarter of the cost of the equivalent amount of coal.

A typical analysis might be: (Hill, 1975)

In periods of rapid inflation absolute levels of cost mean very little but it is clear that modern nuclear plants will generate electricity substantially cheaper than contemporary coal or oil-fired plant. Also, once built they are substantially free from inflation because the fuel costs are so low.

The thermal reactor has been the first to be developed. The first generation of civil reactors operated by the Central Electricity Generating Board, known as Magnox reactors, have been completed and are producing about 5000 MWE (about ten percent of electric power generated in Britain). These reactors are graphite moderated, carbon dioxide cooled and fuelled with metallic uranium bars containing naturally occurring 0·7% U^{235}, with the remainder almost exclusively U^{238}. The fuel bars are sheathed in Magnox (Magnesium - 0·8% aluminium -0·01% beryllium) cans to prevent oxidation by the carbon dioxide coolant gas and to provide a heat transfer surface.

1.2 The Advanced Gas Cooled Reactor (A.G.R.)

A logical development of the successful Magnox reactors is the A.G.R. The use of enriched uranium dioxide fuel, clad in a niobium stabilised 20% Cr/25% Ni austenitic stainless steel, enables the ratings and power densities to be increased, resulting in higher carbon dioxide outlet temperatures. The higher coolant temperature permits generation to be carried out more efficiently and the increased fuel rating means that the size of plant needed to generate a given amount of electricity is reduced with a corresponding decrease in capital cost.

At present, five A.G.R. stations are under construction, each designed to produce approximately 1250 MWE. It is well known that the construction of the A.G.R. stations have been beset by technical difficulties which have been costly and time - consuming to overcome.

However, it is expected that the first A.G.R. will become operational later this year. Figure 1 shows a section through a reactor of Dungeness B power station.

The current design for the A.G.R. fuel pin is a metre long 20Cr/25Ni/Nb steel tube of 0·38mm. wall thickness, containing 7·24 mm. radius enriched uranium dioxide pellets. Heat transfer is improved by the provision of circumferential ribs on the outside of the cladding. A fuel element consists of a bundle of 36 pins (arranged within a graphite sleeve as shown in Fig. 2). Eight such elements are axially suspended on a common central tie bar to form a fuel stringer. The fuel dwell time is between 3 and 5 years and over this period the pins experience peak systematic cladding temperatures of 750°C., with random hot spots of up to 850°C, during exposure to a moist carbon dioxide - based coolant at 40 atmospheres pressure.

1.3. The Prototype Fast Reactor (P.F.R.)

The larger and more advanced thermal reactors are expected to further reduce electricity generating costs. Thus for new nuclear systems under development, it becomes increasingly difficult to penetrate the market and secure contracts to build. Nevertheless there are sound reasons for pressing ahead with the development of fast breeder reactors, particularly sodium cooled reactors.

Three main reasons for fast breeder development are:-

(i) All the countries doing major development work expect to have several thousand megawatts of thermal reactors in operation during the 1970's and therefore much plutonium will be produced. This plutonium must be utilised in an economic manner.

(ii) It is considered that fast breeder reactors, using plutonium for their initial core inventories, will provide lower electricity generating costs than any other power system.

(iii) The fuelling arrangements for fast breeder reactors are such that more fissile material is produced than is consumed.

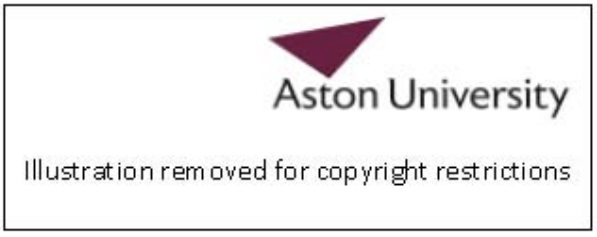
Aston University
Illustration removed for copyright restrictions

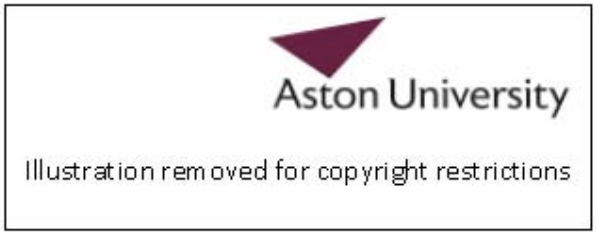
Aston University
Illustration removed for copyright restrictions

Thus fuel costs can be reduced and electricity prices held relatively insensitive to the cost of uranium.

In 1966, the 250 MWE P.F.R. was sanctioned for construction at Dounreay, Scotland, and full power is expected from the reactor during 1975. Fig. 3 shows a section through the reactor.

The core is made up of an array of hexagonal sub-assemblies containing 325 stainless steel fuel pins containing mixed plutonium-uranium oxide. The fuel pins, which are made from a high nickel A.I.S.I. type 316 stainless steel (designated M316), have a diameter of 5·84 mm, and wall thickness of 0·38 mm. Above and below the fuel is the axial breeder consisting of pins containing uranium dioxide. The lowest region of the sub-assembly is the plenum in which fission products can accumulate during irradiation (Fig. 4). The hexagonal sub-assemblies are supported from a diagrid. The fuel sub-assemblies forming the core occupy 78 of the central spaces and are surrounded by reflector and radial breeder sub-assemblies of the same size.

The reactor is enclosed in a single stainless steel tank which contains the whole primary circuit comprising the reactor core, breeder blanket, shielding, six intermediate heat exchangers and three primary pumps for circulating the sodium coolant. To complete the power station, there are three independent secondary loops containing sodium, each connecting a pair of intermediate heat exchangers to a boiler.

1.4. The relevance of the present work.

The integrity of components in A.G.R.'s and P.F.R. is essential for safety and reliability. For fuel cladding, fracture is important because active fission products may be released into the primary circuit. Thus, even before complete disintegration occurs initiation and propagation of cracks may form a leak path through the can wall. Therefore, it is important to understand the criteria controlling crack initiation and propagation.

FIG.3 THE U.K. SODIUM-COOLED REACTOR

(from Bainbridge (1970))

FIG.4 FAST REACTOR POWER STATION FUEL

(from Bainbridge (1970))

Post irradiation examination of failed fuel pins from the Windscale A.G.R.by Skinner and Newbigging (1973) has shown that failure occurred by the development of intergranular cracks which initiated at the can inner surface and propagated through the can wall. The observations suggested that failure was due to localised concentration of strain in the cladding over a fuel pellet crack. Also intergranular failures resulting from high internal fission product pressure have been observed. These types of failure have also been observed in other reactor systems (Steinar, 1972).

Evidence of intergranular attack by reactive fission products, such as caesium or its precursor iodine, on the inner surface of the cladding has been observed in both thermal and fast reactors (Johnson and Crouthamel,1970 ; Batey and Bagley, 1974). This again can cause strain localisation in the cladding. Similarly, interactions between coolant and cladding can cause defects in the outer cladding surface.

Thus the work presented in this thesis considers the initiation and growth of creep cracks from defects. Criteria controlling crack propagation in A.G.R.and P.F.R. cladding materials are considered at both micro and macroscopic levels,and over a range of temperature. Environmental effects relevant to nuclear reactors are considered, e.g. the influence of iodine vapour and neutron irradiation on creep crack propagation.

The work is extended to consider more general application than just cladding since in recent years the increased use of non-destructive testing techniques has revealed the widespread existence of crack - like defects in C.E.G.B. plant in general. Outages in the most efficient plant are very expensive, particularly during the winter, and so considerable savings can be achieved if the growth of cracks can be predicted and repairs either avoided or postponed until the summer.

CHAPTER 2.

LITERATURE REVIEW

A brief review of the structure and precipitates of 20Cr/25Ni/Nb and A.I.S.I. type 316 stainless steels is made. The effect of notches on creep rupture behaviour is reviewed and, after mentioning the concepts and limitations of fracture mechanics, the applicability of the various fracture mechanics methods to creep crack propagation is discussed. The propagation of macroscopic cracks results from microscopic rupture processes. These microscopic aspects are reviewed. Finally, the effect of nuclear reactor environment (neutron irradiation, fission product attack) on these fracture processes is discussed.

2.1. Structure and composition of 20/25/Nb and A.I.S.I. type 316 stainless steels.

2. 1.1. 20Cr/25Ni/Nb Stainless Steel

A typical composition of 20/25/Nb stainless steel is shown in Table 1. The structure consists of a polycrystalline face centred cubic solid solution alloy of low stacking fault energy, γ ($\gamma < 40$ mJ/m^2, Silcock, Rookes and Barford (1966)) initially containing dispersed Niobium carbonitride precipitates (Nb(CN)).These precipitates are commonly nucleated on intra-granular dislocations but also on grain and twin boundaries.

Precipitation in 20/25/Nb steel is complex and the simultaneous occurrence of as many as five phases (Nb(CN), $M_6(CN)$, $M_{23}(CN)_6$, Fe_2Nb, σ, where M is comprised of Cr, Ni and Fe: their relative amounts depending upon the exact composition of the steel) is reported in the literature. Knowles (1973) has shown that a useful method for predicting precipitate phases in terms of alloy composition is to consider the degree to which

TABLE 1.

A Typical Alloy Composition for C.A.G.R.

Cladding (wt.%)

(from Adamson and Martin, 1972)

matrix chromium is stabilised by the addition of niobium a stronger carbide forming element. This degree of stabilisation is expressed as $\frac{\text{wt. \% Nb}}{\text{wt. \% (C + N)}}$. The precipitation of chromium bearing $M_{23}C_6$ is undesirable due to the impairment of corrosion resistance. This can be minimised by control of the niobium to (carbon + nitrogen) ratio in the alloy specification. Thus when the niobium to carbon plus nitrogen ratio is about 7·7 sufficient niobium is retained in solution to completely combine with all the carbon present in solution to form stoichiometric NbC rather than $M_{23}C_6$.

Knowles suggests that the precipitate M_6C has three niobium atoms in its chemical formula and thus for precipitation of carbon as this phase the niobium to carbon plus nitrogen ratio must be 23·1. At ratios greater than 23·1 excess matrix niobium is present allowing the formation of iron niobide.

During high temperature exposure, the niobium carbonitride precipitates coarsen (Healey, Brown and Speight, 1973) and may transform to $M_6(CN)$ or a precipitate similar to a z phase ($Cr_2Nb_2(CN)_2$). Also progressive formation of grain boundary sigma phase (a complex brittle, intermetallic compound of chromium and iron) occurs with time as the temperature is reduced below 820°C. The volume fraction of sigma phase is restricted to less than 10% due to the high nickel content of the alloy.

In compositions of 20/25/Nb steel typical of cladding, boron is present at levels of several parts per million and will be fully precipitated and incorporated into the structure of carbide phases at temperatures of less than 980°C. (Goldschmidt, 1971). Evidence from other steels has shown, for example, that boron can replace carbon in the matrix NbC and grain boundary $M_{23}C_6$ precipitates (Harries and Roberts, 1967).

2.1.2. A.I.S.I type 316 Stainless Steel.

The composition limits of many stainless steels have been standardised by the American Iron and Steel Institute (A.I.S.I.). For A.I.S.I. type 316 steel, the composition is given in Table 2. This austenitic stainless steel is widely used in numerous engineering structures which require good mechanical properties and corrosion resistance at temperatures of up to about 700°C. For fast reactor cladding a version of type 316 steel (designated M316) having a high nickel content has been selected (A typical composition is given in Table 2). This is because leaching of nickel from the cladding by liquid sodium can occur, resulting in enhanced sigma phase formation in the cladding with subsequent impairment of the mechanical properties.

Structurally, the 316 steels are face centred cubic solid solutions initially containing dispersed $M_{23}C_6$ precipitates. The stacking fault energy of 316 steel has been measured as 25 -35 mJ/m^2 (Weiss and Stickler (1972)). The molybdenum partly enters the carbide phase and boron additions act to make the $M_{23}C_6$ precipitates smaller and more numerous (Crussard, Plateau, and Henry (1963)).

Long term exposure of 316 steel to elevated temperature causes decomposition of the austenitic matrix by a complex sequence of precipitation reactions, resulting in the formation of several carbide and intermetallic phases. Weiss and Stickler (1972) have produced time - temperature - precipitation diagrams for 316 steel between 400°C. and 900°C. for aging times of up to 3000 hours. The phases resulting from the various temperature/aging times have been identified as $M_{23}C_6$ and M_6C carbides and the intermetallic phases chi (containing molybdenum, chromium, iron and nickel), Laves (Fe_2Mo) and sigma $[(Fe,Ni)_x(Cr,Mo)_y]$. Cold work prior to aging is shown to accelerate the precipitation of these phases; a result confirmed by Spruiell, Scott, Ary and Hardin (1973).

TABLE 2.

Composition of A.I.S.I. type 316 Stainless Steel (Clauss (1969)) and typical composition of M316 steel (Bagley et al (1974))

	A.I.S.I. type 316 steel (wt. %)	M316 Steel (wt. %)
C	0·08 max.	0·04
Mn	2·00 max.	1·7
Si	1·00 max.	0·6
Cr	16·0 - 18·0	17·0
Ni	10·0 - 14·0	13·5
Mo	2·00 -3·00	2·4
P	0·045 max.	0·01
S	0·030	0·01
Fe	Balance	Balance

2.2. Effect of Notches on Creep-Rupture Behaviour.

Notches are a common cause of brittle failure in metals and their embrittling action is utilised in the standard test for measuring fracture toughness.

Perhaps the first indications of notch embrittlement during creep-rupture were given by the failure of boiler flange bolts after several years service. Such bolts were generally designed with large factors of safety, based on conventional smooth-bar data. Nevertheless, premature failures were reported more than thirty years ago. The breaks usually occurred in threads or at abrupt changes in cross section, where stress concentrations were present. The failures could not be anticipated either from creep-rupture tests on smooth specimens or from short-term tensile tests on notched specimens (Brown and Sachs, (1951)).

Two types of test were commonly used to evaluate the extent of embrittlement during high temperature service. The earlier type of test measured the room temperature impact strength of notched specimens of the material after exposure for various times at elevated temperature. During the past 20 years, there has been an increasing amount of creep-rupture testing with notched specimens to assess the susceptibility of materials to creep crack growth. Generally, such tests are performed in simple tension at constant load upon bars with and without notches. The cross-sectional area at the notch root is made equal to the plain bar area, thus achieving similar nominal stress levels. The notch influence can be expressed as a ratio of time to failure for the notched bar divided by the failure time for the plain bar. Some tests result in notch strengthening, i.e. the life of the notched testpiece is greater than that of the plain bar, while others show notch weakening.

Whether a given material is strengthened or weakened by notching depends upon the test conditions. Variations in the notch geometry, the temperature, the rupture life, and the metallurgical condition of the material all effect its sensitivity to notching. Accordingly, the results of tests performed on a wide variety of materials are so varied that they are contradictory.

The effect of plain bar ductility on notch sensitivity has been commented upon by several authors (Garofalo (1959); Brown, Jones and Newman (1952); Brown and Sachs (1951); Davis and Manjoine (1952)) who suggested that strengthening occurred when plain specimen ductility wasgreater than about 10% and for ductilities less than this, weakening occurred. However, Voorhees, Freeman and Herzog, (1962) found that no value or range of ductility in unnotched specimens could be used to predict the notch rupture behaviour.

The evidence for an effect of notch acuity on notch sensitivity is also conflicting. Voorhees, Freeman and Herzog (1962) have shown that for 19 materials, increasing the notch sharpness first strengthened and then weakened notched bars. However, other workers (Hanink and Voorhees (1962); Manjoine (1962))recorded the opposite effect while Manjoine (1963) showed both weakening and strengthening as the notch acuity rose.

The investigation into size effects also shows confusing trends. The work of Manjoine (1962, 1963) showed that notch sensitivity (either strengthening or weakening) tends towards the unnotched value as the specimen size was increased. Supporting this trend to some extent was the evidence of Goldhoff (1963) which recorded a general and continuous reduction in notch strengthening for increasing size of specimen.

The metallurgical condition of the material has also been shown to cause notch sensitivity. Davis and Manjoine (1952) found that

the appearance of notch weakening or strengthening depended upon grain size, with coarse grained material showing weakening and fine grained material of the same smooth bar ductility showing strengthening. Precipitation on grain boundaries has also been proposed to cause weakening (Brown, Jones and Newman (1952)).

Voorhees, Freeman and Herzog (1962) suggested that the presence of a notch introduced nothing inherently new into the properties of a material. They pointed out that the influence of the notch on rupture behaviour must involve to some extent (i) the resulting stress concentration with the attendant stress gradients and the increase in local strain for any given axial load and/or (ii) the multiaxiality of the stress pattern produced when a notched bar is loaded, which is shown in Fig. 5 for a bar with an external circumferential notch. Relaxation of the radial stress occurs at the notch root so that a biaxial stress system occurs here, whilst the triaxial stess system in the interior of the bar increases to a maximum below the surface of the notch.

During loading, the material near the notch root will undergo localised plastic flow and the stress pattern will then be redistributed by creep relaxation. Clearly, the notch sensitivity of a material will be related to the creep and creep-relaxation strength as well as the ability of the material to accommodate the local plastic deformation. For axial plastic flow to proceed, radial strain must occur but the radially induced stress is resisted by the relatively low stressed surrounding material. This lateral constraint to plastic flow results in notch strengthening. Garofalo (1959) suggested that notch strengthening occurred when crack initiation was delayed by relaxing the triaxial stresses developed on loading. Crack initiation is often found to occur just below the notch root in the position of maximum tensile stress.

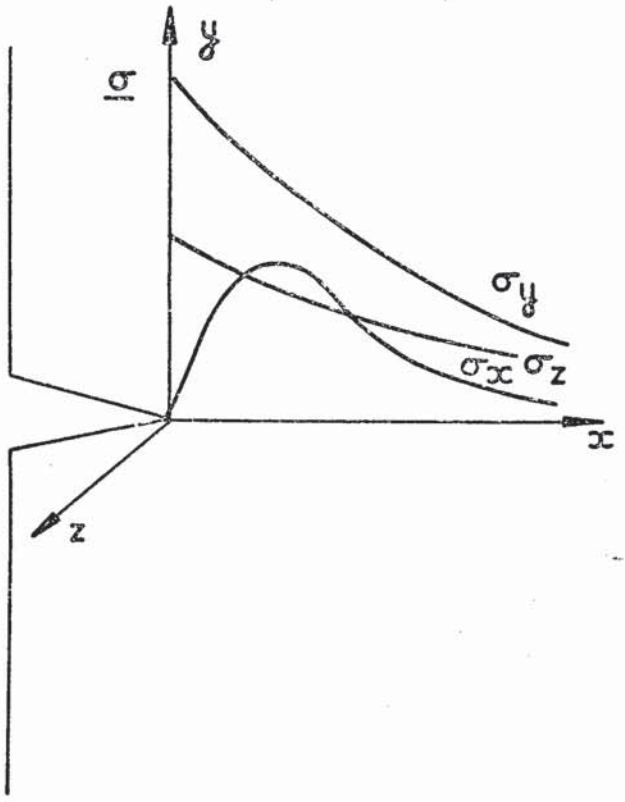

FIG. 5. Schematic Representation of Stresses Ahead of Circumferential Notch.

Taira and Ohtani (1973) suggested that notch weakening was attributed to the short time for crack initiation in notched specimens compared with plain specimens. This resulted from the presence of high local stresses at the notch root which had not relaxed to the same extent as when notch strengthening occurs. Lateral constraint still occurred which would be expected to cause strengthening, but recent results of Dyson (1975) suggest that the rate of cavity nucleation is effected by the stress state such that cavitation occurs more easily in a large triaxial stress system. Thus, macroscopic crack initiation would be easier, resulting in notch weakening.

The early investigations on the effects of notches on the creep-rupture behaviour of materials have lead in recent years to more detailed quantitative examinations of the growth of creep cracks from defects. Crack growth rates have been measured and various fracture mechanics concepts have been proposed as the controlling criteria for creep cracking. However, before this work is reviewed, the various concepts of fracture mechanics and their limitations are described.

2.3. The Concepts and Limitations of Fracture Mechanics.

2.3.1. The stress field around a crack.

To describe the stress field around a crack in a body deforming under some external applied stress, the co-ordinate system shown in Fig. 6 is used. With this system, it is possible to distinquish between the different stress systems as follows:-

(i) Plane stress occurs when the stress component σ_{zz} is zero throughout the thickness of the body (i.e. in the z direction).

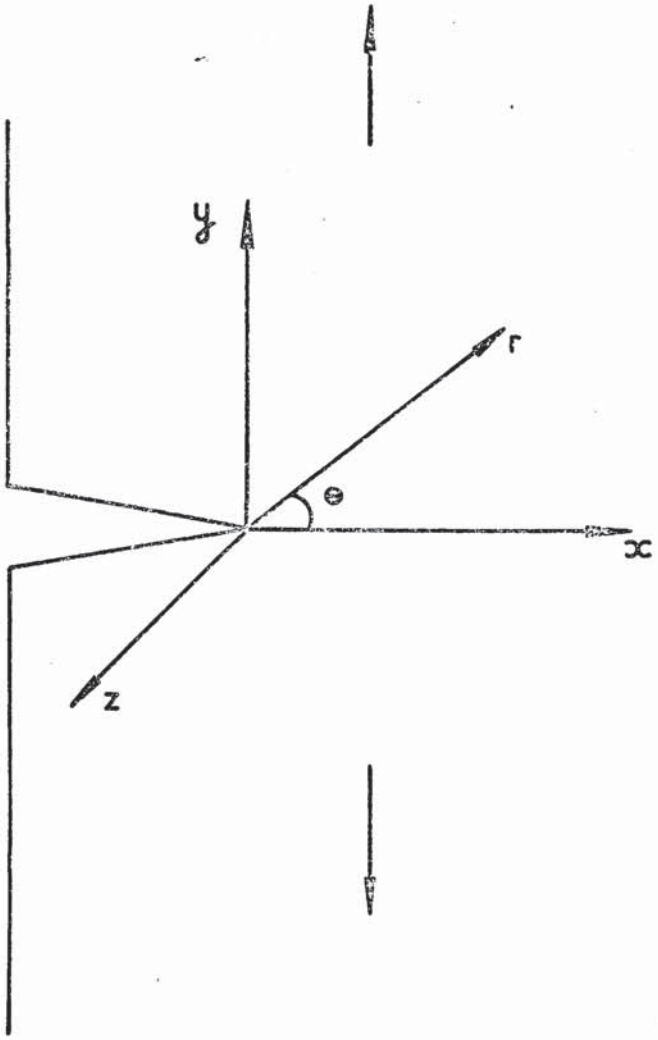

FIG. 6. Co-Ordinate System used to Describe Crack Tip Stresses.

(ii) Plane strain results from the strain component ϵ_{zz} being zero throughout the thickness of the body. For example, this type of elastic field is produced by an edge dislocation and the displacements are confined to the xy plane.

(iii) Anti-plane strain results from displacements only in the thickness direction. A screw dislocation produces this type of stress field.

For the case of simple extension of a crack, length a, in an infinite body the expression for the stresses, given by Westergaard (1939) and later adapted by Irwin (1957) can be written:-

$$\sigma_{xx} = \frac{\sigma\sqrt{\pi a}}{(2\pi r)^{\frac{1}{2}}} \cos\frac{\theta}{2}\left[1 - \sin\frac{\theta}{2}\sin\frac{3\theta}{2}\right] \quad (1)$$

$$\sigma_{yy} = \frac{\sigma\sqrt{\pi a}}{(2\pi r)^{\frac{1}{2}}} \cos\frac{\theta}{2}\left[1 + \sin\frac{\theta}{2}\sin\frac{3\theta}{2}\right] \quad (2)$$

$$\sigma_{xy} = \frac{\sigma\sqrt{\pi a}}{(2\pi r)^{\frac{1}{2}}} \left[\cos\frac{\theta}{2}\sin\frac{\theta}{2}\cos\frac{3\theta}{2}\right] \quad (3)$$

Clearly, the stresses tend to infinity as $r \to 0$. This is a consequence of the fact that the material has been assumed to be linear elastic. Also, it can be seen that the equations can be expressed in the general form:-

$$\sigma_{ij} = \frac{K}{(2\pi r)^{\frac{1}{2}}} f_{ij}(\theta) \quad (4)$$

where $K = \sigma\sqrt{\pi a}$ and is called the stress intensity factor. This equation applies to any geometry provided the appropriate formulation for K is used. It is usual to denote the loading system by a suffix, thus K_1 applies to tensile loading, K_2 to shear loading, and K_3 to antiplane strain. The stress intensity factor is the parameter which characterises the stress field (and the strain field) at the crack tip. It is a function only of the applied stress, the crack length and the geometry of the body containing the crack. Provided the relationship between these parameters is known, the relevant K value can be calculated.

2. 3.2. Linear Elastic Fracture Mechanics.

The stress intensity factor can also be used in describing fracture since it is related to the crack extension force, G, which is defined as the energy required to extend unit length of crack front by unit length:-

$$G = \frac{K^2}{E} \text{ for plane stress (Irwin, 1957)} \qquad (5)$$

or

$$= \frac{K^2 (1 - \nu^2)}{E} \text{ for plane strain} \qquad (6)$$

where ν is Poisson's ratio and E is Young's modulus.
The Irwin analysis proposed that crack propagation occurred at a stress, σ_F, when G was equal to a critical value, G_c. Thus, when $G = G_c$, $K = K_c$ and for tensile opening mode deformation under plane strain conditions is written as K_{1C}, which is called the fracture toughness.

The theory was derived for purely elastic conditions. However, equation (2) predicts that there is a region in the neighbourhood of the crack tip where the stress σ_{yy} is greater than the yield stress of the material, σ_y, and a plastic zone of size d_p forms. This causes

a redistribution of the stresses near the crack tip. To maintain the load carrying capacity of the specimen, d_p must extend further than the point, r_p, at which the elastic stress is equal to the yield stress. To a first approximation, the plastic zone extends a distance ahead of the crack given by:-

$$d_p = 2r_p = \frac{K^2}{\pi \sigma_y^2} \qquad (7)$$

for plane stress and about one third of this value for plane strain.

This equation allows the elastic analysis to be extended to situations where small scale yielding has occurred. This is achieved by proposing a new stress distribution by translating the original distribution a distance r_p ahead of the crack tip (Irwin, 1964). The corrected K value is determined as:-

$$K = \sigma \sqrt{\pi(a + r_p)} \qquad (8)$$

The distribution of stress remains as $r^{-\frac{1}{2}}$ but a "notional" elastic crack the length of the original crack, a, plus r_p is considered to exist.

2. 3.3. General Yielding Fracture Mechanics.

Where extensive plasticity precedes fracture, the assumption of elastic behaviour for K no longer holds and the calculation of the fracture toughness, K_{1c}, is not valid. Under these conditions, test pieces and structural details may be characterised at fracture initiation by a critical crack opening displacement (COD) concept or by the more general approach of the J contour integral proposed by Rice (1968).

The COD concept was proposed independently by Cottrell (1961) and Wells (1961) who reasoned that it should be possible to use the amount by which the crack opened as a measure of the work

done in extending the crack. Thus, fracture occurred whenever the COD, δ, exceeded a critical value, δ_{crit}.

Bilby, Cottrell and Swinden (1963) described the elastic-plastic fields for anti-plane strain by a dislocation distribution in the field of the crack. An array of edge dislocations represented the crack face separation and the displacement in the plastic zone. This enabled the following expression to be derived for the crack opening displacement in tensile opening mode deformation:-

$$\delta = \frac{8}{\pi} \frac{\sigma_y}{E} a \ln \left[\sec \left(\frac{\pi \sigma}{2\sigma_y} \right) \right] \qquad (9)$$

At very low stresses, this may be simplified to give,

$$\delta = \frac{\sigma^2 \pi a}{\sigma_y E} = \frac{K^2}{\sigma_y E} \qquad (10)$$

or, substituting for equation (5) and rearranging gives:-

$$G = \delta \sigma_y \qquad (11)$$

Thus, it can be seen that at these low stresses δ is related to the linear elastic fracture mechanics parameters. The COD is a parameter which appears to characterise fracture both before and after general yield. The possibility arises of measuring the value of the critical crack opening displacement for a material on a small test piece which breaks well after general yield and using the same value to predict the failure stress of a large structure which breaks before general yield.

This same possibility arises from the work of Heald, Spink and Worthington (1972) who have applied the Bilby, Cottrell and Swinden (1963) model of plastic relaxation around the crack to post yield fracture. They derived an equation to relate the apparent fracture toughness, K_A, measured in a "non-valid" toughness

test (i.e. extensive plasticity had occurred before failure) to the "valid" plane strain fracture toughness, K_{1c}. Thus, the applicability of linear elastic fracture mechanics parameters may possibly be extended well beyond linear elastic conditions.

The use of the J contour integral as a parameter to characterise fracture in both the linear elastic and post yield regimes came to prominence following the suggestions of Rice (1968). For a crack aligned in the x-direction, J is defined as:-

$$J = \int_{\Sigma} \left(W \, dy - T \frac{\partial U}{\partial x} \, dS \right) \qquad (12)$$

where Σ is any path anticlockwise around the crack tip from the lower flank to the upper flank, W is the strain energy density, T and U are surface tractions and displacements along the contour and S is the arc length around Σ. For linear elasticity, $J = G = K^2/E$ in plane stress. Its use has been extrapolated to deal with elastic/plastic and fully yielded conditions.

Experimentally, J values have been measured from non-linear compliance measurements by determining the areas between load-deflection curves for successively longer cracks to give $\frac{dW}{da}$ $(=J)$ where W is the work done to a given deflection. J can also be calculated theoretically by Finite Element Analysis. For a single test (3 point bend or compact tension specimen) the J value may be calculated by:-

$$J = \frac{\text{constant.} \quad W}{B \, (w - a)} \qquad (13)$$

where the constant equals 2 for post yield fracture behaviour and is related to the geometry for other cases. W is the energy absorbed (i.e. the area under the load/deflection curve), B and w are the specimen thickness and width respectively and a is the crack length.

Thus, the J-integral can be evaluated for a given specimen and experiments in which the value of J at fracture was measured in two specimen geometries designed to give markedly different stress states, appeared to show that a constant J_{1C} value characterised fracture in both geometries (Bucci et al, (1972)). Landes and Begley (1974) found that J_{1C} versus temperature showed good agreement with previous K_{1C} data. The measurement of J_{1C} is a new testing technique and much work remains to be done to establish fully the applicability of the approach.

2.4. The Application of Fracture Mechanics to Creep Crack Propagation.

The need for the extension of fracture mechanics concepts to creep fracture is important. Cracking may escape non-destructive testing before service, particularly in weldments and further crack growth may occur in service. A problem often arising, therefore, is the estimation of the growth rate of a defect or crack in the creep range during service.

Little information existed previously in this area and consequently over the last five years, considerable effort has been devoted to the study of the factors affecting creep crack growth. As data has become available from these investigations, it has become apparent that various approaches are possible and that interpretation can be affected by differences in material behaviour and in the testing technique employed in the laboratory. To enable precise analyses of defect growth to be made, the applicability and limitations of the various proposed approaches need to be known.

From a detailed examination of creep crack growth at 565°C. in single edge notched tension specimens of quenched $2\frac{1}{4}$Cr - 1 Mo steel,

Siverns and Price (1970, 1973) obtained a correlation between crack growth rate $(\frac{da}{dt})$ and stress intensity factor (K) such that the data were described by the equation:-

$$\frac{da}{dt} = D K^s \qquad (14)$$

Where D and s are material and temperature dependent constants.

Several other authors have found a similar equation to apply and the various material and testing conditions are summarised in Table 3a. Most work was performed on only one specimen geometry so it is not possible to decide whether the K correlation is unambiguous. Conclusions varied where results were presented for two geometries.

Such a correlation appears to be untenable since time dependent plastic strain can occur which will tend to relax the high initial elastic stresses at the crack tip, making elastic theory inapplicable. However, it was argued by the various authors that the rate at which relaxation occurred would be dependent on the material creep properties and the degree of constraint , so that where relatively little plastic strain accompanied crack growth, the stress field equations for a crack in an elastic body (i.e. equation. (4)) may provide a good approximate description of the stresses at the crack tip.

To test the applicability of K to creep crack growth in the aluminium alloy RR58, Kenyon et al (1973) used contoured double cantilever beam (DCB) specimens which were designed to give a constant K value over a wide range of crack lengths. They found that crack growth between 100 and 200°C. occurred in three stages. In stage 1 despite the constant K, decreasing crack growth rates were observed and in stage 3, acceleration of the crack growth rates occurred. In stage 2,

TABLE 3a Summary of References correlating K with creep crack propagation rate.

Reference	Material and Temperature	Apparent K ($MNm^{-3/2}$)	S	Geometry
Popp and Coles (1970)	Inconel 718 538°C	100 - 160	7	CC
Siverns and Price (1970)	2¼Cr - 1 Mo quenched steel 565°C	10 - 90	5·5	SEN
James (1972)	Type 316, cold worked steel 538°C	25 - 40	>20	CC and CKS
Robson (1972)	0·2%C cast steel 450°C	40 - 50	20	CKS and SEN
	0·2%C wrought steel 450°C	30 - 40	14	CKS
Thornton (1972)	1Cr-Mo-V wrought steel 565°C	30 - 70	8	SEN
	½ Cr-Mo-V cast steel "	40 - 50	16	"
	½ Cr-Mo-V wrought steel (Coarse grains) "	17 - 40	6	"
	½ Cr-Mo-V wrought steel (fine grains) "	35 - 50	6	"
Kenyon et al (1973)	RR 58 100 - 200°C	17 - 27	30	DCB

however, the growth rates were correlated with K as in equation (14), the exponent value being 30, which is about the same as the stress exponent in the secondary creep equation:-

$$\dot{\varepsilon} = A\,\sigma^n \qquad (15)$$

where $\dot{\varepsilon}$ is the secondary creep rate and A and n are material and temperature dependent constants. It was suggested that stage 1 was possibly due to stress redistribution. Soaking the specimens at temperature prior to testing was found to significantly reduce the primary stage possibly by allowing residual stresses to redistribute. A similar observation of three stages in crack growth rate has been observed by Soo (1974) in coarse grained solution treated 9Cr - 1Mo steel at 525 to 550°C.

Another investigation of the correlation between crack growth rate and K was made by Pilkington et al (1974) who also measured the rate of crack opening displacement during the test. Despite their calculations showing that the initial nett section stress (i.e. the stress on the uncracked ligament) applied to some of the specimens would have caused considerable yielding, correlations of crack growth rate and K were attempted. A linear relationship was obtained over limited ranges of K values for each individual test, but it was not possible to obtain a correlation from test to test. They suggested that although a local K parameter may be valid, it ought to be related to the rate of change of crack opening displacement rather than crack growth rate, to give an equation:-

$$\frac{d\delta}{dt} = B\,K^m \qquad (16)$$

where δ is the crack opening displacement, and B and m are constants, with m varying between 5 and 30.

Harrison and Sandor (1971) have presented data obtained by

Brothers (unpublished work) for tests on 1 Cr-Mo-V steel at 538°C. using centre cracked specimens. The authors correlated the crack growth data with both K and the nett section stress, and found that the latter provided the better correlation, and linear elastic fracture mechanics was dismissed as inappropriate since creep deformation was certain to have occurred.

Taira and Ohtani (1973) have also found a correlation between crack growth rate and nett section stress in circumferentially notched bar and double edge notched specimens of 1 Cr-Mo-V steel. Their equation was:-

$$\frac{da}{dt} = N \sigma_{Nett}^{b} \qquad (17)$$

where b is 8·8 and N depends upon specimen geometry, being smaller for the bar specimens.

Siverns and Price (1970, 1973) found that the correlation of crack growth rate with nett section stress was poor but the assymetric nature of their specimens subjected the uncracked ligament to additional stresses from bending moments. Thus a more refined analysis is required before the validity of various stress criteria (other than K) can be assessed in these tests.

Ellison and Walton (1973) have found that the growth rates obtained from tests on single edge notched specimens of normalised and tempered 1 Cr-Mo-V steel at 565°C. could not be correlated with K alone, but introduced a time function, t_p, where t_p is the time during which the crack propagates across the specimen. Their equation for 1 Cr-Mo-V steel was:-

$$\frac{da}{dt} = 4{\cdot}56 \times 10^{-20} \quad t_p^{\,0{\cdot}93} \; K^{7{\cdot}46} \qquad (18)$$

They suggested that the K represented the initial local

stress conditions and that the time component described the rate at which the stress was relaxed due to the creep strain. However, they did not attempt to correlate the growth rates with any other function despite acknowledging that K-distribution of stresses was inapplicable.

The linear elastic fracture mechanics approach (equation(14)) does not describe a critical displacement for crack initiation at high temperature as has been observed in many tests (Haigh (1973)). An alternative approach has been suggested by Wells and McBride (1967) namely that crack growth is controlled by local displacements at the crack tip. This is very attractive in principal since it is easily visualised as the deformation and fracture of a small tensile specimen at the crack tip (Cottrell, (1961)) and is a method that has been used to describe unstable crack growth at low temperatures. In addition, for a creep process, the accumulation of strain is an accepted physical picture. Haigh (1973) considered this approach to be relevant in controlling creep crack growth in 1 Cr-Mo-V steel at 565°C, where significant deformation accompanied crack growth. He found the following equation to be applicable:-

$$\frac{da}{dt} = 2\left(\frac{d\delta}{dt}\right)^{0\cdot 8} \qquad (19)$$

The three stages of crack growth observed by Soo (1974) corresponded to the stages of the creep curve also suggesting a relationship between growth rate and displacement rate.

The application of crack opening displacement as the controlling parameter for crack growth requires data on cracked specimen deformation, which is controlled by an equivalent stress (Ewing and Richards (1972)):-

$$\sigma_H = \frac{P}{mBW} \qquad (20)$$

where σ_H is the equivalent stress,

P is the applied load

B is the specimen thickness

W is the specimen width.

and m is the ratio of the load to cause yield in the cracked section compared with that in the uncracked section. The value of m was derived from an examination of the fully plastic slip line field analysis. A major conceptual difficulty is to relate a completely plastic analysis based on time independent yield with a time dependent creep process.

Another criterion for creep crack propagation has been suggested by Turner and Webster (1974), Webster (1975) and Nikbin and Webster (1975), who suggested that growth was controlled by a function of the J contour integral. Reanalysis of the results of Kenyon et al (1973) on RR 58 and results from quenched $\frac{1}{2}$ Cr-Mo-V steel tested at 565°C suggested that growth could be described by the equation:-

$$\frac{da}{dt} = \alpha \dot{J} \qquad (21)$$

where $\dot{J}$ is the rate of doing work on the specimen. For a particular geometry, $\dot{J}$ and K are related and so an apparent correlation with K could be found. Similarly, when the stress exponent, n, in equation (15) is large, $\dot{J}$ is proportional to the nett section stress and correlation with this term would be expected. However, further experiments are required over a wider range of testing conditions to determine whether non-linear fracture mechanics concepts can be extended to predict creep crack growth.

Neate and Siverns(1973) and Neate (1975), in an attempt to rationalise the various approaches, have shown in tests on $2\frac{1}{4}$ Cr-Mo, 1 Cr-Mo-V and $\frac{1}{2}$ Cr-Mo-V steels of differing heat treatment to give varying creep strengths and ductilities, that these properties are of prime importance in determining the applicability of the various fracture mechanics parameters. Other attempts have been made to rationalise the criteria controlling creep cracking, some of which are shown in Table **3b**. This Table summarises the various criteria which have been suggested for crack growth in $\frac{1}{2}$ Cr-Mo-V and 1 Cr-Mo-V steels. It is apparent that in the approaches specified above there can be difficulty in reconciling the various models in terms of creep mechanisms. An important observation in this respect is the inherent differences in ductility shown by creeping materials, as shown by Neate and Siverns (1973) and Neate (1975). Siverns and Price's original data were for a material of low ductility (less than 1-2% under the particular test conditions), whereas the data of Thornton, Robson and Haigh were for relatively ductile materials. The fracture mode was also found to be different in the different tests with transgranular cracking occurring in James' tests but Siverns and Price found that intergranular cracking occurred in the quenched $2\frac{1}{4}$ Cr-Mo steel. These differences in mechanism imply differences in the distribution and accummulation of creep damage in the various materials. Hence, any theory presented for general application should be able to account for intergranular failure and for the more ductile transgranular crack growth mechanism.

Williams and Price (1974) have tried to rationalise the various criteria. They considered the crack tip stress distribution resulting from creep deformation and showed that the stress distribution

TABLE 3b Various Creep Crack Growth Criteria in 1Cr-Mo-V and ½Cr-Mo-V

Material	Heat Treatment	Temperature	Geometry	Criterion	Reference
1 Cr-1Mo-¼V	Normalised and Tempered	600°C	Circumferentially Notched Bar Double edge notched strip	$\dot{a}$ = constant x $\sigma_{Nett}^{8.8}$	Taira and Ohtani (1972)
1 Cr-1Mo-¼V	N & T	538°C	Centre cracked Plate (C.C.P.)	$\dot{a}$ = constant x σ_{Nett}^{10}	Harrison and Sandor (1971)
1 Cr-Mo-¼V	Normalised and Tempered	565°C	Single Edge Notched (S.E.N.)	$\dot{a}$ = constant x $t_p^{0.98}$ $K^{7.46}$	Ellison and Walton (1973)
1 Cr-Mo-V	Normalised and Tempered	550°C	Wedge Opening-Loading (W.O.L.)	$\dot{a} = 2\dot{\delta}^{0.8}$	Haigh (1973)
1 Cr-Mo-V ½ Cr-Mo-V	N & T	550°C	W.O.L.	$\dot{a} = 2\dot{\delta}^{0.8}$ $\dot{a} \propto$ Equivalent Stress, σ_d	Haigh (1974)
½ Cr-Mo-V	N & T Quenched	565°C	S.E.N. C.C.P. W.O.L.	$\dot{a}$= constant x $\sigma_d^{7.4}$ $\dot{a}$ = constant x $t^{-\frac{1}{2}} K^{3.24}$	Neate (1975)
½ Cr-Mo-V	Q	565°C	S.E.N.	$\dot{a}$ = const. x $K^{3.4}$	Neate and Siverns (1973)
½ Cr-Mo-V	N & T	550°C	S.E.N.	$\dot{a} \propto K$ $\dot{\delta} \propto K^m$	Pilkington et al (1974)
½ Cr-Mo-V	Q	565°C	Double cantilever beam	$\dot{a} = \alpha \dot{J}$	Webster (1975)

was strongly affected by the value of the stress exponent in the operative creep equation (i.e. n in equation (15) or p in the equation $\epsilon = R\sigma^{p}t^{x}$). Barnby (1974) used an elastic analogy to evaluate the crack tip stress distribution and has also arrived at a similar conclusion, showing that the larger the exponent, the less was the resulting stress gradient. Williams and Price showed that for $p=1$, the distribution was identical to the linear elastic stress distribution, and for $p = \infty$, was identical to the fully plastic stress distribution. Thus the model covers the values of p from purely elastic to purely plastic stress distributions. A major difficulty is to identify the deformation mode and stress index relevant to particular test conditions and plant operation. To overcome this difficulty, Williams and Price used a reference stress, defined as that stress which when applied to a uniaxial specimen will give the same displacement rate. They suggested that for high values of n or p, i.e. greater than 5, the effect of the stress concentration is minimised and the reference stress should be used to describe the behaviour of components containing cracks. The reference stress becomes identical to the equivalent stress used by Haigh when $p = \infty$. For $p < 5$, K is suggested as a suitable criterion. Thus, from a knowledge of the stress index, Williams and Price suggested that either the reference stress or K should be the controlling criteria. It can be inferred that there should be differences in the microstructural aspects of creep deformation and crack growth depending upon whether K or the reference stress is controlling failure. In the former, since the relaxed stresses in the vicinity of the crack tip remain high and decrease rapidly with distance, the creep damage will be confined to this region. However, when the residual stress concentration is low and more widely spread across the uncracked ligament,

the creep damage will also be less localised. The concept of a damage front spreading ahead of a crack in a creep ductile material is used by Goodall and Chubb (1974). They assumed failure occurred when a damage front, followed some way behind by the actual macroscopic crack, had propagated across a structure. Since they used finite element analysis, it should be possible to carry out these calculations for any stress index, but in practise the procedure is extremely expensive and time consuming.

2.5. Microscopic Aspects of Creep Fracture.

The preceding section has largely neglected the detailed microscopic mechanisms operating at the tip of the macroscopic crack. Whilst observations have been made on the fracture mode, i.e. intergranular, transgranular or mixed, little effort has been made to link the micro-structural mechanistic work that exists from plain specimen tests to the processes operating at the crack tip. The considerations of stress distribution ahead of the tip have pointed to the extent of localisation of the crack tip fracture processes and to the occurrence of a damage zone ahead of the crack.

Williams (1973) has shown in ductile A.I.S.I. 316 stainless steel that a region of microscopic creep cracking extending over several grains occurred at the root of the notch before macroscopic crack growth occurred. Haigh (1974) has found extensive damage distributed over a region of similar size to the notch diameter in normalised and tempered ½ Cr-Mo-V steel. In contrast, Soo (1974) found in coarse grained (> 125 μm) 9 Cr-Mo steel that intergranular cavitation was confined to a region approximately 20 μm wide, and King (1975) found that damage was very localised in brittle heat affected zone simulated ½ Cr-Mo-V steel, extending only about one grain diameter in front of the crack.

Clearly the growth of macroscopic cracks is controlled by microscopic rupture processes. Accordingly, the nucleation and growth of the microscopic creep cracks ahead of the main crack is of importance when considering creep crack propagation from a defect.

2. 5.1. The nucleation of microscopic creep cracks.

The nucleation and growth of these creep cavities has been widely studied since their full significance in limiting life under creep conditions was first realised by Greenwood (1952)

although voids had been observed previously by Jenkins (1944). Greenwood, Miller and Suiter (1954) observed rounded cavities located mainly along grain boundaries oriented perpendicular to the applied stress in specimens of copper that had been creep tested. The inter cavity spacing decreased with decreasing temperature and was approximately equal to the spacing between slip bands. Greenwood et al concluded that cracks were formed by the growth and linking of these cavities and related cavity formation with the ductility minimum observed at high temperature. Jenkins (1954) confirmed the observation of Greenwood et al that the cavities formed preferentially on grain boundaries oriented perpendicular to the stress axis.

Eborall (1954) suggested that viscous sliding could lead to stress concentrations at obstacles, such as triple points (the line along which 3 grains meet), in a manner proposed by Zener (1948). McLean (1957) rejected this possibility "because many cavities do not start at grain corners." He added, however, that too few observations had been made for definite conclusions to be drawn. Accordingly, McLean (1956 - 1957) conducted creep tests on Nimonic 80A over a wide range of stresses and temperatures. At high temperature or low stress, the rounded cavities were located preferentially on the grain boundaries oriented normal to the stress axis, similar to the results of Greenwood, et al (1954). At lower temperature and higher stress, the cracks assumed a different morphology being wedge shaped with the widest end of the wedge at a triple - point junction between boundaries on which sliding had occurred. McLean termed these configurations B and A type cracking, but since then "r" (for the rounded cavities) and "w"(for the wedge shaped cavities) have become the accepted designations.

The classic work on "w" type cracking is by Chang and Grant (1956). Fig. 7 illustrates three forms of wedge crack that can develop at triple points.

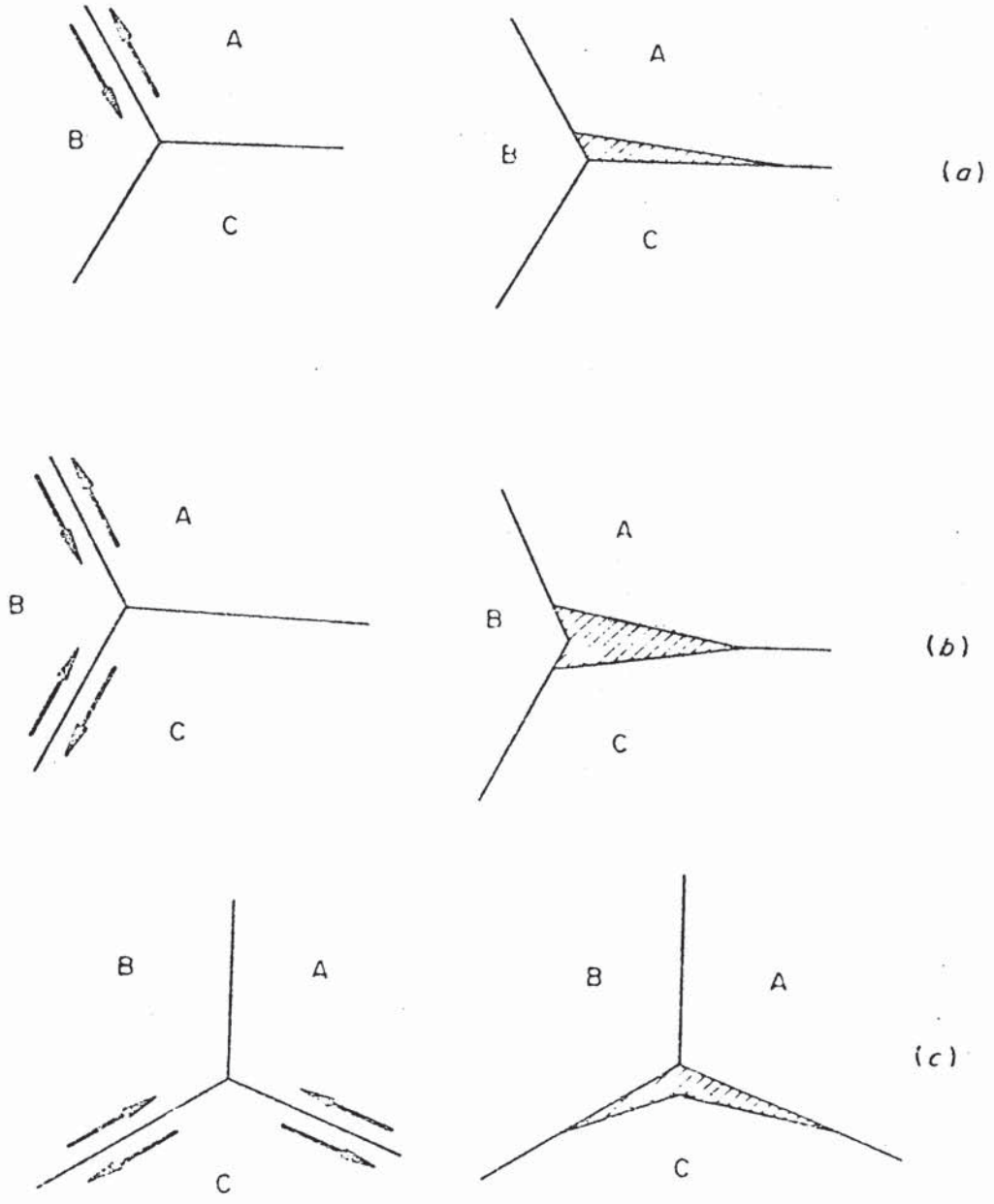

FIG. 7 Schematic illustration of possible means of forming wedge cracks by grain boundary sliding.

The observation that the nature and location of the cracks depended on temperature and stress suggested that basically different processes were responsible for the two types. Since then, research has concentrated on uncovering the different mechanisms believed to be responsible for the nucleation and growth of the two types of cracks.

As mentioned previously, Zener (1948) proposed that if grain boundary sliding was blocked at a triple point, a stress concentration would be produced which could be hydrostatic in nature. This hydrostatic stress would not be relaxed by dislocation movement and could nucleate cracks. McLean (1957) tried to quantify this approach using the stress concentration at the head of a single pile-up of dislocations derived by Stroh (1954). To nucleate a crack, the following relationship must be achieved:-

$$\tau > \sqrt{\frac{12\ \gamma\ G}{\pi\ L}} \qquad (22)$$

where τ is the shear stress across the boundary γ is the specific surface energy, G the shear modulus and L the length of sliding boundary. However, this equation relates to perfectly elastic bodies and thus plastic creep deformation will introduce errors in the use of this equation. Mclean showed that the creep failure of Nimonic 80A agreed with this approach.

Further work by Smith and Barnby (1967a)examined the double pile - up model (Fig. 7(b) and derived the relationship for nucleation in this case:-

$$\tau > \sqrt{\frac{2\gamma\ G}{\pi\ (1-\nu)\ L}} \qquad (23)$$

where ν is Poisson's ratio. These factors reduced the stress necessary to nucleate a crack by about a factor of two for $\nu = 0{\cdot}33$.

Weaver (1959-60) added to McLean's work with additional studies on Nimonic 80A but with specimens in which the microstructure was varied. In specimens containing precipitate particles distributed along grain boundaries, cracks developed between the particles and rupture lives were shortened. In interpreting the results, Weaver equated the grain-boundary length, L, in McLean's equation, with the interparticle spacing and obtained a specific surface energy in agreement with McLean's original estimate. However, Eborall (1961) argued that in this case the shear was blocked or supported at discrete points rather than at an effectively infinite medium as in the case of a triple point. Smith and Barnby (1967b) also considered the situation and pointed out that because of the restriction of sliding by precipitate particles, cracks may not be able to form until stresses high enough to fracture the particles were reached.

At the time he first observed the cavities, Greenwood (1952) proposed that they arose from the condensation of vacancies generated within the grains by plastic deformation. He assumed homogeneous nucleation on the grain boundaries. Baluffi and Seigle (1955) and Machlin (1956) argued that the vacancy supersaturation obtained under creep conditions was not sufficient to cause homogeneous nucleation. Therefore, discontinuities at the boundaries were required, irrespective of the growth process. Baluffi and Seigle (1957) suggested that impurity particles or deformation-induced nuclei were possible sources of the cavities and cited some observations by Reswick and Seigle (1955) that impurity particles enhanced cavitation in alpha-brass. McLean (1957) argued that nucleation probably occurred on pre-existing sites, possibly holes, since cavities were also observed to form readily in diffusion experiments (Kirkendall effect). Oliver and Girifalco (1962) supported the existence of pre-existing nuclei,

but Garofalo (1965) argued that this was unlikely to be a general condition otherwise "r" type cavities would be observed at high as well as at low stresses. Gifkins (1965) also dismissed this idea since such nuclei had never been observed even though they should be easily detectable. As a result of these arguments deformation-induced mechanisms for the nucleation of cavities have been proposed. Most of these involve grain boundary sliding and some irregularity in the boundary that blocks the sliding.

Impurity particles or precipitates could provide effective obstacles to sliding at which stress concentrations could be produced. For crack nucleation to occur, the stress concentration must not be relaxed by the formation of "folds" of plasticity in the grain (Chang and Grant (1956)). Nucleation at grain boundary precipitates is supported by the results of Weaver (1959-60) for Nimonic 80A. The distribution of particles is crucial to the mechanism. The particles must be spaced sufficiently wide to enable stresses to build up to overcome the cohesion at the particle/matrix interface, but at the same time, they must be present in a high enough concentration to take the load off the triple points. Other work has shown the association of cavities with impurity particles or precipitates, as shown in Fig. 8 (Kutumbarao & Rama Rao (1973); Greenwood (1969); Wilson (1973); Rukweid (1972); Harris (1965); Venkiteswaran, Bright, and Taplin (1973)). However, Gifkins (1965) has pointed out that such an association may be fortuitous since when cavities have grown large enough to be observed it is impossible to tell whether they actually formed at the particle or simply nucleated elsewhere and grew until they encountered it.

Sliding concentrates stress as any point where the boundary deviates from a perfect plane. Gifkins (1956) and Chen and Machlin

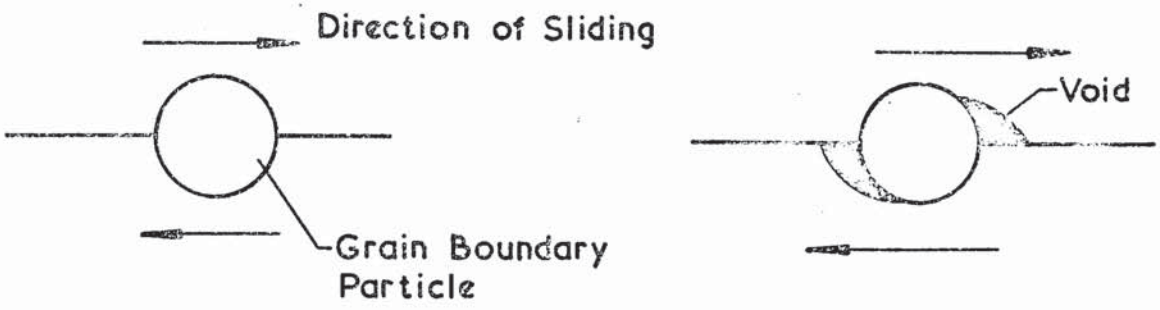

FIG. 8. Nucleation of Void at a Particle by Grain Boundary Sliding.

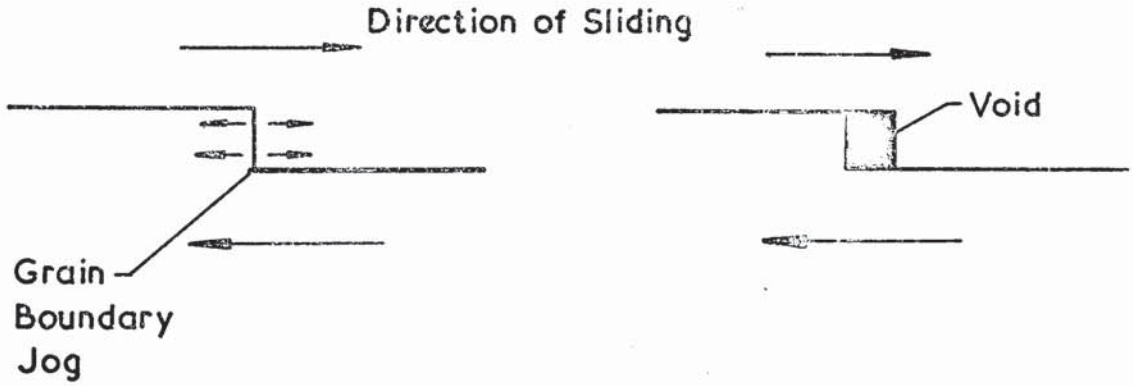

FIG. 9. Nucleation of Void at Grain Boundary Jog.

(1956) suggested that ledges or jogs in the grain boundary could obstruct sliding and produce stress concentrations high enough to overcome atomic cohesion and, upon further sliding, open into cavities (Fig. 9). Chen and Machlin (1956) proposed that ledges were a natural feature of grain boundaries, but Gifkins (1956) proposed that ledges were formed where slip bands penetrated a grain boundary. Davies and Wilshire (1961) extended this proposal by suggesting that slip-produced ledges were not straight but were themselves stepped because of intersection by dislocations from secondary slip systems. Further sliding then produced a string of isolated cavities that eventually linked up to form a large crack. This explained the strings of cavities often observed in materials that fail by cavitation.

Whilst the possibility of ledges forming on grain boundaries is generally accepted, there is little direct experimental evidence to support this. Indirect evidence was provided in the original observations by Greenwood, Miller and Suiter (1952) that in their tests on copper, the cavity spacing increased with increasing temperature and was about equal to the slip band spacing. McLean (1963) used electron microscopy to examine an iron creep specimen and observed an area of grain boundary containing several ledges up to 100Å high. However, he pointed out that this was not a typical structure. Li (1963) referred to structures of atomic dimensions which may be sites at which individual dislocations have entered or left the boundary.

McLean (1963) and Harris (1965) pointed out that once the cavity has nucleated, it must grow at a rate greater than the rate of sintering. Harris concluded that for very small cavitities sintering should predominate. This conclusion does not however consider the stabilising effects that dissolved gases could have. Gittins (1967) and Walker and Evans (1970) showed that dissolved gases do collect in cavities and that the volume change introduced by creep deformation

cannot be fully recovered by post-test annealing.

Nucleation of cavities is clearly a difficult problem to examine experimentally since very high resolution techniques are required to observe the cavities at their earliest stage of existence. Johannesson and Tholen (1972) have examined grain boundaries in copper after creep deformation in a 1 MeV electron microscope. Cavities were observed in the very early stages of formation and were always associated with obstacles in the grain boundaries such as triple points or kinks. They proposed that the stress concentration at these obstacles resulted from grain boundary sliding, and stress concentrations as high as 10^3 were suggested. Another high voltage electron microscope study of cavity nucleation in a copper base alloy by Fleck, Taplin and Beevers (1975) also revealed the association of cavities with grain boundary obstacles, in this case grain boundary particles. The particles were not fractured and so the proposal of Rukweid (1972) that nucleation occurred by the shearing of the particles by the movement of grain boundary dislocations was inapplicable to this case. Harris (1965) has proposed a mechanism for cavity nucleation at non-shearable grain boundary particles when the stress concentration resulting from grain boundary sliding is sufficient to cause matrix/particle separation. Fleck et al (1975) suggested that a similar mechanism was operating and proposed that dislocation pile-ups at the particles after a critical amount of sliding caused a sufficient stress concentration for nucleation. The cavities observed in this study showed a polyhedral shape in the early stage of formation as has been observed by Johannesson and Tholen (1972), Cane and Greenwood (1975) and Stiegler, Farrell, Loh and McCoy (1967). This contrasts with the results of Dyson and co-workers (Dyson and Henn (1973); Dyson (1973); Dyson and Rodgers (1974)) who observed spherical cavities in Nimonic 80A using high voltage electron microscopy. The material had been prestrained at room temperature and then creep

tested at 750°C. It suffered progressive loss of creep strength, life and ductility as the amount of prestrain was increased. Metallography revealed a concomitant increase in the number of spherical creep cavities. It was found that simply by prestraining and then heating for a short time at 750°C. was sufficient to produce many sub-micron cavities. The cavities formed during annealing as a result of grain boundary decohesion during prestrain. Thus, the nucleation mechanism of these spherical cavities was different from those discussed previously.

The recent application of high voltage and scanning electron microscopy to the study of cavity nucleation has proved to be fruitful. Clearly there remains a need for further evidence concerning the nucleation mechanisms but the electron metallographic studies have indicated that the critical cavity nucleus size for growth is comparable with that anticipated theoretically (Greenwood, (1973)).

2. 5.2. Microscopic creep crack growth

The mechanisms of crack growth have been the subject of much debate. Cottrell (1961) considered the following possible processes for crack growth:-

1) by spreading along the boundary, like a cleavage crack, through the breaking of atomic bonds by the concentrated stress at its ends;

2) by changing volume through elastic deformation, as a result of changes in the applied stress or in the length of the cavity;

3) by spreading along the boundary at constant volume (apart from elastic deformation) through the migration of atoms, mainly by surface diffusion, from the ends to the sides of the cavity;

4) by spreading along the boundary, with changing

volume, through the removal of atoms from the ends by atomic migration along the boundary or into the grains.

Also variations in crack morphology have been observed with the tendency to form wedge cracks diminishing at higher temperatures and lower stresses and rounded cavities developing on grain boundaries oriented normal to the stress axis. These cavities show no preference for triple points. The differences in shape and location of these cracks, along with the different stress and temperature regimes in which they occur have lead to two different mechanisms of growth to be postulated. For a long time, bitter struggles ensued between supporters of the opposing vacancy controlled and grain boundary sliding controlled mechanisms, but it has become increasingly apparent over the years that conditions can be established to favour one mechanism. For the general case, however, both mechanisms can occur and the relative proportions of each depend upon material and test conditions.

2. 5. 2.1. Diffusion - controlled growth of creep cavities

Greenwood (1952) originally suggested growth by vacancy condensation and this mechanism has been widely examined both theoretically and experimentally. Baluffi and Seigle (1955) first considered the thermodynamic conditions for void growth in the presence of a stress. They considered the case of a void on a grain boundary oriented with the boundary normal at some angle θ to the stress axis. They considered the changes in chemical potential associated with taking an atom from the surface of the void and inserting it into the grain boundary. The void is therefore enlarged increasing its surface area and energy. The elastic strain energy in the specimen changes and finally the specimen changes volume allowing the applied stress to do work. Baluffi and Seigle demonstrated that the strain energy term could be neglected in comparison with the surface energy term and showed

that the critical tensile stress, σ^*, at which a cavity of radius, r, will grow by accepting vacancies from the grain boundary is $\sigma^* = \frac{2\gamma}{r \cos^2\theta}$, i.e. voids of radius r will grow if the stress is greater than σ^* and will sinter if the stress is less than σ^*. This treatment predicts a strong orientation dependence for cavity growth since the critical stress is inversely proportional to $\cos^2 \theta$. Increasing θ from 0 to 60^o increases the stress by a factor of 4. This provides a rationalisation for the preferential appearance of r-type cavities on boundaries perpendicular to the stress axis ($\theta = 0^o$).

Hull and Rimmer (1959) extended the treatment of Baluffi and Seigle to consider the kinetics of void growth by vacancy condensation. They considered that growth could occur either by a void accepting vacancies only in a narrow band intersecting the grain boundary where transport would occur by grain boundary diffusion, or over its entire surface where transport would occur by bulk diffusion. They demonstrated that for all reasonable sized voids, the effect of the latter mechanism would be small. They then adopted the simplified picture in which voids grew only by accepting vacancies diffusing from the grain boundary in a narrow disc of thickness z centred on the void. They also considered only boundaries oriented normal to the stress axis, so that the chemical potential for vacancies was $-2\gamma\Omega$ at the surface of the void and $-\sigma\Omega$ at a point midway between the voids, where Ω is the volume of a vacancy. They assumed that the gradient in chemical potential was linear between these extremes and that surface diffusion allowed the voids to maintain a spherical shape. They derived an equation for the rate of growth of a void,

$$\frac{dr}{dt} \sim \frac{D_g z \sigma \Omega}{2 KT\eta r} \qquad (24)$$

where Dg is the grain boundary diffusion coefficient, K is Boltzmann's constant, T is the absolute temperature and η the average spacing between voids. They also showed that if the specimens were subjected to hydrostatic pressure during the test, the value of the pressure must be subtracted from the stress.

Hull and Rimmer tested this model by performing creep tests on copper wire which contained oxide inclusions. They verified metallographically that grain boundary cavities grew and linked together to form cracks. They were unable to find cavities in an experiment in which a hydrostatic pressure equal to the uniaxial stress was applied. They calculated that the activation energy for the process was close to that for grain boundary diffusion. Additionally they observed that the intercavity spacing decreased with increasing stress, suggesting that cavity nucleation was stress induced.

Speight and Harris (1967) modified the treatment by using Fick's second law to describe the vacancy concentration profile around the void. Radial symmetry was assumed and the concentration was set at zero at a point midway between the voids. The chemical potentials used by Hull and Rimmer were used to fix the vacancy concentrations at the void surface and at the midpoint between voids. The resultant equation was:-

$$\frac{dr}{dt} \sim \frac{z\, Dg\, \Omega\, (\sigma - 2\gamma/r)}{2kTr\left\{\ln\left(\frac{\eta}{2r}\right) - \left(\frac{\eta^2 - 4r^2}{2\eta^2}\right)\right\}} \left(\frac{1}{r} - \frac{4r}{\eta^2}\right) \qquad (25)$$

The principal difference occurs at large void spacings or in the early stages of void formation where equation (25) gives growth rates appreciably larger than the Hull and Rimmer equation (equation 24)).

Several modifications have been proposed to these two models. Dobes and Cadek (1970) criticised the assumptions of Speight and Harris that the only flux of vacancies was along the grain boundaries into the voids and that the rate of vacancy production is constant. They described the vacancy concentration in the boundary by considering the vacancy flux within the grains to the boundaries (analagous to that in Nabarro -Herring creep (1950, 1948)) and their equation for cavity growth predicts faster rates than equations (24) and (25) if the intercavity spacing is greater than 25 times the void radius. Also, unlike the other two models, Dobes and Cadek predicted the rate of cavity growth to be independent of intercavity spacing for large void spacing. Weertman (1973) also suggested that relatively widely spaced voids grow much more quickly than the Hull and Rimmer theory suggests. Weertman also pointed out that Speight and Harris had used an improper boundary condition in the derivation of their equation. The corrected expression for the void growth rate can be many orders of magnitude greater than the Hull and Rimmer predicted values.

Another modification to the Hull and Rimmer theory is by Vitovec (1972) who derived an expression for the rate of void growth taking into account the fact that the voids cause a reduction in the load - bearing area and thus an increase in the nett stress. This results in an increase in growth rate for large voids.

Recently, Speight and Beere (1975) have presented a treatment of void growth incorporating some physical concepts which have been previously neglected, such as the fact that the rate of vacancy production is equivalent to a corresponding rate of precipitation of atoms which causes adjacent grains to move apart and so increase

the volume of each cavity. This factor is of particular importance when the void size becomes comparable with the spacing. Fig. 10 compares the void growth rate/relative separation predicted by the various models. The Speight and Beere curve differs slightly from the Speight and Harris curve (by a factor of 2 at a relative spacing $\frac{2r}{\eta}$ of 0·5). The Speight and Beere and Weertman curves are identical for widely spaced voids ($\frac{2r}{\eta} < 0{\cdot}2$).

The transference of atoms from the surface of voids to the normal grain boundary constitutes a creep mechanism and has been studied theoretically by Harris, Tucker and Greenwood (1974). Creep curves were generated and it was shown that both time and strain to failure depend critically upon the initial void spacing. Also, the conclusions of Vitovec were supported since it was shown that the increase in nett stress as the cavities grow has a marked influence on the derived creep curves. However, these authors assumed that no further cavity nucleation occurred after time zero. Skelton (1975) has, therefore, developed the Harris et al model to allow for continuous nucleation and found that for similar failure times, the elongation was lower when voids were continuously nucleated. No allowance was made for the nett stress increase in these calculations. The creep model by Harris et al does not necessarily apply only to spherical cavities but most models of cavity growth have assumed spherical cavities on the assumption that surface diffusion is sufficiently fast. Dobes (1973) and Spark(1969) suggested that this is not necessarily correct and cavities may be unable to mimimise their surface energy and thus may be ellipsoidal, as observed by Wingrove and Taplin (1969); Steigler, Farrell, Loh and McCoy (1967). Ashby and Raj (1975) also considered the shape of voids during growth.

FIG. 10 Normalized void growth rate($\frac{1}{K}\frac{dV}{dt}$, where K is factor independent of void spacing, V is void volume) v. relative separation($\frac{2r}{\ell}$). (from Speight and Beere (1975))

Curve (1):- Speight and Beere (1975)
(2):- Hull and Rimmer (1959)
(3):- Speight and Harris (1967)
(4):- Weertman (1973)

The void shape is determined by the relative rates at which atoms are drawn from the void and surface atoms redistributed, i.e. the shape is determined by kinetics not by equilibrium considerations.

Considerable effort has gone into producing experimental evidence to support the theoretical models discussed above. Boettner and Robertson (1961) studied cavity formation in copper by means of density measurements. They were unable to detect volume changes in single crystals or in polycrystals made by recrystallising single crystals. They also observed that specimen purity affected the formation of cavities and that directional solidification reduced volume changes to below their level of detection. They concluded that grain boundaries or possibly grain boundary diffusion and some form of nucleus were necessary conditions for cavity formation. They found that cavities formed initially near the free surface and argued that the free surface was the ultimate source of vacancies diffusing into the cavities. The apparent activation energy for cavity growth was considerably less than that for bulk diffusion and suggested that grain boundary diffusion controlled the process.

Ratcliffe and Greenwood (1965) performed a series of creep experiments on magnesium in which the stress was changed at times during the test by application of a hydrostatic pressure equal to the stress. Negligible cavitation occurred if the pressure was applied for the duration of the test. Creep rates were not influenced by the pressure, but tertiary creep started earlier in the absence of pressure. The specimen tested under pressure necked to failure while that tested without pressure failed intergranularly with little reduction in area. Density measurements showed that if the pressure was applied during the test, cavity growth ceased, even when large cavities were already present. In experiments in which the pressure

was initially applied and then released, the change in density with further strain parallelled the change for specimens tested without pressure. Ratcliffe and Greenwood (1965) concluded that cavity growth occurred solely by vacancy precipitation and that it was independent of any shear deformation that occurred during creep (at least for their test conditons). However, the measured density changes were proportional to (time) $^{2\cdot5}$, which is significantly greater than the expected value of 1·5 for growth from vacancy condensation on a constant number of cavities. They concluded that nucleation of cavities occurred continuously during the test. Greenwood (1969) extended the argument in the form of a model in which the cavity concentration was proportional to strain, in both primary and secondary creep, and in which the growth rate was constant (valid for widely spaced cavities growing by vacancy condensation (Fig. 10)). This gave a relationship in which the total cavity volume was equal to the product of creep strain and time and independent of the shape of the creep curve.

Ratcliffe and Greenwood (1965) found an approximately linear relationship between the number of observable cavities and creep strain (or time) as did Price (1966) in studies of oxygen-free silver. Intrater and Machlin (1959) also found a nearly linear relationship between cavity concentration and grain boundary sliding in copper bicrystals.

However, Gittins (1967) found that the number of cavities increased as (time)$^{0\cdot5}$, and Oliver and Girifalco (1962) deduced that the number of cavities remained constant during the test. Greenwood (1969) and independently Woodford (1969) showed that Gittins (1967) data were consistent with a linear relationship between the number of cavities and creep strain for both primary and secondary creep. Dyson and McLean (1972) found in Nimonic 80A at 750^{o}C that the

number of cavities increased linearly with strain up to about 0·75 of the creep lifetime and suggested that this may be useful in assessing the remaining lifetime of service components.

In nearly all the work, therefore, the cavity concentration increased with increasing strain and it was concluded that cavity nucleation occurred continuously during creep, presumably as a result of some deformation process. However, Spark (1969) and Evans and Waddington (1969) considered continuous nucleation to be unproven. Evans and Waddington pointed out that optical metallography revealed only those cavities greater than about 1 μm in diameter. They showed that an approximately linear relationship between the number of observable cavities and the creep strain could be derived for the case of a fixed number of cavities, having sizes following a log-normal distribution growing at a uniform rate that was proportional to the grain boundary sliding displacement.

Spark (1969) also considered that continuous nucleation was unproven and developed a model to explain the experimental results without assuming continuous nucleation. If the cavities are unable to minimise their surface energy by surface diffusion, there is no direct relationship between the volume of a cavity and the area it occupies on the grain boundary. Therefore, Spark postulated that the volume increase might be due to grain boundary diffusion but the increase in area of cavitated boundary is determined primarily by strain.

Continuous nucleation of cavities was invoked by Ratcliffe and Greenwood (1965) to explain their observation that in creep, density decrease varied as $(\text{time})^{2\cdot5}$, whereas the Hull and Rimmer model, with a constant number of cavities, gave a power dependence of 1.5. As was mentioned earlier, Ratcliffe and Greenwood favoured growth by vacancy condensation because of their observation that

application of hydrostatic pressure could suppress cavity growth. If all the cavities were nucleated at the beginning of creep life, the discrepancy between measured and predicted growth rates was sufficiently large to invalidate the agreement between the experimental results and the theory.

Some other observations have shown that cavity growth is more dependent on strain or strain rate than on time as would be the case if growth were diffusion controlled. Davies, Davies and Wilshire (1965) studied a series of nickel-cobalt alloys and found that the product of rupture life and creep rate was a constant, independent of cobalt content. In these specimens, fracture occurred by the growth and linking of grain boundary cavities. Since the stress necessary to produce a given creep rate increased appreciably with increasing cobalt content, Davies et al concluded that rupture life and hence the cavity growth rate were independent of stress; a result incompatible with the Hull and Rimmer model. They added that the growth of cavities was not simply diffusion controlled but depended on other plastic deformation mechanisms, grain boundary sliding or dislocation motion. However, they did not investigate whether there were any affects of alloying additions and stress on cavity nucleation. Nevertheless, it does question the general validity of the concept of diffusion-controlled growth and has led to the development of an alternative approach based on deformation-controlled growth.

2. 5. 2.2. Growth of Creep Cracks by deformation processes.

Williams (1967) experimentally determined crack growth rates in a single phase aluminium - 20% zinc alloy as a function of stress and angle between the crack plane and the stress axis. It was shown that for growth normal to the stress axis, the growth rate was proportional to the opening rate of the

wide part of the wedge crack which in turn was found to have an approximately 1:1 correlation with the grain boundary sliding offset resolved parallel to the wedge opening. The crack length increased steadily as sliding occurred and the extent of stable crack growth was controlled by metallurgical features ahead of the crack tip such that if the plastic zone of the crack is restricted, the crack could become unstable and grow to the adjacent triple point. Similar effects can be shown from the data of Soderberg (1969).

Waddington and Williams (1967) studied crack growth and fracture in the single phase aluminium - 20% zinc alloy in the presence of a hydrostatic pressure. Application of a pressure equal to the applied stress increased rupture lives and ductility and reduced the crack density. Waddington and Williams argued that the hydrostatic pressure decreased the crack growth rate. The reduced crack densities were believed to be due to a reduction in the number of cracks that had grown to a visible size, not in the total number of cracks. They argued that pressure reduced the normal stress at the tip of the crack and thereby reduced the growth rate. They did not measure the effect of hydrostatic pressure on grain boundary sliding. They interpreted the occurrence of cracks in the pressurized specimens as evidence that the cracks nucleated by sliding or shear processes rather than by vacancy condensation.

Recently, Needham and Greenwood (1975) have shown evidence that grain boundary sliding was decreased by hydrostatic pressure in tests on copper at 500°C. They confirmed Waddington and Williams' (1967) observation that pressure had no effect in suppressing cavitation but substantially reduced the total volume change that occurred through the formation of cavities. They also found that application of a hydrostatic pressure increased the rupture lives and found that failure time varied as $(\sigma - P)^{-4}$, where σ= tensile stress, and P= hydrostatic pressure.

Another approach to define differences in crack growth mechanism has been the measurement of the angle between cracked boundaries and the stress axis. If shear is the controlling process, the distribution should peak at an angle of 45° and if vacancy condensation is controlling, it should peak at 90°. However, from the simple model proposed by Chang and Grant (1956) (Fig.7), it is clear that varying orientations of cracked boundaries can be produced by grain boundary sliding alone. For example, the optimum angle will vary from about 70° (Fig 7 (a)), about 90° (Fig. 7 (b)) and about 45° (Fig 7 (c)) (Williams (1975)).

Similarly, if the applied stresses are reduced, "r" type cavities have been found to peak at 45° at the higher stresses and at 90°in the lower stress regime, as might be expected (Gittins and Williams (1967)). The angular distribution of cavities has also been studied by Rama Rao, Kutumba Rao and Pandey (1973) who found in a Cr-Ni austenitic stainless steel, that there was a marked shift in the peak from 90° to 45° as the grain size was decreased from 180 to 30μm, suggesting increasing importance of grain boundary sliding. In contrast, they found that the peak of the distribution in Cr-Mn-N steel remained constant around 90° over the grain size range 104 to 10μm suggesting that the distribution in this steel was predominantly governed by cavitation at precipitate/matrix interfaces, since precipitation was a common feature of all specimens irrespective of the grain size. The effect of grain size on cracking has also been studied by Fleck, Beevers and Taplin (1975) in a copper-based alloy. They found that decreasing the grain size increased the contribution of grain boundary sliding to total deformation and thus resulted in increased cavitation. They found that for grain sizes of less than 100μm, failure occurred by void formation and

subsequent interlinkage. For large grain size material, fracture was controlled by the length of the longest crack such that failure occurred when it reached a certain critical length.

Davies, Williams and Wilshire (1968) have studied the orientation distribution of cracked boundaries and found that it did not depend on creep rate over a strain rate range of nearly three orders of magnitude. In all cases, the cavities were located preferentially on boundaries at 90° to the stress axis. By compressing the specimens at the test temperature prior to creep testing, they showed a large increase in the frequency of cavities on boundaries at 45° to the stress axis. They interpreted this as additional cavity nucleation that occurred at jogs or ledges formed by the compressive strain. Johanneson and Tholin (1969) found cavities in copper and steel located preferentially on boundaries nearly normal to the stress. However, cavity growth rates were much too large to be explained by the Hull and Rimmer model, and they suggested that deformation processes must play a prominent role in cavity growth.

Much work has been performed to try and clarify the role played by deformation processes, mainly grain boundary sliding, on the cavity growth process. Davies and Wilshire (1965) tested nickel - 1% palladium and copper - 15% aluminium alloys to the beginning of tertiary creep, reversed the direction for an equal time, and then returned to tension until fracture occurred. The specimens failed in the same time as they would have had the compressive stage not occurred. Davies and Wilshire then argued that this occurred because the cavities did not sinter under compression as would be expected if the Hull and Rimmer mechanism was operative, but that growth had occurred by grain boundary sliding that could not

be reversed. However, Gittins (1967) showed that gases may diffuse into cavities to prevent or retard their sintering.

Davies and Dutton (1966) performed a series of experiments on changing the direction of stress in a copper - 15·4% aluminium alloy in the sequence shown in Fig. 11. Initially, they strained a specimen in tension to the tertiary creep stage in which the grain boundary sliding occurred as shown in Fig. 11(a). They then cut a cube from the specimen and tested it in compression (Fig. 11 (b)). They found that many of the cavities closed and much of the density decrease was recovered. They then took a second cube from the tensile specimen which they tested in compression, applying the stress at 90° to the direction chosen previously. This produced sliding as shown in Fig 11 (c), which was equivalent to the original tensile condition. Continued cavity growth was found, and they concluded that diffusional processes were unimportant and that under these conditions only sliding contributed to cavity growth.

Taplin and Gifkins (1967) criticised this type of experiment since void closure due to sintering could explain these results. Gittins (1967) had also found that sintering can occur on reversed stressing at room temperature. In response to these comments, Davies and Williams (1969a) repeated the experiment with copper and obtained essentially the same result. In addition, they performed some compression tests at room temperature on specimens containing cavities and found essentially no shrinkage.

Davies and Williams (1969 b) argued strongly in favour of cavity growth by grain boundary sliding by pointing out that growth controlled by the diffusion of vacancies could not explain the general observation that rupture life is inversely proportional to secondary creep rate. They proposed a model for cavity formation based on dislocation motion and grain boundary sliding as shown

FIG. 11 Sequence of stressing operations used by Davies and Dutton (1966). Grain boundary is designated X-X.

in Fig 12. In this model, slip dislocations entering a grain boundary form jogs which are opened into cavities by sliding (Figs. 12(a) and 12(b)). Continued slip and sliding finally opens the cavity to the form shown in Fig. 12 (c).

Applying Ishida and McLean's (1967) suggestion that grain boundary sliding occurs by the glide and climb of slip dislocations along a grain boundary, Davies and Williams proposed that when a dislocation enters a cavity on a boundary, the component of the Burger's vector normal to the boundary widens the cavity and the component parallel to the boundary lengthens it. Surface diffusion of atoms occurs simultaneously to attempt to change the shape of the cavity to minimise surface energy. This model is only qualitative, but it does have the advantage over the diffusion-controlled growth model of being able to explain the relationship between cavity size and total creep strain.

Various problems arise in the use of metallographic observations to allow distinction between the diffusion and deformation controlled growth models. Optical microscopy techniques simply do not have the resolution necessary to provide specific information on the shapes and locations of cavities. Transmission electron microscopy suffers from the disadvantage that foils must be thinner than a few tenths of a micron to obtain adequate transmission and any cavities must be smaller than this to be contained within the foil. Taplin and Barker (1966) devised a shadowgraphic technique in which thick, non-transparent foils were examined. Large cavities within these thick foils were often transparent to electrons and could be examined. However, such cavities were usually exposed to the polishing solution, at least on one side, and may have been distorted and enlarged during preparation of the electron microscopy specimens. In addition, Cocks

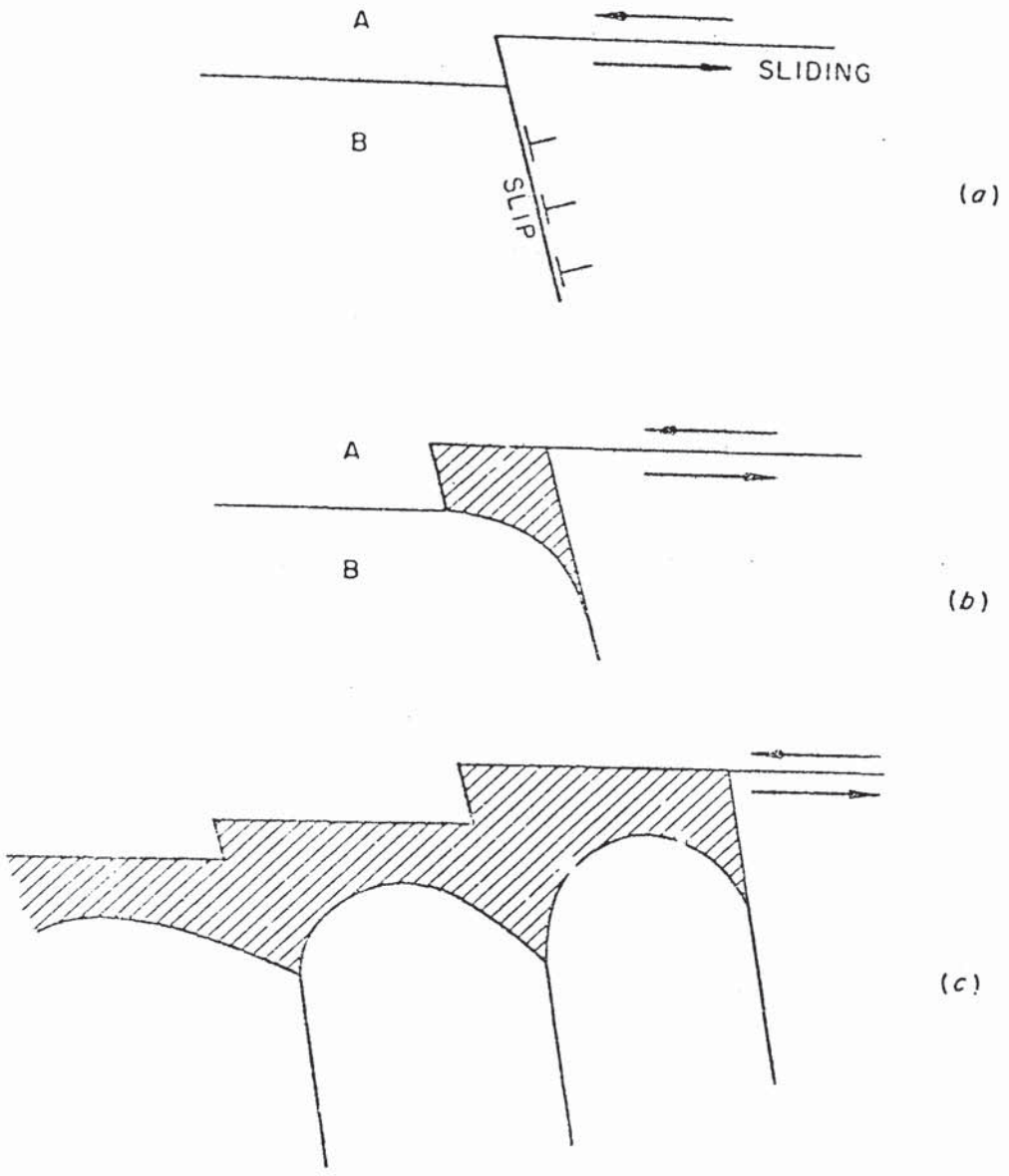

FIG. 12 Schematic illustration of the formation of creep cavities by the combination of grain boundary sliding and crystal slip.

and Taplin (1967) later showed that the shape of a cavity examined by this technique depended critically on its orientation to the electron beam. They demonstrated that an apparently equiaxed cavity can appear elongated with sharp ends if the foil is tilted through a relatively small angle. The shadowgraphic technique is also limited by inability to supply information on the structural features of the grains and grain boundaries adjacent to the cavity.

Electron fractography offers the possibility of overcoming many of these disadvantages. The techniques of fractography and scanning electron microscopy have proved to be well suited to the assessment of cavity shape, size and distribution, particularly if the material is brittle at room temperature and below. Creep specimens can then be broken open to expose cavities formed at elevated temperatures. This technique has been applied to the study of creep cavities in various materials (Wingrove and Taplin (1969); Davies and Williams (1969); Stiegler, Farrell, Loh and McCoy (1967); Summerling and Hyam (1961); Cane and Greenwood (1975)). However, the scanning electron microscope is unable to reveal features of the lattice structure that may be relevant to cavity nucleation. It is in this area that the 1 MeV transmission electron microscope is of use.

The fractographic studies show that in general, creep cavities seem to be equiaxed and polyhedral in materials tested at elevated temperatures and low stresses, and flat and irregularly or dendritically shaped at lower temperatures or higher stresses.

The mechanisms proposed to account for the nucleation and growth of r- and w-type cracks have evolved independently of one another, so that when combined to give an overall picture of the fracture process, they contain a number of inconsistencies. For example, both r - and w - type cracks are generally believed to originate from stress concentrations produced by grain boundary sliding.

Why they are observed at triple points at higher stresses and on two-grain interfaces is not clear. If jogs and other irregularities are able to nucleate cavities in specimens tested at low stresses, why are these sites apparently ineffective at high stresses?

It is apparent from the literature that no single mechanism is applicable to all creep cracking. Indeed, the work discussed here suggests that several mechanisms may operate and each may become dominant at different stages of the creep life.

2.6 The Effect of Nuclear Reactor Environment on Creep Rupture.

2.6. 1 Irradiation Embrittlement.

It has been widely observed that neutron irradiation causes high temperature embrittlement of various metals. Amongst these are austenitic steels and nickel-based alloys and because of their technological importance, considerable research has been undertaken to establish the mechanisms of embrittlement and thus to show how the irradiation effects the microscopic fracture processes for unirradiated materials discussed in section 2.5.

The magnitude of the high temperature embrittlement has been found to be sensitive to alloy composition and structure, test temperature, strain rate, and irradiation conditions (for instance, Harries (1966); Bloom (1972); Steigler and Weir (1967); Holmes, Lovell and Fish (1973); and Waddington and Lofthouse (1967)).

Metallographic examination of irradiated materials strained at high temperature shows that intergranular fracture occurs and the cracks have similar morphologies to those in unirradiated materials. For example, at lower temperature and higher stresses, wedge cracks are formed and at higher temperatures and lower stresses, cavitation is observed. Bloom (1972) has divided the deformation and fracture behaviour of austenitic steels into 3 regions of irradiation

and test temperature (Fig. 13). For lower irradiation temperatures, Region I, metallographic examination of failed specimens shows that the cracks near the fracture extend over several grain facets. Creep curves of 316 stainless steel irradiated to high fast neutron doses in this region exhibit little or no tertiary creep suggesting very rapid crack growth. In region II, the ductility is greater and significant tertiary creep occurs. The cracks are wedge shaped and extend over about one grain facet. In Region III, above about 650°C, little tertiary is observed and extensive cavitation is observed on nearly all grain boundaries which are perpendicular to the stress axis.

Harries (1966) showed that thermal neutrons can be responsible for the detrimental effects of irradiation on the high temperature properties by a transmutation reaction with the boron in the steel. Natural boron contains about 18·8% of the boron - 10 isotope, the remainder being boron - 11. The reaction between the boron - 10 and the thermal neutrons produces helium and lithium:-

$$_{5}B^{10} + {}_{o}n^{1} \rightarrow {}_{2}He^{4} + {}_{3}Li^{7} \qquad (26)$$

This production of helium by irradiating with neutrons is an example of an (n,α) reaction.

Martin, Weir, McDonald and Franklin (1965) showed that at very low concentrations of boron in 304 stainless steel, the contribution of helium from (n,α) reactions between fast neutrons and Fe, Ni and other constituents of the alloy was also important. The most important of these fast neutron (n,α) reactions is the two stage reaction starting from nickel:- (Birss and Ellis (1971)

$$_{28}Ni^{58} + {}_{o}n^{1} \rightarrow {}_{28}Ni^{59} + \gamma \qquad (27a)$$

$$_{28}Ni^{59} + {}_{o}n^{1} \rightarrow {}_{26}Fe^{56} + {}_{2}He^{4} \qquad (27b)$$

FIG 13 Variation in fracture mode in annealed austenitic stainless steels with irradiation and test temperature(from Bloom (1972))

The helium produced has a very low solubility in the metal lattice (estimated to be less than 10^{-9} at 700°C and 1 atmosphere pressure (Steigler and Weir (1967)) and precipitates to form bubbles. The distribution of the helium produced by thermal neutrons is largely determined by the distribution of the boron, since the helium recoil range is about 2 μm. Boron segregation to grain boundaries is frequently observed (for instance William, Harries and Furnival (1972), Elen, Van Witzenburg, de Vries and Glas (1972)) and thus greater numbers of helium bubbles are observed at the grain boundaries. This increased concentration also results from the migration of bubbles from the matrix into the grain boundary. In the absence of a driving force, the bubbles will migrate randomly until they reach obstacles or collide with other bubbles, coalescing to form bubbles too large to diffuse further. At low helium concentrations, the collisions will be rare so that the bubbles may reach the grain boundaries where they will be held because of a reduction in the total energy. Any subsequent movement will be confined to the plane of the grain boundary where the probability of bubbles colliding is greater and further growth occurs by coalescence or absorption of additional helium atoms. Generally, helium bubbles are subjected to driving forces provided by stress and temperature gradients. Harries (1966) showed that if migration occurred by surface diffusion then very small bubbles would move rapidly under the action of the driving force, but the bubbles would virtually cease to move as they became larger.

In the early stages of bubble growth, the bubble radius, r_o, is regulated by the equilibrium between internal pressure, P_o, and the surface tension, γ. In the absence of a stress, removal of an atom from the surface of a bubble increases the surface energy,

$(\frac{2\gamma}{r_o})\ \Omega$, where Ω is the atomic volume, and does work, $P_o\Omega$, in expanding the gas. Equilibrium exists when these terms are equal:-

$$P_o = \frac{2\gamma}{r_o} \qquad (28)$$

For bubbles situated on grain boundaries perpendicular to the stress, σ, additional work, $\sigma\ \Omega$, is done in transferring an atom from the bubble to the grain boundary. The equilibrium condition becomes:-

$$(\sigma + P) = \frac{2\gamma}{r} \qquad (29)$$

where $P < P_o$ and $r > r_o$. Assuming ideal gas behaviour, Hyam and Sumner (1962) showed that the stress in equilibrium with a bubble of radius r is given by:-

$$\sigma = \frac{2\gamma}{r}\left[1 - (\frac{ro}{r})^2\right] \qquad (30)$$

This function has a maximum at a critical stress, σ_c, equal to $0{\cdot}77\ (\frac{\gamma}{r_o})$. If the applied stress is below this value, the bubble will grow to a new equilibrium radius. If the stress is maintained above σ_c, the bubble will continue to grow, unable to attain equilibrium, with the growth rate controlled by vacancy diffusion.

The presence of these grain boundary helium bubbles will clearly have a marked effect upon the nucleation and growth of grain boundary cracks. The different crack morphologies found in irradiated stainless steel suggest that different mechanisms are operating under different conditions of stress and temperature, in a similar way to those discussed for unirradiated material.

Bloom and Steigler (1970) suggested that embrittlement at high temperature can result from stress-induced growth of grain boundary helium bubbles which subsequently interlink to cause failure. They suggested that the cavity nuclei are the grain boundary helium bubbles and growth occurs by vacancy condensation. They modified

the Speight and Harris equation (equation (25)) to account for the internal helium gas pressure to give:-

$$\frac{dr}{dt} \simeq \frac{z\, Dg\, \Omega}{2\, K\, T\, r} \frac{(\sigma + P - \frac{2\gamma}{r})}{\left[\ln\left(\frac{\eta}{2r}\right) - \frac{\eta^2 - 4r^2}{2\eta^2} \right]} \left[\frac{1}{r} - \frac{4r}{\eta^2} \right] \qquad (31)$$

By inserting suitable numerical values into this equation, Bloom and Steigler found that the growth rates were sufficiently fast to account for the cavities observed on the grain boundaries, despite the short-comings of the Speight and Harris equation discussed previously.

Steigler and Weir (1967) and Reiff (1972) have considered the growth of wedge cracks and suggested that the cracks can be easily nucleated by inhomogeneous bubble distributions particularly chains of bubbles along triple points. These wedge cracks will be filled with gas (Reiff (1972)). Such cracks can grow in the same manner as in unirradiated material. Thus the effect of the bubbles is simply to nucleate the cracks with little prior strain or increase the rate of propagation by expansion of sub-critical size bubbles by the stress concentration ahead of the crack. Therefore, it appears likely that gas bubbles enhance both the nucleation and growth of cracks.

Bloom (1972) applied these mechanisms to explain the various crack morphologies in Regions I, II and III of Fig. 13. In Region I, the temperature is sufficiently low for the point defects produced by fast neutrons to persist. The matrix flow stress is increased and results in deformation being localised at grain boundaries that because of helium embrittlement are less able to withstand shear than before irradiation. Thus, the embrittlement is more severe than if the helium embrittlement had occurred alone. Under these conditions, cracks grow in a stable manner along several grain facets until they reach

a critical size. Then unstable propagation along grain boundaries leads to rapid failure. The mechanism of stable growth is not clearly understood. Bloom (1972) suggests that the crack tip stress concentration may cause enhanced cavity growth compared with cavities on uncracked boundaries.

With increasing irradiation temperature (Region II), the matrix hardening decreases and wedge type cracking is observed. This is caused by helium embrittlement alone.

Region III results from the stress-induced growth of grain boundary helium bubbles.

The conclusions of Bloom (1972) and also Bloom and Weir (1968) were based on fast neutron irradiation of 316 stainless steel to a dose of $1 - 3 \times 10^{22}$ n/cm^2. Holmes, Lovell and Fish(1973) have arrived at similar mechanisms of intergranular fracture but they considered a wider range of dose (i.e. $2 \times 10^{21} - 7 \times 10^{22}$ n/cm^2). Fig. 14 shows a schematic representation of the various mechanisms operating as a function of temperature and neutron dose. It can be seen that this figure extends the work of Bloom and shows that the operative mechanisms are also neutron dose dependant. For example, at 650°C. significant ductility loss occurs at fast neutron doses of less than 5×10^{21} n/cm^2. This dose is sufficiently low that no appreciable matrix hardening has occurred. Therefore, this early ductility loss is attributed to helium embrittlement alone. However, for doses beyond about 2×10^{22} n/cm^2 sufficient matrix hardening develops to amplify the helium embrittlement. Since no low dose ductility loss was found at 540°C., matrix hardening probably dominates failure at all doses at this temperature. At 760°C., helium embrittlement alone controls the ductility loss since no irradiation hardening occurs.

FIG. 14 Various embrittlement processes in AISI type 316 stainless steel as a function of temperature and neutron dose. (from Holmes, Lovell and Fish (1973))

Kangilaski, Perrin and Wullaert (1969) have suggested an alternative mechanism for embrittlement in type 347 stainless steel, irradiated to $2{\cdot}1 \times 10^{22}$ n/cm^2. They observed that after long-term irradiation, transmutation reactions had produced significant amounts of copper, vanadium and zinc whilst the manganese content had fallen. They suggested that the embrittlement was caused by segregation of these products to the grain boundaries preventing grain boundary migration. Helium bubbles at the grain boundaries were not thought to be the main cause of embrittlement. However, the importance and exact role of solid transmutation products in other steels after differing irradiation conditions is still uncertain.

The extensive study of irradiation embrittlement mechanisms has resulted in methods being proposed to reduce or even prevent the embrittlement. Martin and Weir (1967) showed that post-irradiation ductilities can be increased by reducing the boron content from a few parts per million to 0·1 ppm. However, for fast reactor applications this would be of little use due to the production of helium by other (n, α) reactions.

Another method of reducing the boron available for transmutation is to form stable borides within the matrix by the addition of Group IVA elements (Titanium, Zirconium Hafnium) to the steel (Bloom and Weir (1972)).

Other suggestions (summarised by Harries (1966)) include retention of the helium bubbles within the grains by producing stable intragranular precipitates with suitable interfacial energies to trap helium bubbles. McLean (1957) has shown that the stress necessary to produce an intergranular crack is proportional to $(2\gamma_s - \gamma_{gb})$ where γ_s is the surface energy and γ_{gb} is the grain boundary energy. Thus, the addition or removal of elements to alter γ_s or γ_{gb} such that the nett effect is an increase in $(2\gamma_s - \gamma_{gb})$ would make grain boundary

fracture more difficult. It has been suggested by Kramer, Garr, Rhodes and Pard (1972) that a grain boundary heavily decorated with precipitates is unable to slide and hence the nucleation and growth of creep cracks is impaired. Harris (1973) has shown that the presence of intergranular precipitates prevented the boundary from acting as a vacancy source, thereby inhibiting void growth, and this may be the dominant effect of the grain boundary precipitates. The presence of these precipitates could act as pegs in the boundary preventing void growth by vacancy condensation and the concomitant plating out of atoms along the boundary. Harris (1975) has developed this idea and has proposed a model enabling an estimate to be made of the size and distribution of precipitates necessary to inhibit the growth of gas bubbles and thus prevent them from developing into creep cavities.

2. 6. 2. Fission product attack.

Although irradiation effects and cladding/coolant compatibility have been studied extensively, the additional effect of chemical interaction between fission products and cladding on cladding integrity has received much less attention. Post-irradiation examination of fuel pins from a number of reactor systems has revealed the formation of reaction products at the inner clad surface and intergranular penetration extending from the inner clad surface (e.g. Johnson, Crouthamel, Chen and Blackburn (1969); Garlick (1971); Hilton and Robins (1973); Batey and Bagley (1974)). The principal reactive fission products have been identified as caesium or its precursor iodine, tellurium and molybdenum (Johnson and Crouthamel (1970)). A comprehensive review of fuel/clad reactions has recently been made by Robins (1974).

The effect of iodine vapour on the fracture behaviour of unirradiated zirconium alloys has been studied by Rosenbaum (1966), Garlick and Wolfenden (1971), Garlick (1973), Wood (1973, 1974) who found that the alloys were susceptible to embrittlement at elevated temperatures (up to 300°C.) by transgranular stress corrosion cracking. Cox and Wood (1975) summarised the available evidence and showed that cold work and irradiation hardening increased the susceptibility to stress corrosion cracking but other factors such as surface oxide conditions, crystallographic texture, and residual stress could also have appreciable effects.

The effect of iodine and tellurium on the creep rupture properties of unirradiated 20/25/Nb stainless steel at 750°C. was investigated by Lobb and Jones (1973). They found that both iodine and tellurium vapours promoted surface nucleated intergranular cracking which significantly reduced the specimen rupture life and strain to failure compared with tests in vacuum. However, a stress corrosion

mechanism was not thought to be operative in this case. Lobb and Jones attributed the embrittlement to a selective corrosion process forming small surface grain boundary cracks in all parts of the creep specimens. In the stressed gauge length, these cracks propagated into the specimen reducing the cross-sectional area. Final failure occurred when the load bearing area had reduced and the stress had increased to the level for rapid shear. The mode of selective attack suggested by Lobb and Jones involved iodide formation (Fe I_2, Ni I_2 and Cr I_2). The accompanying compositional and structural changes in the metal beneath the scale could produce enhanced intergranular penetration.

Ring, Busboon and Spalaris (1972) have performed short term tube burst tests on several irradiated 316 and 304L stainless steel fuel pins which had suffered from intergranular attack from fission products. The results indicated that although ductility is sharply reduced due to the intergranular attack, rupture strength properties were higher than anticipated using a calculation allowing for the reduction in wall thickness due to the intergranular attack. However, these tests were performed in the absence of fission products and were of short duration so that any time dependent corrosion processes would not be observed.

There is a clear need for further investigation of the effect of fission products attack on the mechanical properties of austenitic steels.

Steel	Batch	C	Mn	Si	S	P	Ni	Cr	Mo	B	N	Nb	Fe
A.I.S.I. type 316 Stainless Steel	1	·06	1·79	·51	·018	·023	11·72	17·82	2·76	*	*	*	Bal.
M 316 Stainless Steel	1	·051	1·81	·40	·009	·008	13·69	16·79	2·43	·0018	·04	*	Bal
20Cr/25Ni/Nb Stainless Steel	1	·030	*	*	*	*	25	20	*	·0009	·02	·62	Bal
	2	·040	·54	·72	·005	·003	24·39	19·67	*	·0024	·01	·63	al

TABLE 4 Composition of Stainless Steels

(* Not analysed)

CHAPTER 3.

EXPERIMENTAL

3.1. Specimen Preparations

3. 1.1 Materials and Heat Treatment.

Tests were performed on the stainless steels shown in Table 4, which also shows their compositions.

The type 316 stainless steel was initially 20% cold worked and was in the form of 50 mm x 0·74 mm strip. Specimens were either punched or machined from the strip to the dimensions given in section 3. 1.2. The M316 steel specimens were punched from 0·5 mm thick 20% cold worked strip supplied by the United Kingdom Atomic Energy Authority from P.F.R. stock. The 20Cr/25Ni/Nb steel specimens were produced from C.A.G.R. plain drawn cladding tubes of 15·84 mm outside diameter and 0·67 mm wall thickness. The tubes were split longitudinally and each semicircular segment was rolled flat to produce 0·67 mm thick strip. The specimens were then punched from the strip.

The specimens were deburred, some were notched as described in section 3. 1.2, degreased and sealed in silica capsules evacuated to better than 0·013 μbar. The heat treatments given to the specimens were according to Table 5:-

Table 5.

Steel	Heat Treatment	Linear Intercept Grain Size.
A.I.S.I. type 316 stainless steel.	Solution treatment (1 hr. at 1050°C) Air cool	33 μm
M316 Stainless Steel	Solution treatment (1 hr. at 1050°C) Air cool	38 μm
20Cr/25Ni/Nb Stainless Steel	Primary Recrystallisation (930°C for 1 hr.) Water quench.	17 μm(Batch 1) 17 μm(Batch 2)

Temperature was controlled to ± 1°C. of the values shown in Table 5. Also shown are the mean linear intercept grain sizes resulting from the heat treatments. The silica capsule containing the 20Cr/25Ni/Nb steel specimens shattered on entering the water, but the capsules containing the other specimens had to be broken after cooling.

3. 1.2. Specimen Dimensions

Most of the specimens tested were shaped like the strip tensile specimen shown in Fig. 15. The actual specimen sizes are given in Table 6.

The large type 316 steel specimens were milled from the strip whilst all the others were punched. Some of the specimens had notches machined into them using a circular slitting saw, 0·1 mm thick. The resulting notches had u-shaped roots and were about 0·14 mm wide with lengths depending upon the size of specimen, but in the range 0·08 to 0·14 $(\frac{a_o}{W})$, where a_o = length of the starter notch, W = specimen width (dimension F in Fig. 15). The specimens were either single or double edge notched with a maximum variation in notch length for a given specimen size of 0·013 mm.

Some large notched centre hole specimens were also milled from the 316 strip, the dimensions of which are given in Fig. 16. The centre notches were introduced by spark machining and were the same width and had similar notch roots to the machined defects. One specimen was made with the central hole 12·75 mm. diameter and with starter notches of 1 mm.

Some specimens, 10 mm wide x 0·74 mm thick and 150 mm long, were also milled from the 316 stainless steel strip and double edge notches, 0·7 mm deep, were cut in the middle of the specimen. A large head was not required for these specimens since they were

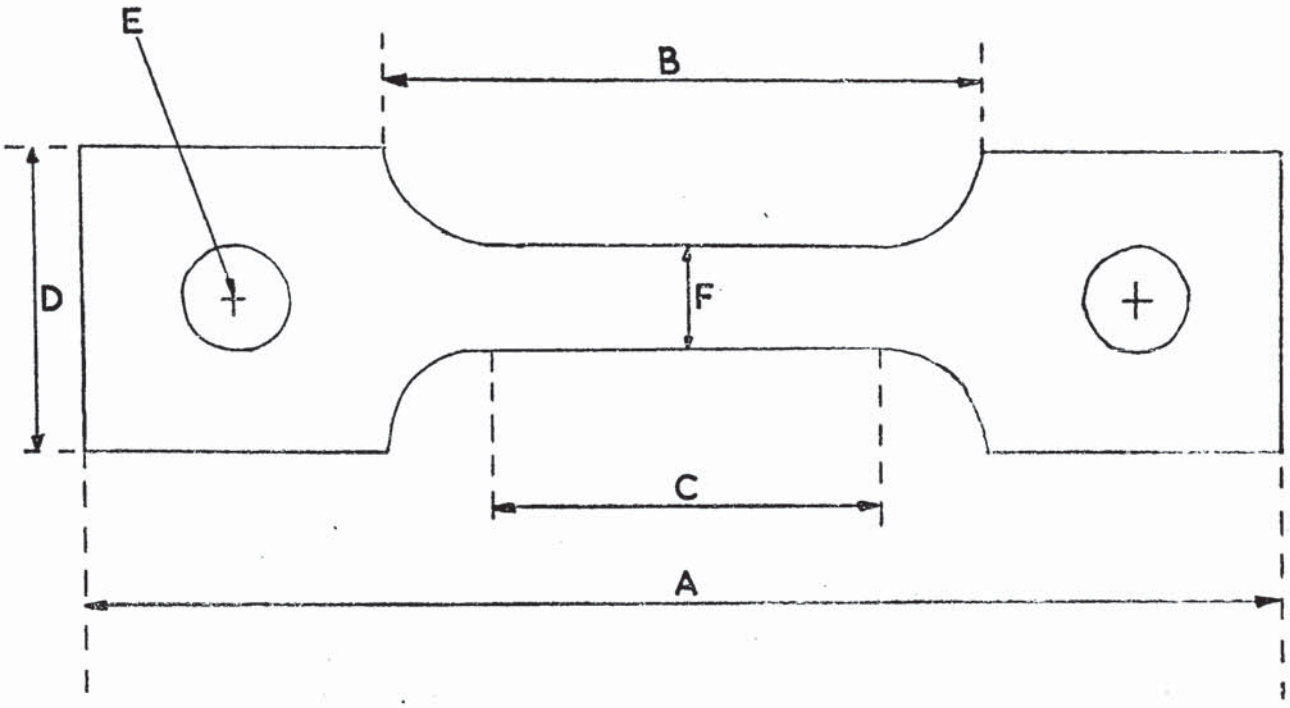

FIG 15 Typical strip tensile specimen

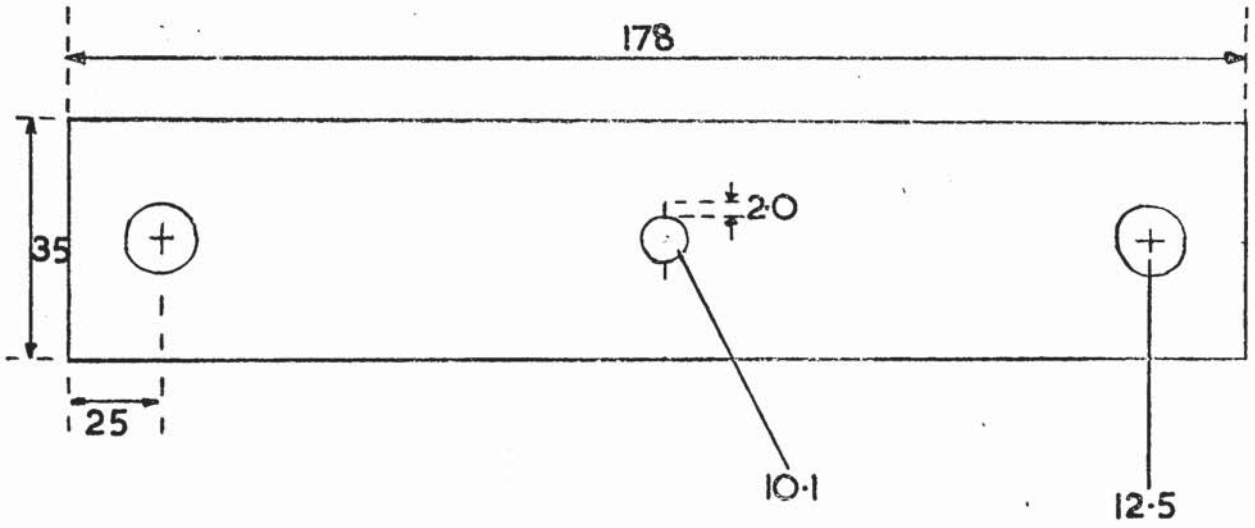

FIG 16 Dimensions (in mm.) of notched centre hole specimens.

Material	A	B	C	D	E	F	
A.I.S.I. type 316 steel	76 178	39 76·4	25 50	19 44	8 12·5	6·3 15·9	(Small specimen) (large specimen)
M 316	53·3	25	20·3	11·5	4·8	4·2	
20Cr/25Ni/Nb steel	76	39	25	19	8	6·3	

TABLE 6. Actual Dimensions (mm) of specimens

to be gripped over a large area by wedge-type grips, rather than be pin loaded like the other specimens. The specimens were polished to a 6 μm diamond finish and parallel lines (approximately 0·1 mm apart) were then scribed across the surface in the region of the notches using a vernier marking gauge.

3.2. Creep Rupture Testing

Prior to testing, the specimen dimensions were measured using a travelling microscope and the specimen thickness was obtained from several measurements using a micrometer.

Four types of creep rig were used for the tests depending upon the testing environment.

Constant load cantilever beam Denison rigs were used for air tests. Displacement measurements were obtained from changes in the position of the beam using dial gauges which were calibrated to show the movement along the line of the specimen rather than the amplified deflections of the beam. The specimen extensions were measured with a sensitivity of 2·5 μm. No corrections were made for changes in specimen compliance as cracks propagated from the notches because this was a negligible source of error. The temperature was controlled to within $\pm$ 1°C. of the required temperature using a Eurotherm controller and by having the control thermocouple close to the furnace windings. A second thermocouple was always positioned beside the specimen and the output from this thermocouple was recorded continuously. The input to each of the 3 furnace windings could be controlled to give a constant temperature zone about 25 mm long in the middle of the furnace. Generally, the specimens were heated to the test temperature in about one hour and were then left for about three hours for the temperature to equilibrate. The load was then applied as quickly as possible (in less than 30 seconds) and the test was defined as starting once the desired load was attained.

For other environments (e.g. vacuum, Iodine vapour), the rigs were of a different design with the constant load applied directly to the bottom stainless steel pull rod and with the specimen and pull rods enclosed by a silica tube (Fig. 17(a) shows the rig used for vacuum tests). The bottom pull rod, connecting the specimen and the weights, emerged from the silica tube through a double "O" ring sliding seal. Displacement of the bottom pull rod was monitored continuously using linear variable differential transformer (LVDT) transducers connected to a data logger. For iodine vapour environments, the silica tube was evacuated by rotary and diffusion pumps to better than 0·13 μbar. The pumps were then isolated and the tap connecting the side-arm of the silica tube was opened to introduce iodine vapour (Fig.17(b)). The start of the test was defined as the time when this operation was completed. For vacuum tests, the pressure was measured at the top of the silica tube (the point furthest from the specimen and diffusion pump) during the tests was about 0·03 μbar. Loading of these rigs was achieved by using a hydraulic jack to support the weight whilst the specimen was being heated up and then the jack was slowly lowered until the weights were supported by the specimen.

For tests in vacuum on irradiated specimens, a very similar rig was used but a stainless steel tube replaced the silica tube and the rig was surrounded by 75 mm thick lead bricks. No problems with radioactive contamination were encountered during these tests.

The fourth type of rig used was a modified Hounsfield tensometer giving constant cross-head displacement rates. Fig. 18 shows a view of the apparatus with a vacuum chamber located in the modified Hounsfield tensometer, surmounted by a microscope and cine camera which were positioned above a viewing window in the vacuum chamber. The vacuum chamber incorporated water jackets around the

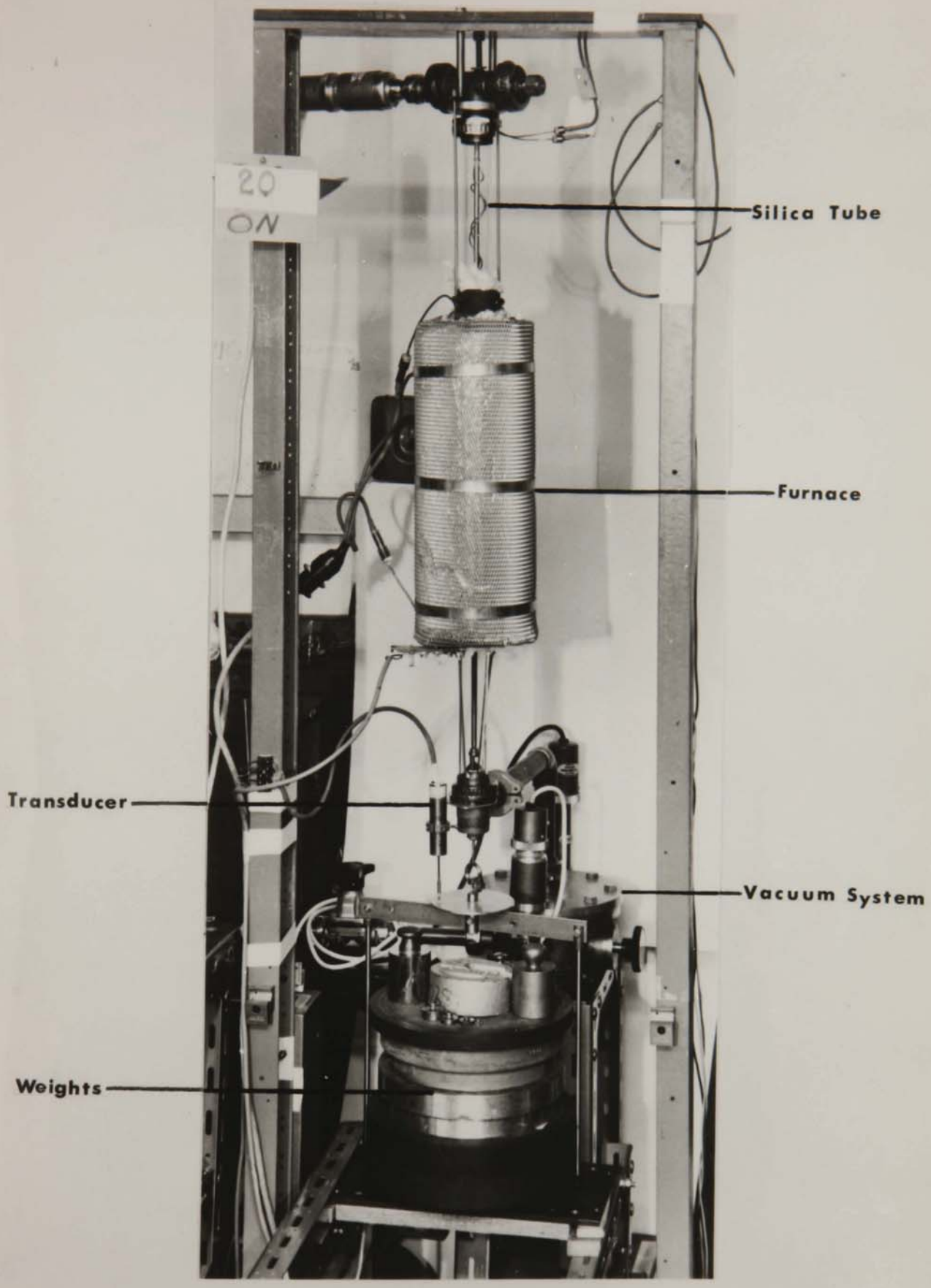

FIG 17(a) Creep rig used for vacuum tests

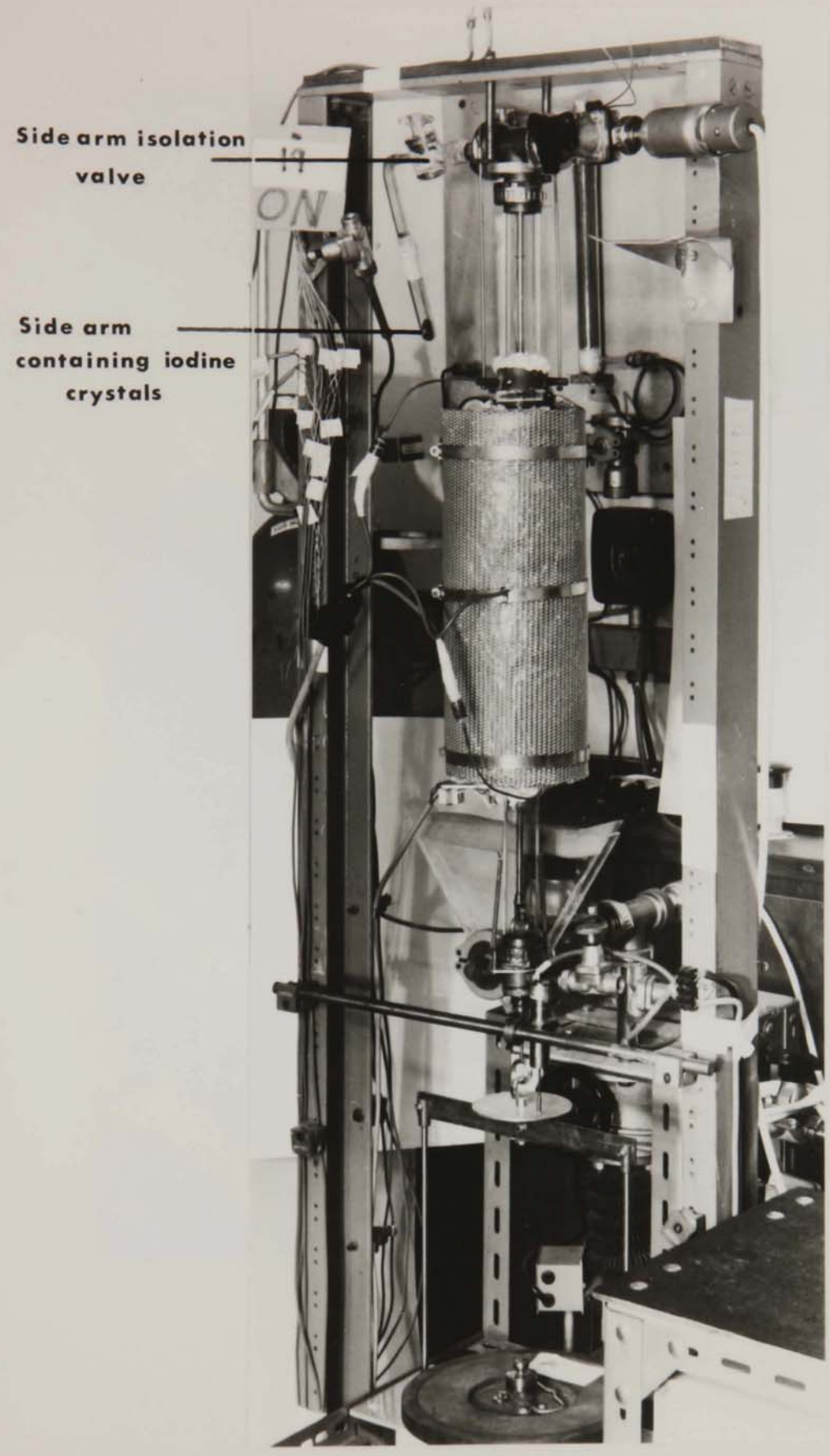

FIG 17(b) Creep rig used for tests in iodine vapour

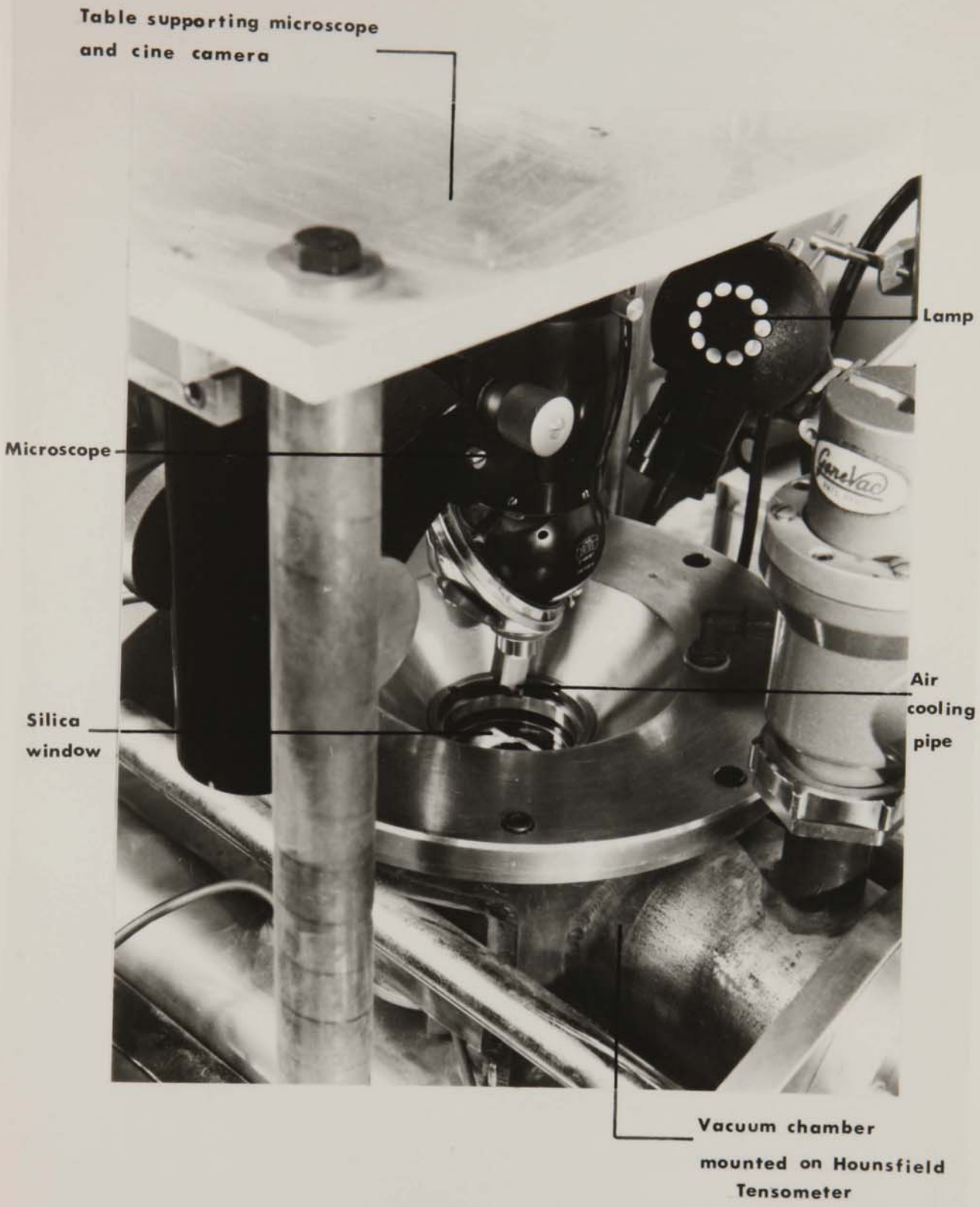

FIG 18 Modified Hounsfield Tensometer

"O" ring locations and bonded inserts in the wall, to provide insulated, vacuum tight seals around the furnace and thermocouple leads. The viewing window was made from optically flat silica. The furnace consisted of a fused alumina cylinder with a circular viewing port wound with 87/13 platinum-rhodium wire and surrounded by tantalum heat shields. Heating and cooling were rapid and the temperature variation over a 25 mm gauge length was less than 5^{o}C. at 750^{o}C. in vacuo despite the unheated opening over part of the specimen.

A standard Zeiss microscope was inverted on its stand so that the base of the support column could be mounted on the underside of the table straddling the vacuum chamber (Fig. 18). The microscope could be moved relative to the frame of the table and therefore to the specimen by slides moving at right angles to one another. A long focus objective lens was used. A Vinten Mark III 16 mm. scientific cine camera was used which can be automatically controlled to give single shots at preset intervals.

Various constant cross-head displacement rates were produced by an electric motor driving through a series of gears. In the other rigs, the specimens were pin loaded but wedge-type grips were used in the modified Hounsfield tensometer.

3.3. Measurement of Creep Crack growth rates.

3. 3.1. D.C. Potential Drop Method.

Initially the technique used to monitor crack growth in specimens in air was the D.C. potential drop method (Gilbey and Pearson (1966)). The method involves passing a constant direct electric current through a notched specimen of rectangular cross-section and comparing the potential measured between points either side of the notch (V_c) with the potential over unit length of uncracked material (V_o) (Fig.19). For a given specimen geometry, as the crack grows the cross-section of the specimen is reduced and its resistance

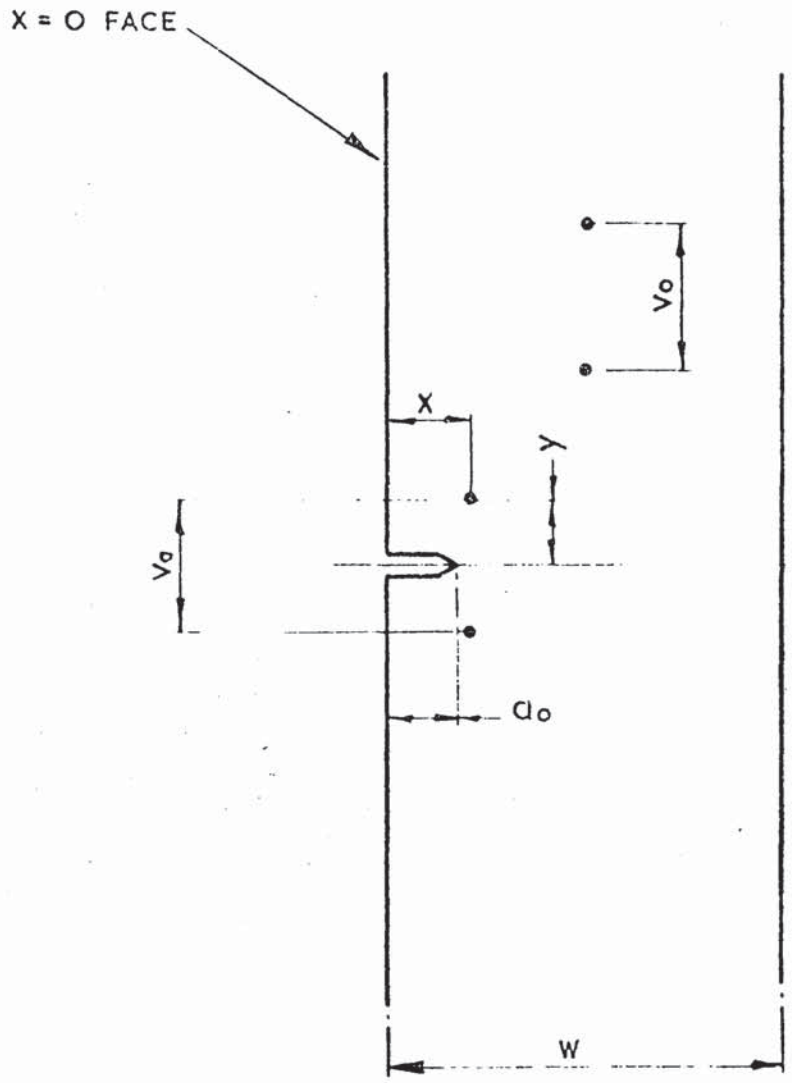

FIG. 19 SCHEMATIC DRAWING SHOWING THE POSITION OF THE Va AND Vo LEADS.

increases causing an increase in V_a. V_a is measured by spot welding wires either side of the notch at positions $(x \pm y)$ in Fig. 19. The initial value of V_a is determined by the exact positioning of the leads. The V_o leads are spot welded along the centre line of the specimen well away from the notch. The current is introduced into the specimen by spot welding strip contacts to the specimen at either end of the gauge length. If V_a is monitored throughout the test, the growth of the crack can be ascertained from suitable calibration curves relating potential increase to crack length. Gilbey and Pearson (1966) have produced calibration curves of $(\frac{V_a}{V_o W})$ versus $(\frac{a}{W})$, where W = specimen width and a = crack length, for single edge notched specimens and, by symmetry, in centre notched plate specimens, for differing positions of the V_a potential leads (i.e. different x and y co-ordinates in Fig. 19).

For the notched centre hole specimens tested here, it was necessary to generate new calibration curves. This was done by making full size specimens (as in Fig. 16) from aluminium foil glued to cardboard for support. Probes to measure V_a and V_o were positioned along the centre line of the specimen.

To monitor crack growth in the large single edge notched and notched centre hole specimens of type 316 steel, the potential leads were 0·35 mm nichrome wire enclosed in alumina beads. The thermal E.M.F.'s generated between the nichrome wire and the stainless steel were negligible. The current leads consisted of several 0·5 mm diameter nickel wires twisted together and enclosed by alumina insulators. A constant current of 10 amps was used in all tests and the potential was measured with a sensitivity of 10 μv.

Although the electrical potential method has the advantage of being relatively cheap and of giving a continuous record,

there are a number of high temperature situations where its use is either difficult or impossible, such as in neutron irradiated specimens or specimens in closely controlled reactive environments such as liquid sodium or corrosive vapours. Therefore, the Notch Region Extension Method described below was developed primarily for these applications.

3. 3.2. The Notch Region Extension (NRE) Method.

For a single edge notched specimen in a tensile creep rupture test, at the beginning of the test, time t_o, the starter notch has a width w_o and a length a_o, as shown in figure 20(a). During the test, the notch strains open and at time t_i and notch opening displacement w_i, cracking initiates from the notch, figure 20 (b). At time t_1, the creep crack length will be a_1. Clearly, the extension in the notched region, as defined by the dotted lines in figure 20 (c), is $(x_1 + y_1) - w_o$. As the crack length increases, the fracture surface behind the crack tip remains effectively 'frozen' into the shape it adopted when fracturing, so that for any crack length, the corresponding notch region extension can be measured. Any strain redistribution that occurs behind the crack tip is assumed to be negligibly small for most materials, but in some very ductile materials, where blunting of the crack tip occurs, some shape change in the fracture surface can occur.

Accordingly, after failure the fracture surfaces can be measured relative to the dotted lines to produce a graph of crack length versus notch region extension. Figure 20 (d) shows three such sets of measurements. Also the measurement of $(x_o + y_o)$ gives the notch opening displacement for crack growth, w_i. The fracture angles observed between the crack surfaces are thus an indication of the notch region ductility.

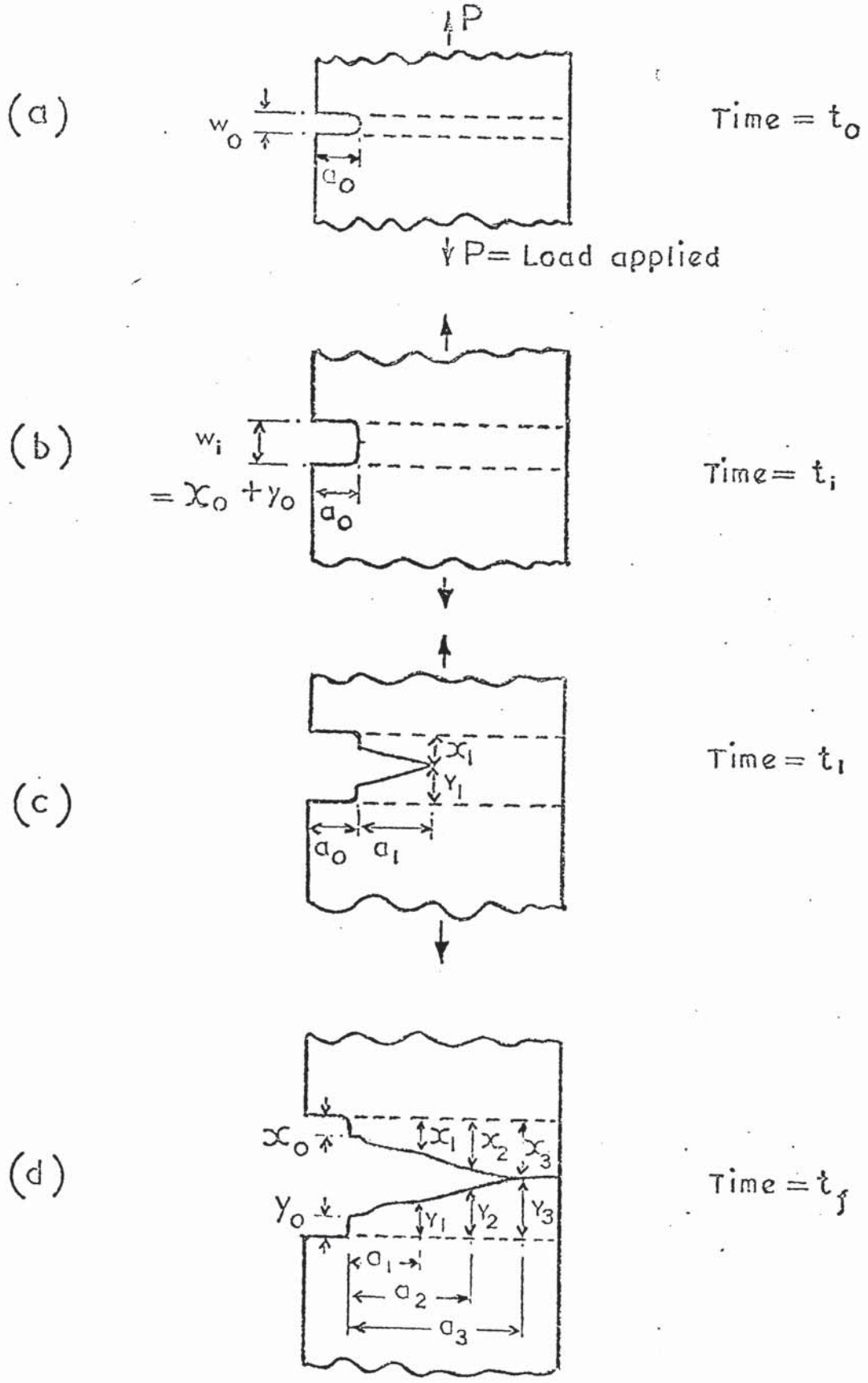

FIG. 20 Straining of the notched region of a single edge notched specimen during a tensile creep rupture test.

(a) Initial condition, time = t_o.
(b) Cracking initictes from notch, time = t_i.
(c) Creep crack length = a_1 at time = t_1.
(d) Failed specimen, time = t_f

During the creep-rupture test, the overall specimen extension can be measured as a function of time. To a good approximation the overall extension comprises the extension of the notched region and the extension of the remainder of the specimen gauge length. The notch region component can be found by the following method.

After failure, the total extension of the specimen is measured (AC in figure 21). The NRE at failure is measured as above and thus the extension of the gauge length at failure can be found (CB and BA respectively). The extension of the remainder of the gauge length consists of primary and secondary creep components and these may be found experimentally by performing creep tests on plain specimens of the same material at the test temperature enabling curve OB to be constructed.

By this means, the contribution to the overall extension from the unnotched portion of the gauge length can be found and so permits the evaluation of the shaded part of figure 21 which represents the change in extension with time in the notched region. Accordingly, the increase in creep crack length with time can now be estimated since for a particular extension, the crack length and the time are both known.

The time for crack initiation, t_i, from the starter notch can also be determined since the notch opening displacement for crack initiation, w_i, has been measured. Thus the time when the notch region extension plus the initial notch width, w_o, equals this value is the time from crack initiation.

The discussion so far has concerned idealized single edge notched specimens. However, as a crack propagates in such an asymmetrical specimen, the uncracked ligament experiences an increasing

bending moment and if the strength of the material is unable to withstand this, the cracked region hinges open. The dotted lines in figure 20 define the notch region for a single edge notched specimen that has not deformed under the action of this bending moment. Clearly, the hinging will cause the cracked specimen to rotate relative to these dotted lines, so that fora particular crack length, the notch region extension measured after the test will differ from that which would have been measured had the test been interrupted at that crack length. The error will be small for small rotations, as is the case for high creep strength materials. However, for other materials it is advisable to use a symmetrical specimen geometry, e.g. double edge notched or centre notched, so that specimen hinging does not occur.

The variation in NRE with time, as shown by the shading in figure 21, is obtained by the difference between the overall extension measured thoughout the test and the extension of the plain part of the specimen calculated from plain specimen control tests. The secondary creep rate found by the plain specimen control could differ by up to a factor of three from the actual strain rate of the plain part of the specimen. However, even without a plain specimen control some idea of the extension of the plain part of the specimen with time can be obtained. Clearly, the extension of the plain part of the specimen at any time must be greater than line (1) in figure 22, which represents the case where all the observed primary creep is from notch region. The extension must also be less than line (3), which represents the case where all the primary creep is due to the extension of the plain part of the specimen, and no extension occurs in the notched region until the end of primary creep. Thus, lines (1) and (3) define lower and upper bounds to the extension of the plain part of the

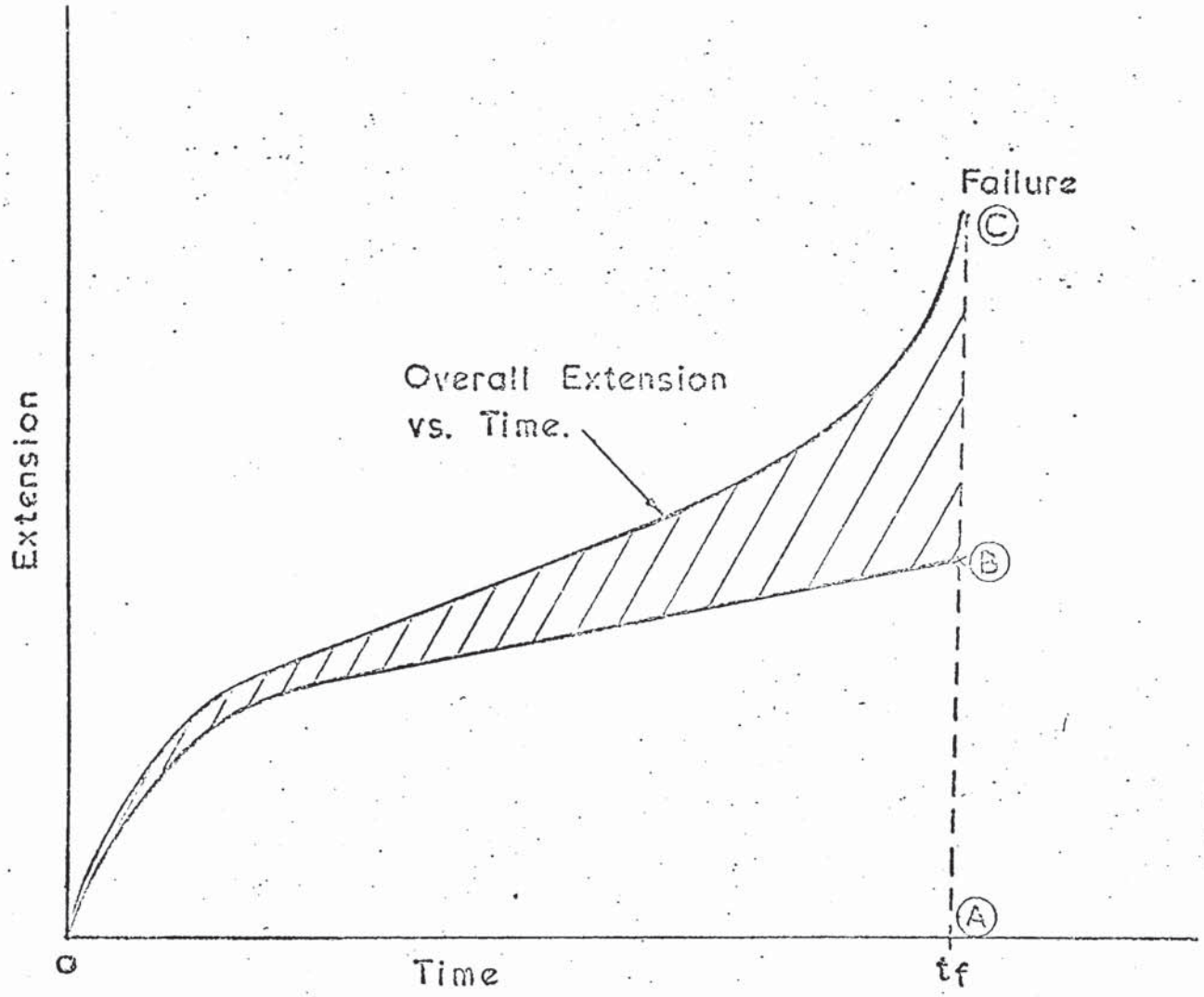

FIG. 21 Schematic overall extension v. time graph. OC is graph of overall extension v. time, OB is extension of plain part of specimen and shaded area represents change in notch region extension with time.

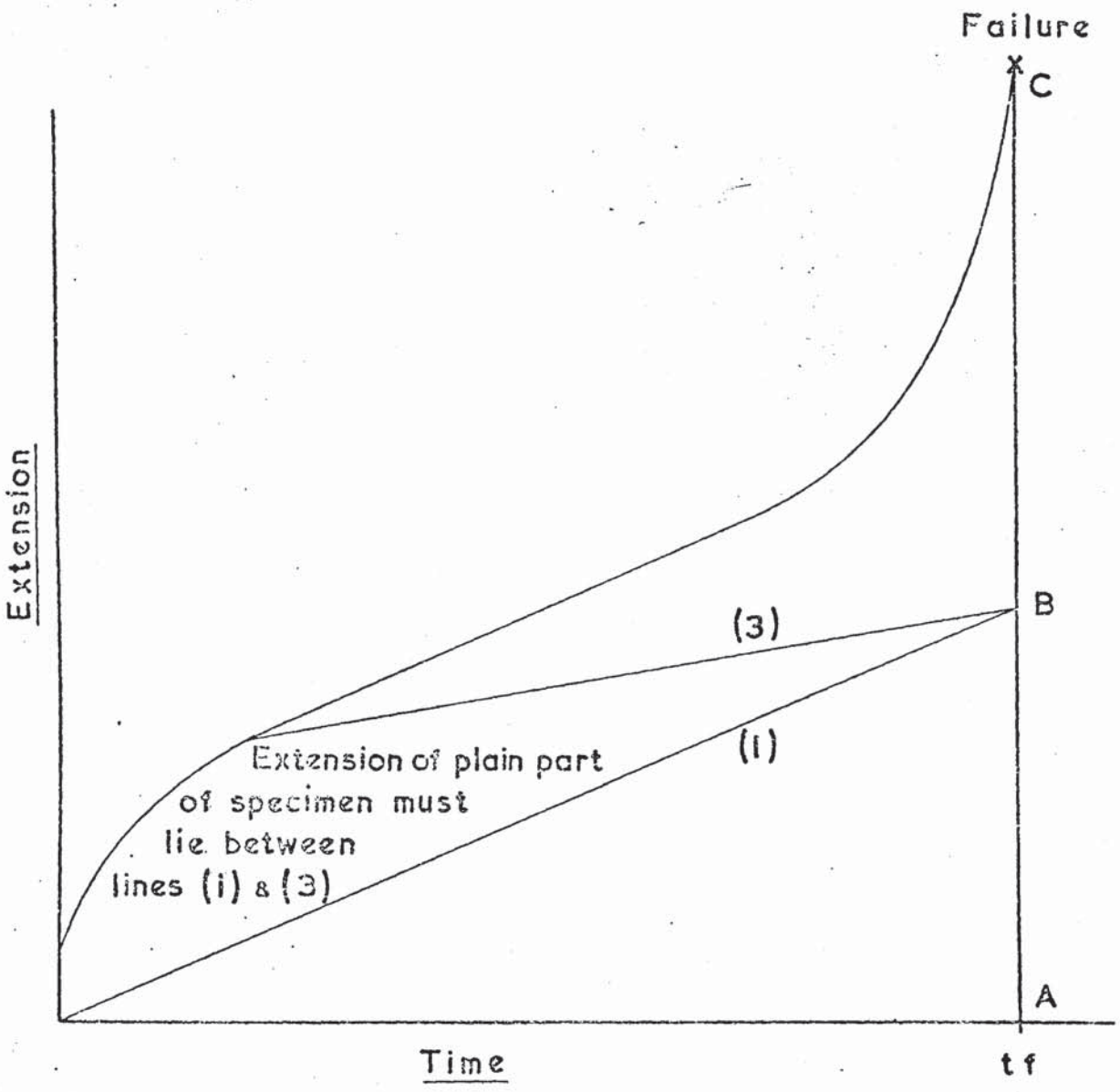

FIG 22 Schematic overall extension v. time graph. Lines (1) and (3) define lower and upper bounds to the extension of the plain part of the specimen with time.

specimen with time. The extension derived from the plain specimen controls must fit between these lines, and any that do not can be rejected.

3. 3.3. Direct Measurement.

The modified Hounsfield tensometer described in section 3.2. allowed direct observation of the growing creep cracks to be made and so the crack length at various times could be measured from the cine film.

3.4. Post-test examination techniques.

3. 4.1. Post-test measurements.

Most tests were continued until the specimen failed. After each test, the fractured specimen halves were placed together and measured with a travelling microscope to obtain the total elongation at failure. Thus for plain specimens, the failure strain could be calculated. Reduction of area measurements were also made on the fracture surfaces of some of the specimens by measuring the cross sectional area of the fracture surfaces using a Reichart microscope.

The measurements needed to calculate crack growth rates were made on some of the notched specimens either by photographing the notched region at a magnification of 50X and measuring the crack length versus notch region extension from the photograph, or magnifying the notched region 50X (to an accuracy of within $\pm$ 0·075%)using a Nikon 6 CT-2 Profile projector,then tracing the magnified image and making the measurements from the tracing.

3. 4.2. Optical metallography.

Selected specimens were prepared for examination in the optical microscope. Longitudinal sections of the specimens were mounted in bakelite and polished to a 1 μm diamond finish by normal metallographic procedures. The specimens were examined in both

the as-polished and the etched condition. The various etchants and etching conditons used are shown in Table 7.

3. 4.3. Electron Microscopy

Some of the specimens were sectioned and the fracture surfaces were examined in a Cambridge scanning electron microscope.

For notched specimens that had been interrupted before final failure, longitudinal sections of the cracked regions were prepared as for optical metallography, then lightly etched with dilute aqua regia and examined in the scanning electron microscope.

Etchant	Conditions	Remarks
10% oxalic acid	10 gm. oxalic acid in 100 cc. distilled H_2O. Electroytic etch at 70°C using stainless steel cathode, 3V, 1·5A, 2-30 secs.	General reagent revealing inter and intragranular precipitates, and grain boundaries
Dilute aqua regia	25cc distilled H_2O, 25cc HCl, 10cc HNO_3, Chemical etch at room temperature	General reagent. Attacks austenite uniformly leaving carbides clearly outlined and in relief.
10% HCl in methanol	10cc HCl in methanol Electrolytic etch at room temperature 3V, 1·5A, 2-10 secs.	As for 10% oxalic acid.

TABLE 7

Etchants and conditions used on stainless steel specimens

CHAPTER 4.

EXPERIMENTAL RESULTS

4. 1. Creep crack growth in A.I.S.I. type 316 stainless steel.

4. 1.1. Comparison of methods for measuring creep crack growth.

Crack growth in 316 stainless steel specimens has been measured by the three methods described in section 3. 3 and the results have been compared.

Single edge notched specimens of 316 steel were tested at 740°C. and the crack lengths during the tests were monitored continuously by the D.C. potential drop technique. The extension of the specimens were recorded during the tests and after failure, the notched regions were measured so that crack growth rates could be calculated by the NRE method. The results of the variation in crack length with time for the two techniques are shown in Fig. 23. The most significant difference between the two sets of results for the test at a gross section stress of 69·7 MN $m.^{-2}$ was in the time to initiate cracking from the notch: the NRE method predicted a time of 61 hours whilst the DC method gave a time of 84 hours. This was thought to be due to a lack of sensitivity in the DC method at very small crack lengths and to the experimental errors in the measurement of the small displacements involved. However, for larger crack lengths the two sets of results compare favourably. Also shown are the results for a second test at the same temperature but with the specimen loaded under a gross section stress of 59 MN $m.^{-2}$ and again the two techniques compare favourably.

Comparisons between the results of the NRE method and the direct observation of crack growth have been made on double edge notched specimens at650 and 750°C.. Fig. 24 shows the results of the two tests. The tests at 750°C. showed that at a given time, the two

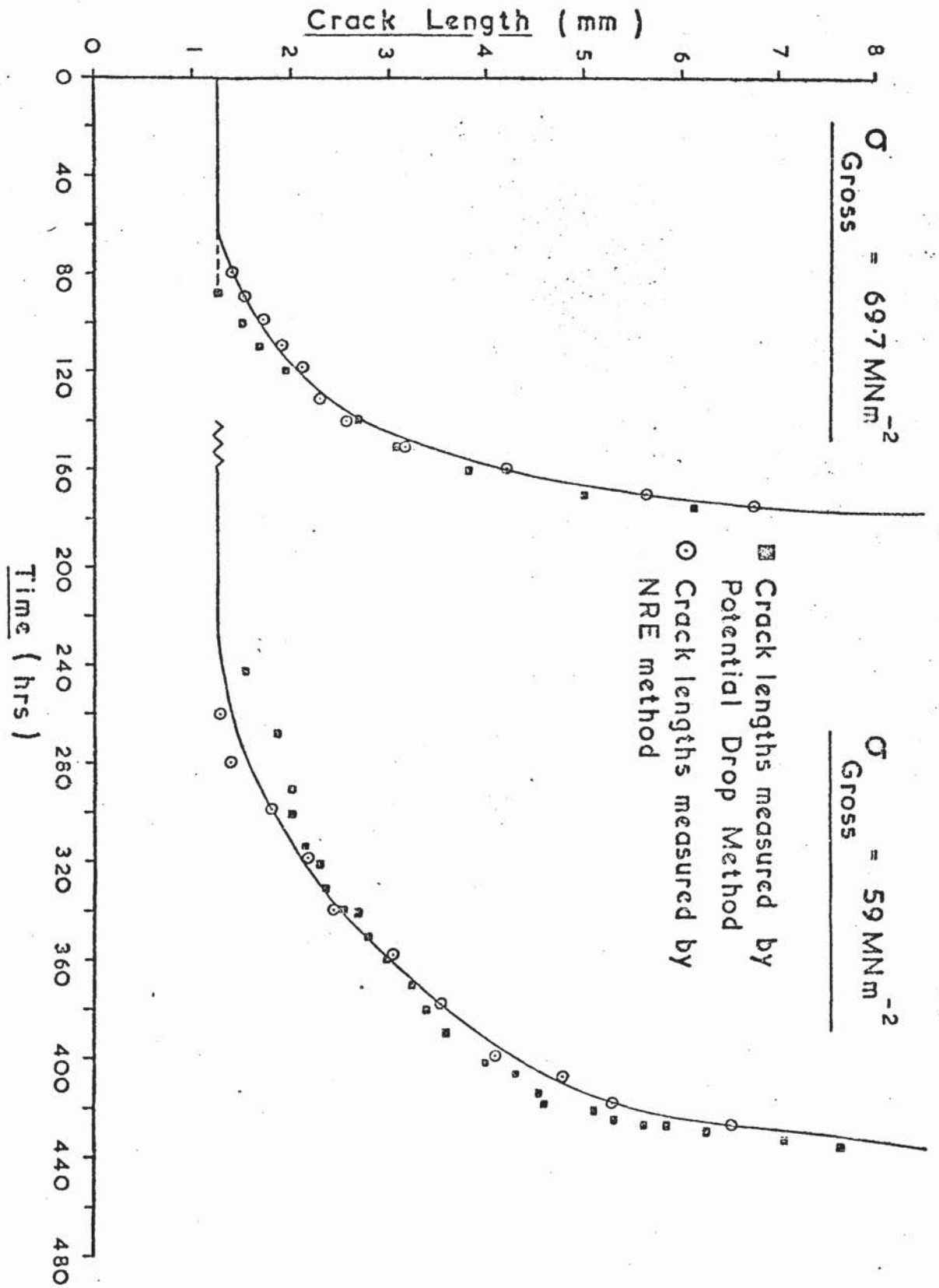

FIG 23 Crack length v. time graphs showing results obtained by the NRE method and the DC potential drop method.

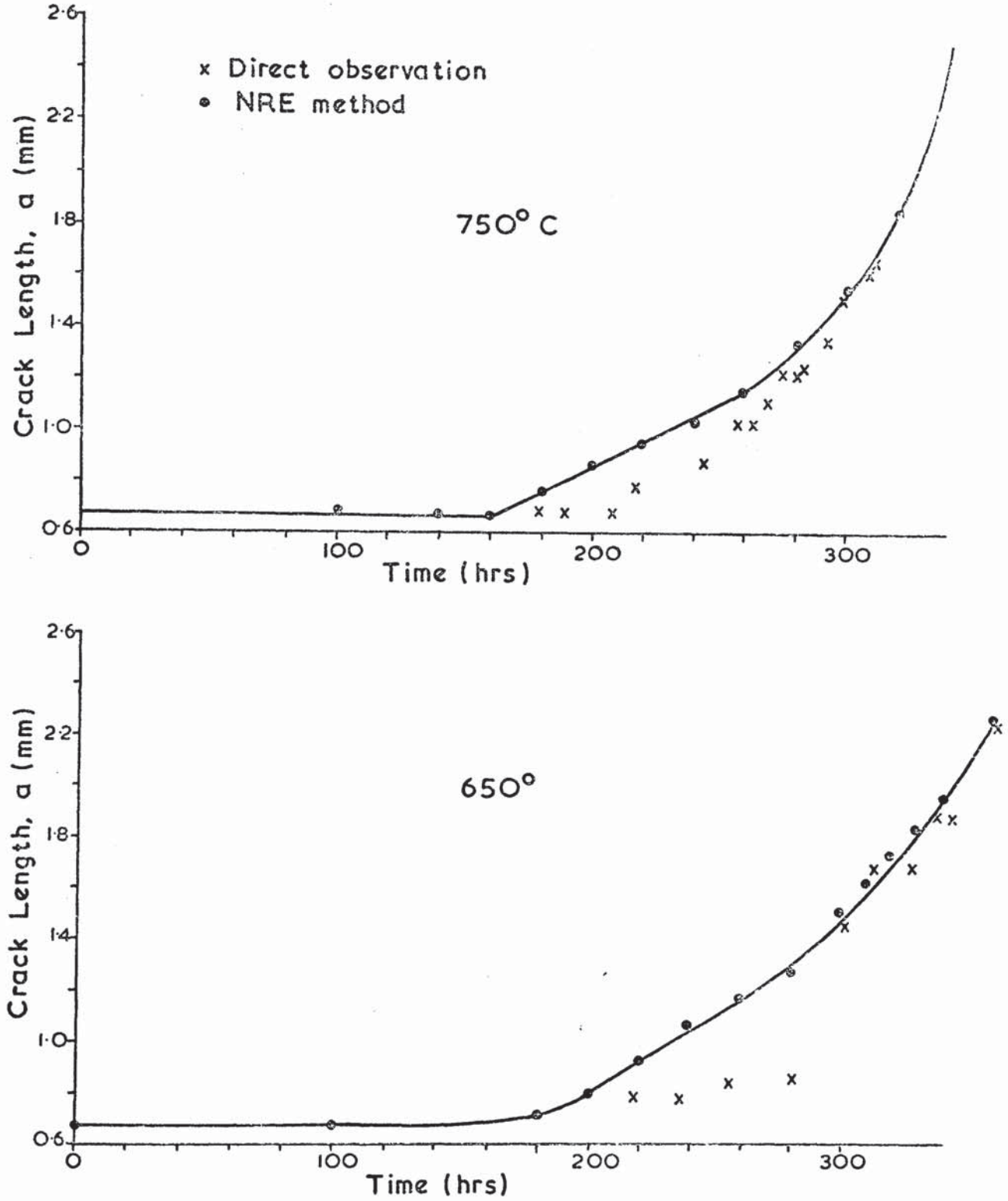

FIG. 24. Creep Crack Growth in 316 Stainless Steel Predicted by NRE Method and Direct Observation.

methods gave crack lengths to within about 0·1 mm of each other, consistent with the experimental accuracy of the two methods. At 650°C., there was a greater difference at short crack lengths (up to 0·4 mm) but for crack lengths greater than 1·4 mm, the two methods gave very similar results. It is thought that the discrepancy at short crack lengths arises from difficulties in accurately identifying the crack tip on the photographs due to extensive surface rumpling, thus, resulting in incorrect crack length measurements. However, in general it can be seen that similar results would be obtained whichever method of measuring crack growth was used.

4. 1.2. The validity of various fracture mechanics methods at 740°C.

Tensile creep rupture tests were performed in air on single edge notched specimens (large size) and notched centre hole specimens of 316 stainless steel at 740°C. Crack growth was monitored continuously by the D.C. potential drop technique and on a couple of specimens was checked by the NRE method as described above. The initial nett section stresses (i.e. before cracking initiated from the notch) were from 63 to 90 MN m^{-2} and Table 8 shows the various failure times.

Figs. 25 and 26 show the crack growth rates plotted against stress intensity factor and nett section stress respectively. For the single edge notched specimens, the stress intensity factor (K_I) used was given by (Brown and Srawley (1966)):-

$$K_I = Y \cdot \frac{La^{\frac{1}{2}}}{BW} \qquad (32)$$

where $Y = 1{\cdot}99 - 0{\cdot}41\left(\frac{a}{W}\right) + 18{\cdot}70\left(\frac{a}{W}\right)^2 \ldots$ and L is load, B is specimen thickness and W is width.

For the notched centre hole specimens,

$$K_I = \sigma_{gross} \sqrt{a\pi} \quad f\left(\frac{a}{r}\right) \qquad (33a)$$

TABLE 8.

Creep Rupture of notched specimens of 316 stainless steel at 740°C.

Type of Specimen	Initial Nett Section Stress ($MN\ m^{-2}$)	Failure Time (hrs).
Single Edge Notched (S.E.N)	89·4	25·8
S.E.N.	75·5	180·6
S.E.N.	63·6	442·1
S.E.N.	88·4	115·8
Notched Centre Hole (N.C.H)	86·2	48·5
N.C.H.	77·5	318·0
N.C.H.	65·9	511·2

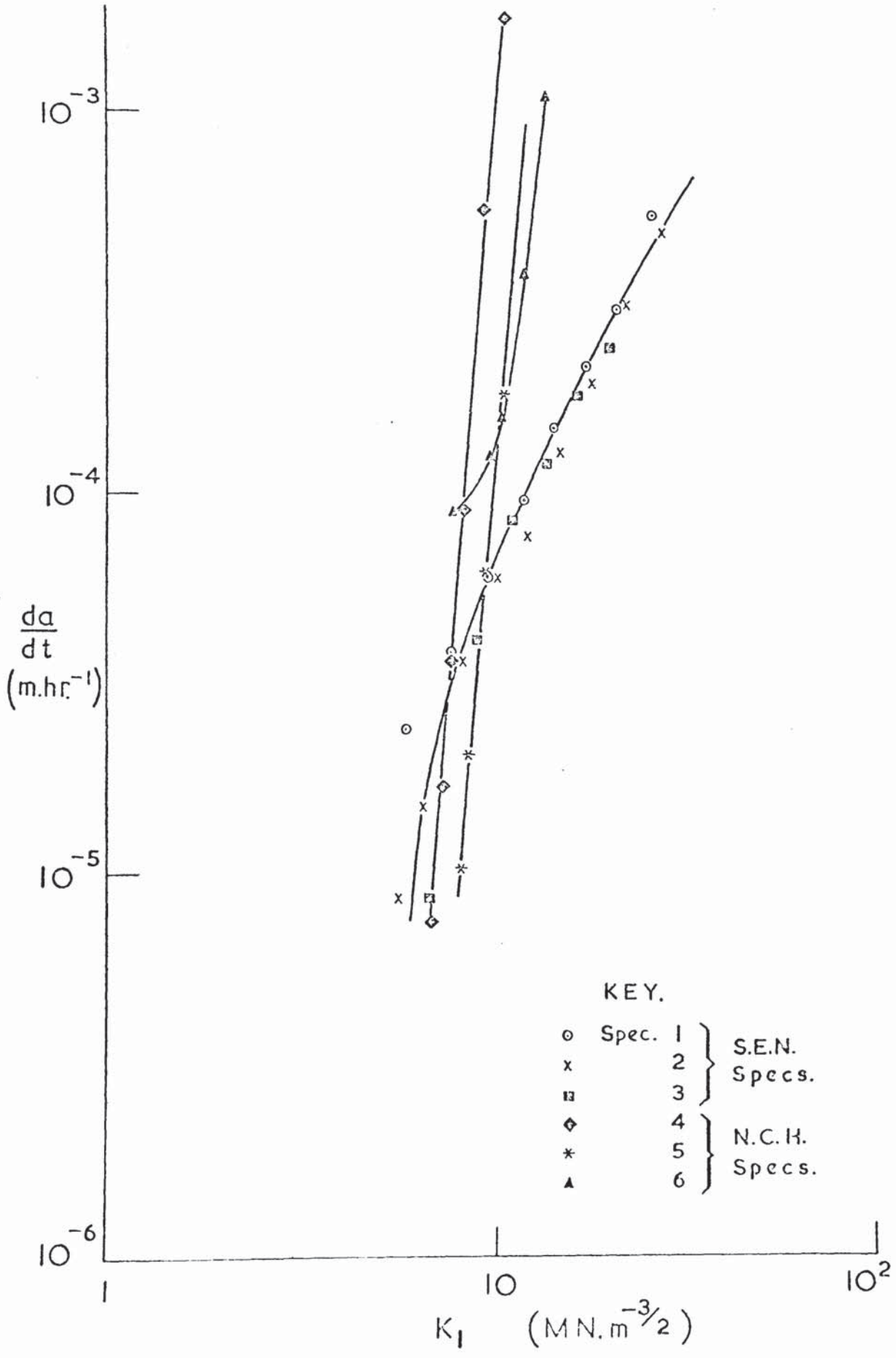

FIG. 25 Creep crack growth rate $(\frac{da}{dt})$ versus stress intensity factor (K_I).

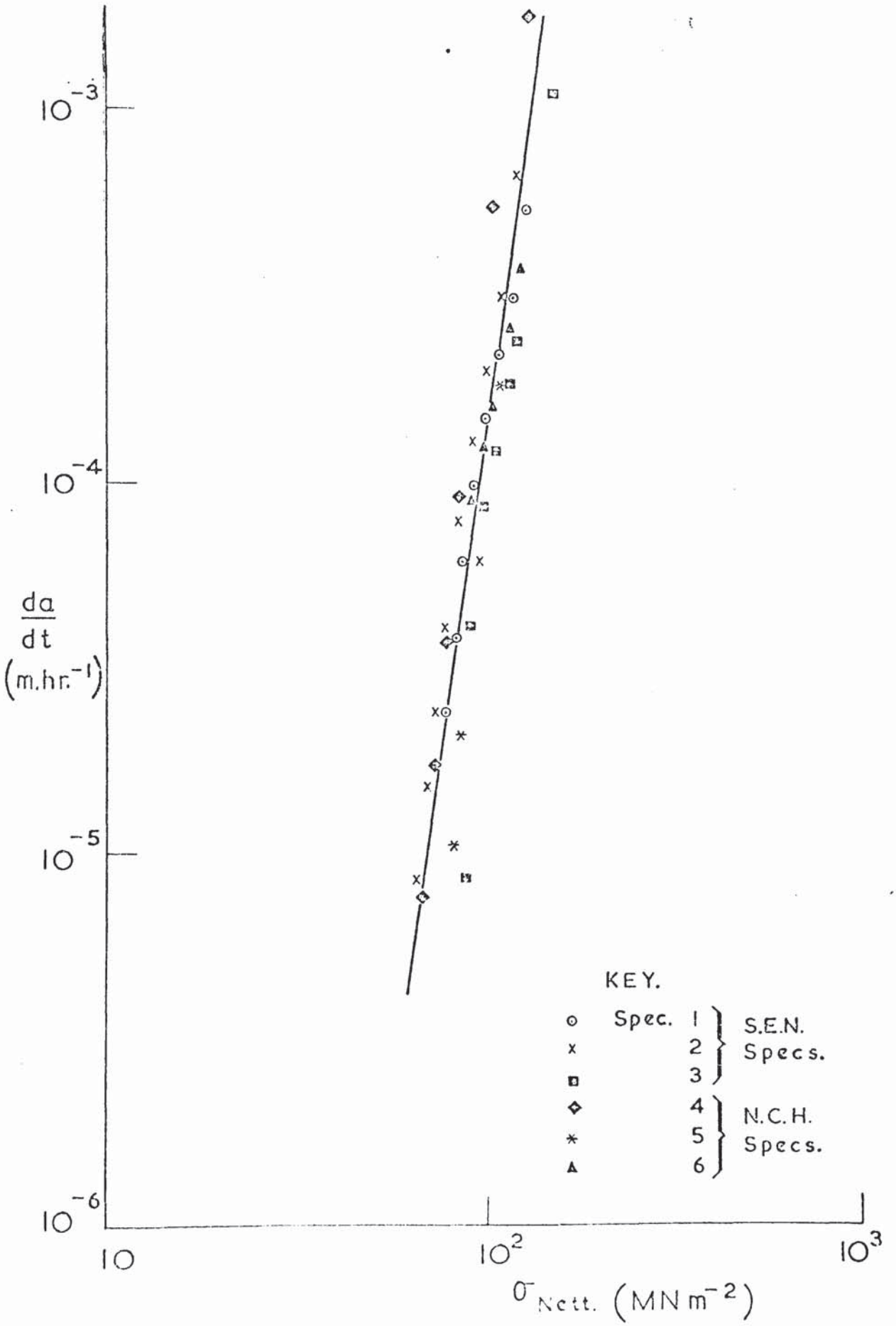

FIG. 25 Creep crack growth rate ($\frac{da}{dt}$) versus nett section stress ($\sigma_{Nett.}$).

where $a \leq 0{\cdot}2\ R$ and R is the hole radius and $f(\frac{a}{R})$ is evaluated by Paris and Sih (1964). When $a > 0{\cdot}2\ R$,

$$K_I = Y' \cdot \frac{La^{\frac{1}{2}}}{BW} \qquad (33b)$$

where $Y' = 1{\cdot}77 + 0{\cdot}227\ (\frac{2a}{W}) - 0{\cdot}510\ (\frac{2a}{W})^2 \ldots$ (Brown and Srawley (1966)).

When the crack growth rates were plotted against K_I (Fig. 25) a single relationship was found for the single edge notched specimens, but the same relationship was not found in the notched centre hole specimens which showed great changes in growth rate for very slight changes in K_I. If a real link existed between K_I and and crack growth rate, $\frac{da}{dt}$, all the points from both types of specimen should have fallen on one curve. When plotted against the nett section stress (Fig. 26), all points do in fact fall on one curve and obey the relationship:-

$$\frac{da}{dt} = N\ \sigma_{Nett}^{p} \qquad (34)$$

where N and p are constants, of values $1{\cdot}8 \times 10^{-18}$ m. $hr^{-1}(MN\ m.^{-2})^{-7}$ and 7 respectively. The stress exponent for secondary creep at 740°C. is, in fact, close to 7 (McLauchlin (1975)).

4. 1.3. The Effect of Temperature on the criteria controlling Creep Crack growth.

Double edge notched specimens (small size) of 316 stainless steel were tested in air at temperatures of 600, 700,740,800 and 850°C. and crack growth rates were calculated by the NRE method.

Plain specimen tests at various stresses were also performed at the same temperatures. The secondary creep rate, $\dot{\varepsilon}$, was measured at each stress level and used to obtain a value for the stress exponent, n, in the secondary creep equation (equation (15)).

The creep crack growth rates are plotted against nett section stress in Fig. 27 and it can be seen that between 600 and 850°C., equation (34) is obeyed. The value of p at each

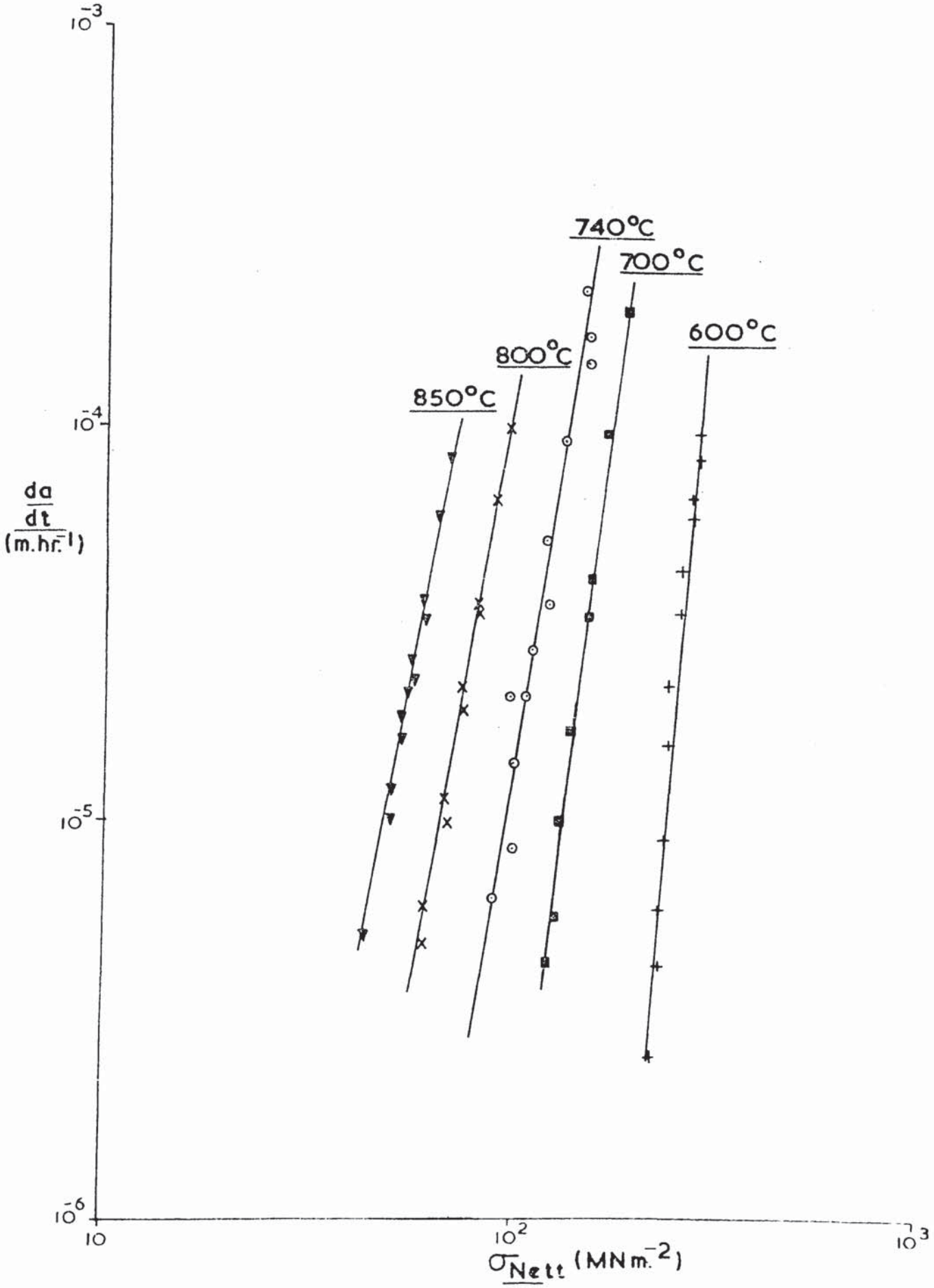

FIG. 27 Creep crack growth rate v. nett section stress between 600 & 850°C.

temperature was determined by linear regression analysis and is shown in Table 9. Also shown are the values of the stress exponent, n, in equation (15) calculated from the plain specimen tests, the results of which are shown in Fig. 28. Values of n found by other authors at about the same temperatures are also included in Table 9. The values of n and p are plotted at each temperature in Fig. 29 and it can be seen that within the accuracy of the experiments, n = p.

Fig. 30 shows the notched region of a specimen with the crack opening displacement (δ) and notch region extension (NRE) indicated at a particular crack length. It can be seen that the NRE = δ and thus the NRE method of measuring creep crack growth gives $\frac{d\delta}{dt}$ also. Fig. 31 shows $\frac{da}{dt}$ plotted against $\frac{d\delta}{dt}$ at temperatures of 600, 740 and 850°C. The gradients of the lines have been calculated by linear regression analysis and in the temperature range 600 to 850°C all fall in the range $1{\cdot}2 \pm 0{\cdot}2$.

Fig. 27 shows that crack growth rates at constant σ_{Nett} increase with increasing temperature. Assuming an Arrhenius-type equation to apply, i.e.

$$\frac{da}{dt} \quad \alpha \exp\left(-\frac{Q}{RT}\right) \qquad (35)$$

where Q = Activation energy for crack growth, R and T have their usual meanings, graphs of log $(\frac{da}{dt})$ versus $(\frac{10^3}{T^oK})$ have been constructed and are shown in Fig. 32 for the temperature range 700 to 850°C. A few of the points were found by extrapolating the curves in Fig. 27, but the extrapolation was never over more than one order of magnitude in crack growth rates. Between 740 and 850°C, apparent crack growth activation energies of between 339 and 372 KJ $mole^{-1}$ were found for nett section stresses of between 100 and 65 MN m^{-2}.

Creep activation energies have been calculated for

TABLE 9

CREEP AND CRACK GROWTH PARAMETERS

$T^{o}c$	p	n (present work)	n (Other Authors)	Author
600	14.2 ± 1.2	11.9 ± 1.4	12.5 at 593.3°C	Garofalo et al (1961)
700	9.4 ± 0.8	8.8 ± 1.2	6.6 at 704.4°C	Garofalo et al (1961)
740	6.8 ± 0.6	7.2 ± 0.5	7.0 at 750°C 7.3 at 760°C 6.8 at 732°C	McLauchlin(1975) Cornell Aero Lab. Report (1950) Challenger et al (1973)
800	6.4 ± 0.3	6.3 ± 0.8	5.9 at 816°C 5.5 at 816°C	Challenger et al (1973) Garofalo et al
850	5.9 ± 0.4	5.6 ± 0.5	-	-

FIG. 28 Plain specimen secondary creep rate v. applied stress between 600 & 850°C.

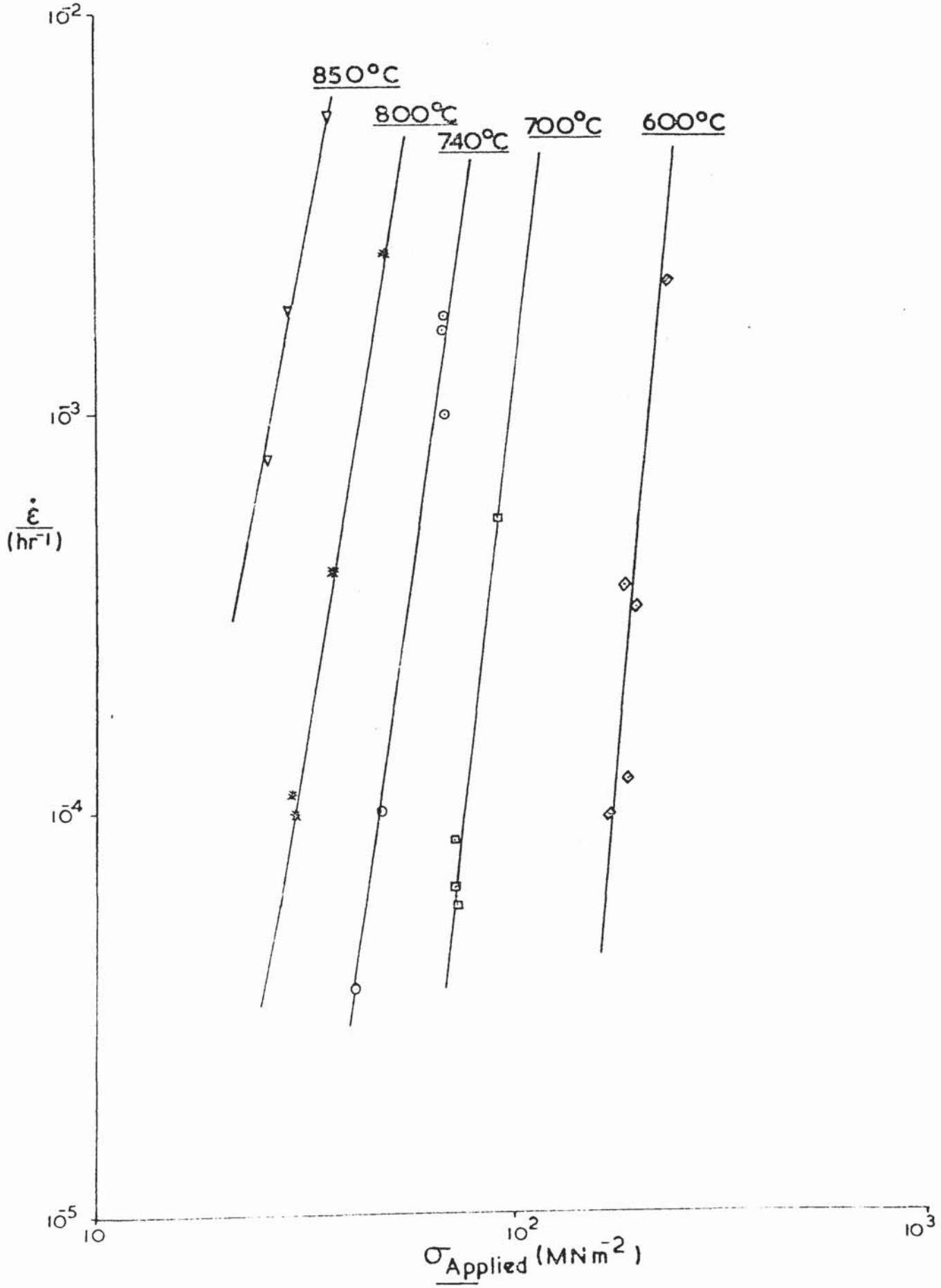

FIG. 29 The relationship between exponents n and p and temperature

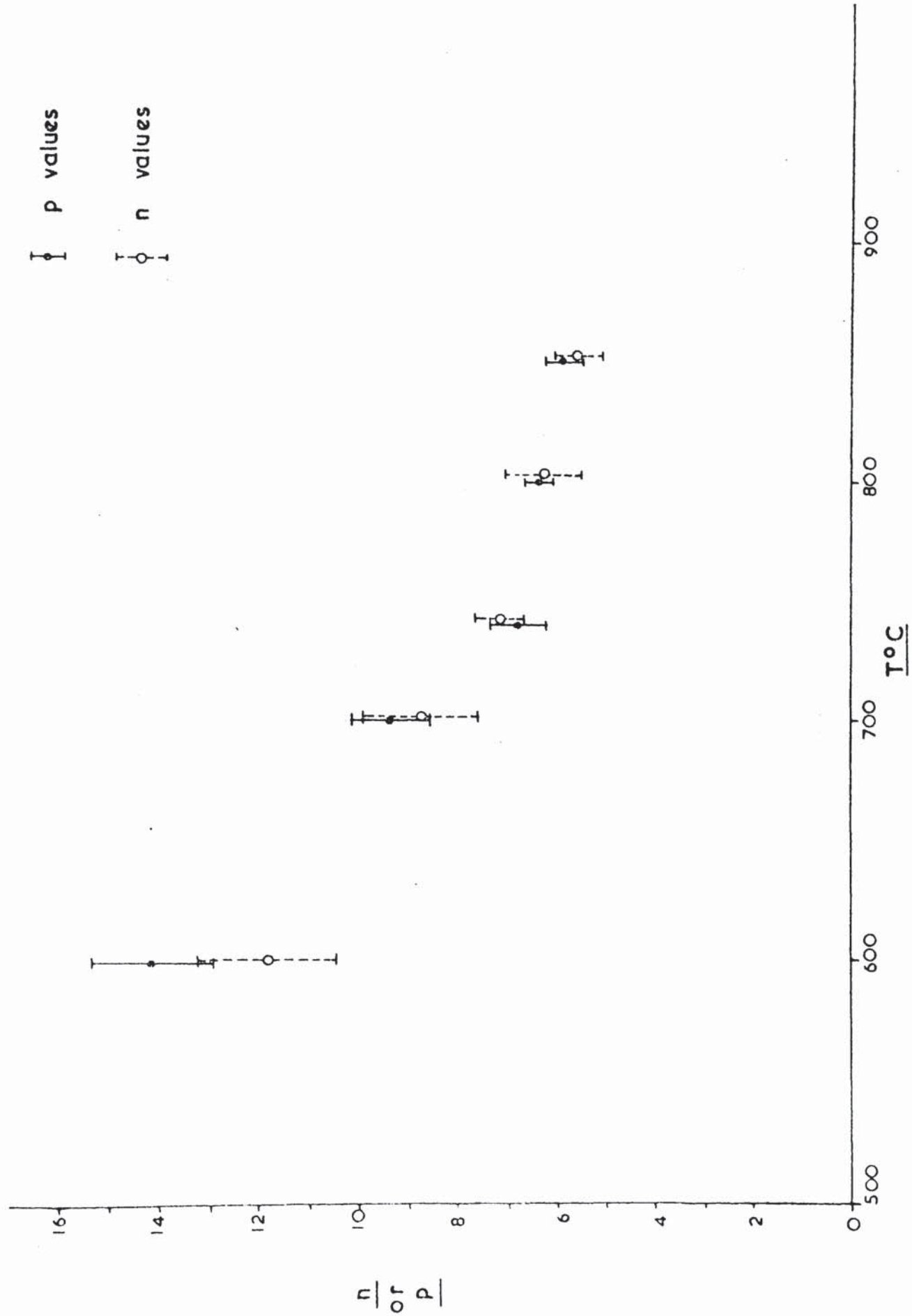

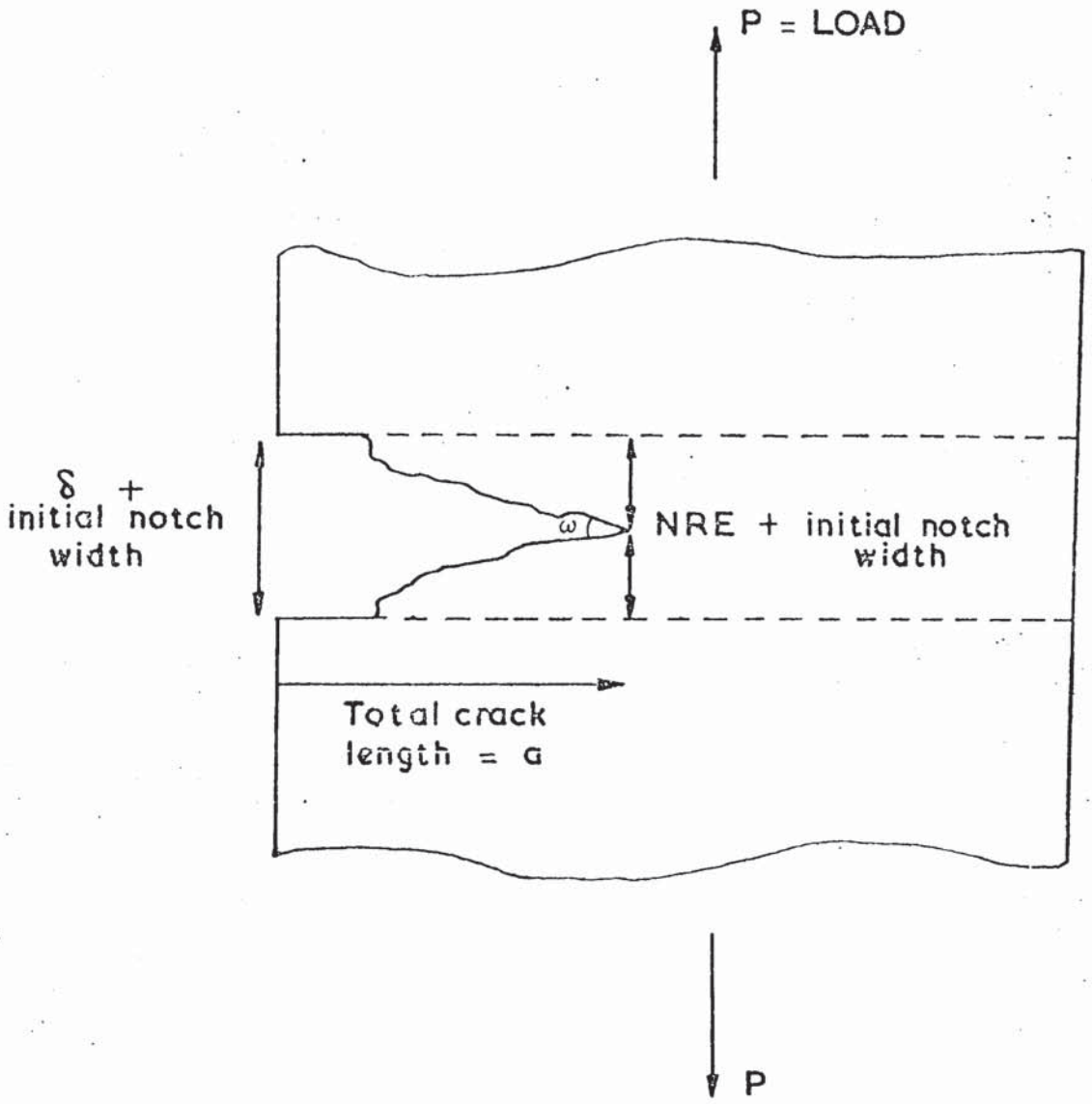

FIG. 30 Notched region of specimen showing that the notched region extension = crack opening displacement, δ, measured at outside of starter notch.

FIG. 31 Crack growth rate v. crack opening displacement between 600 & 850°C.

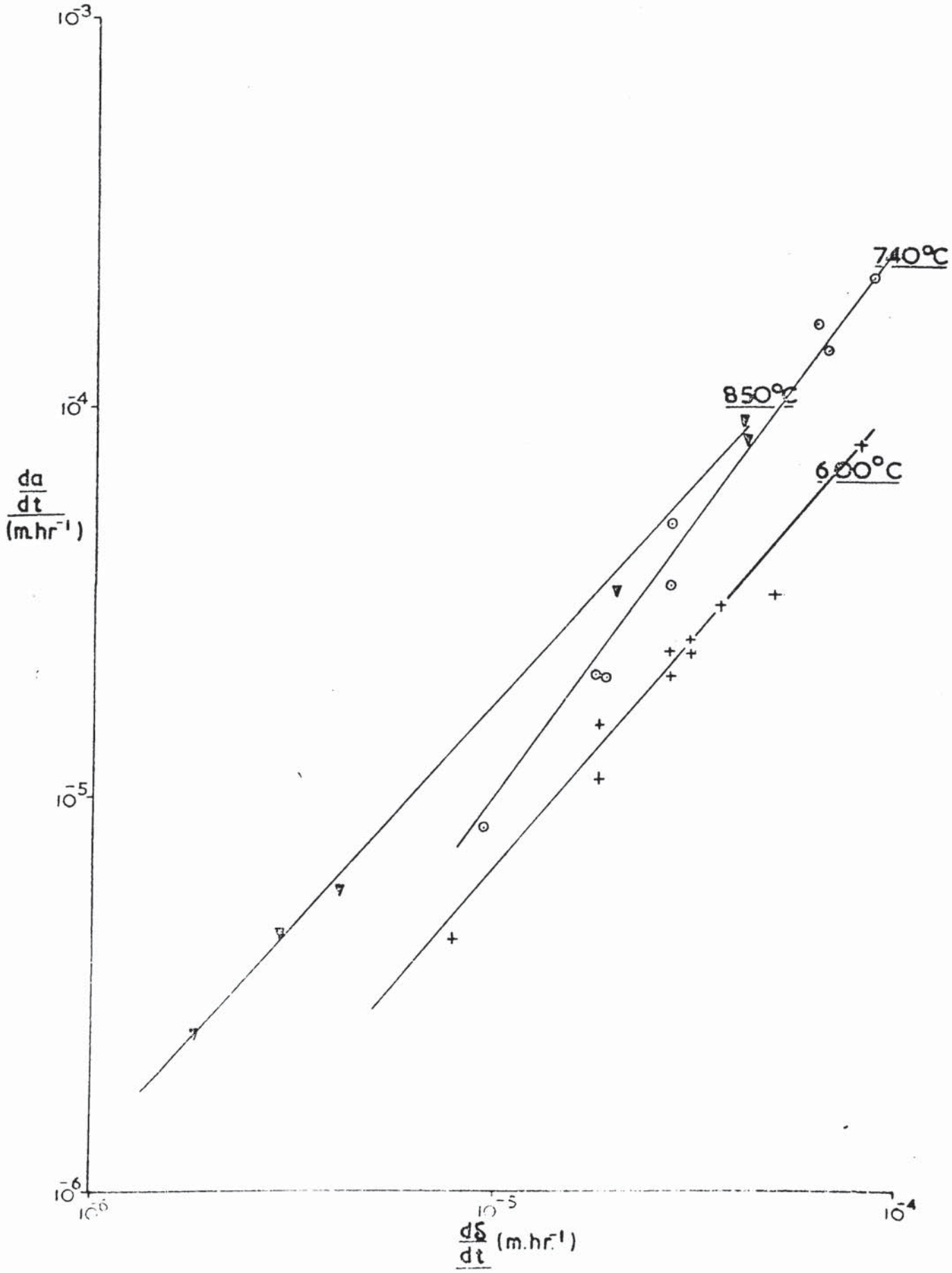

FIG. 32 Arrhenius plot of creep crack growth rates to calculate activation energy for crack growth

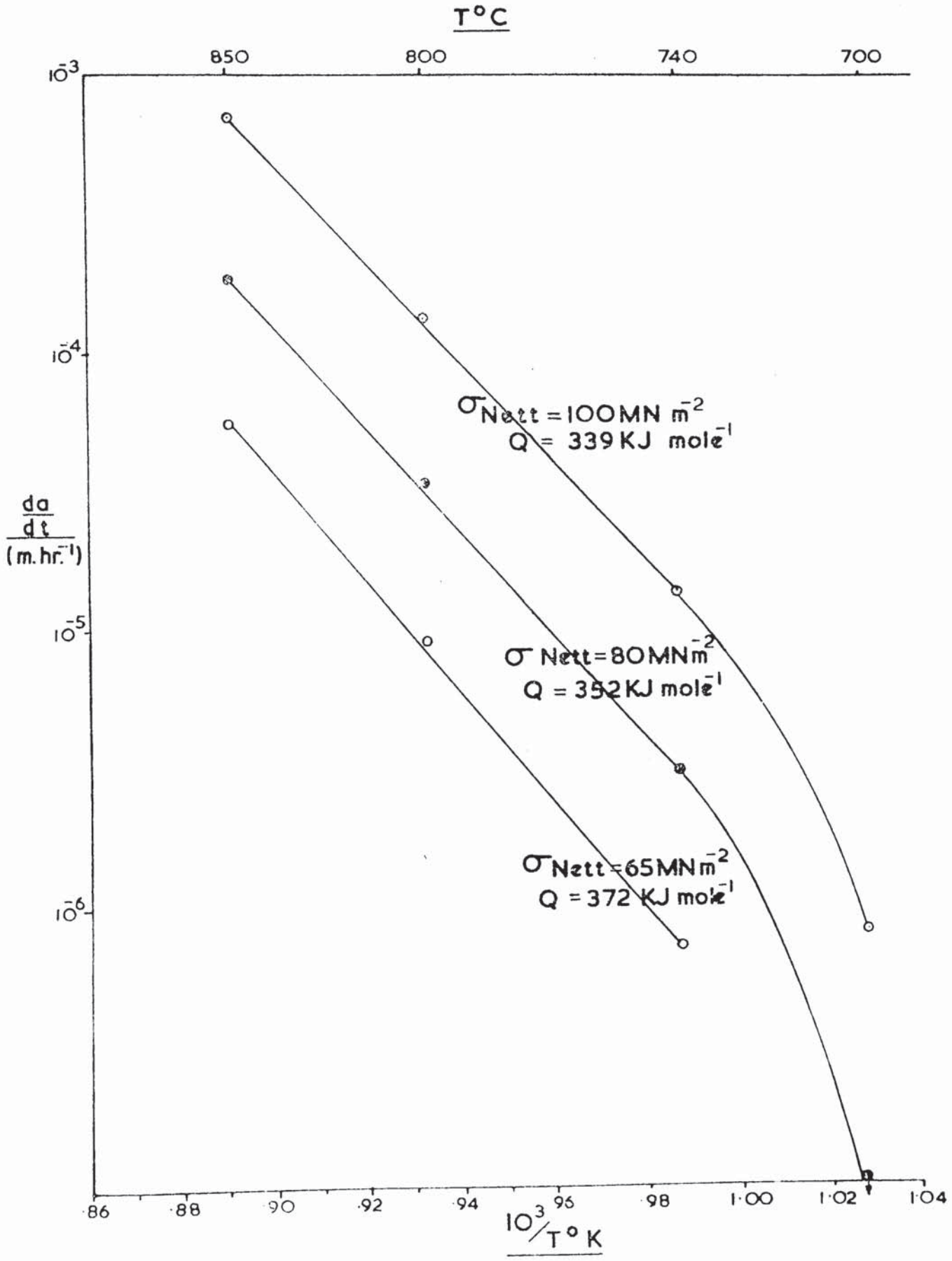

the plain specimen data shown in Fig. 28. Fig. 33 shows the Arrhenius plot for the temperature range 700 to 850°C. Between 740 and 850°C, apparent creep activation energies of between 345 and 470 KJ mole^{-1} were found for a stress range of 80 to 50 MN m^{-2}.

For the temperature below 740°C, the available data in Figs. 32 and 33 shows that both creep and crack propagation processes decreases more rapidly with temperature than would be expected from the apparent activation energies obtained at higher temperatures. However, the lack of comprehensive information prevents any further quantitative comparison.

4. 1.4. Macroscopic Aspects of Crack Growth from notches.

4. 1.4.1. Crack initiation and propagation

It was observed in each test on type 316 stainless steel that certain minimum displacements must be achieved for crack initiation and propagation; this being the basis of the NPE method of measuring crack growth. The displacements to initiate cracking, δ_i, can be measured at the notch root. A measure of the displacement associated with propagation is the angle included at the crack tip by the fracture surfaces, ω, (i.e. the fracture angle) (Formby (1972), McLintock (1968)). These quantities are illustrated in Fig. 30.

It was found in the type 316 stainless steel specimens that as the crack propagates from the notch, the fracture angle remains about constant for part of the specimen width and then decreases to zero as final failure occurs. Fig. 34 shows a typical result obtained from a type 316 steel specimen (large size) tested at 740°C. Therefore, after failure of the notched specimens tested in air at temperatures betweeen 600 and 850°C., δ_i and ω were measured. For a given specimen size, tests at various loads, and therefore various times to failure, showed that ω and δ_i decreased as the

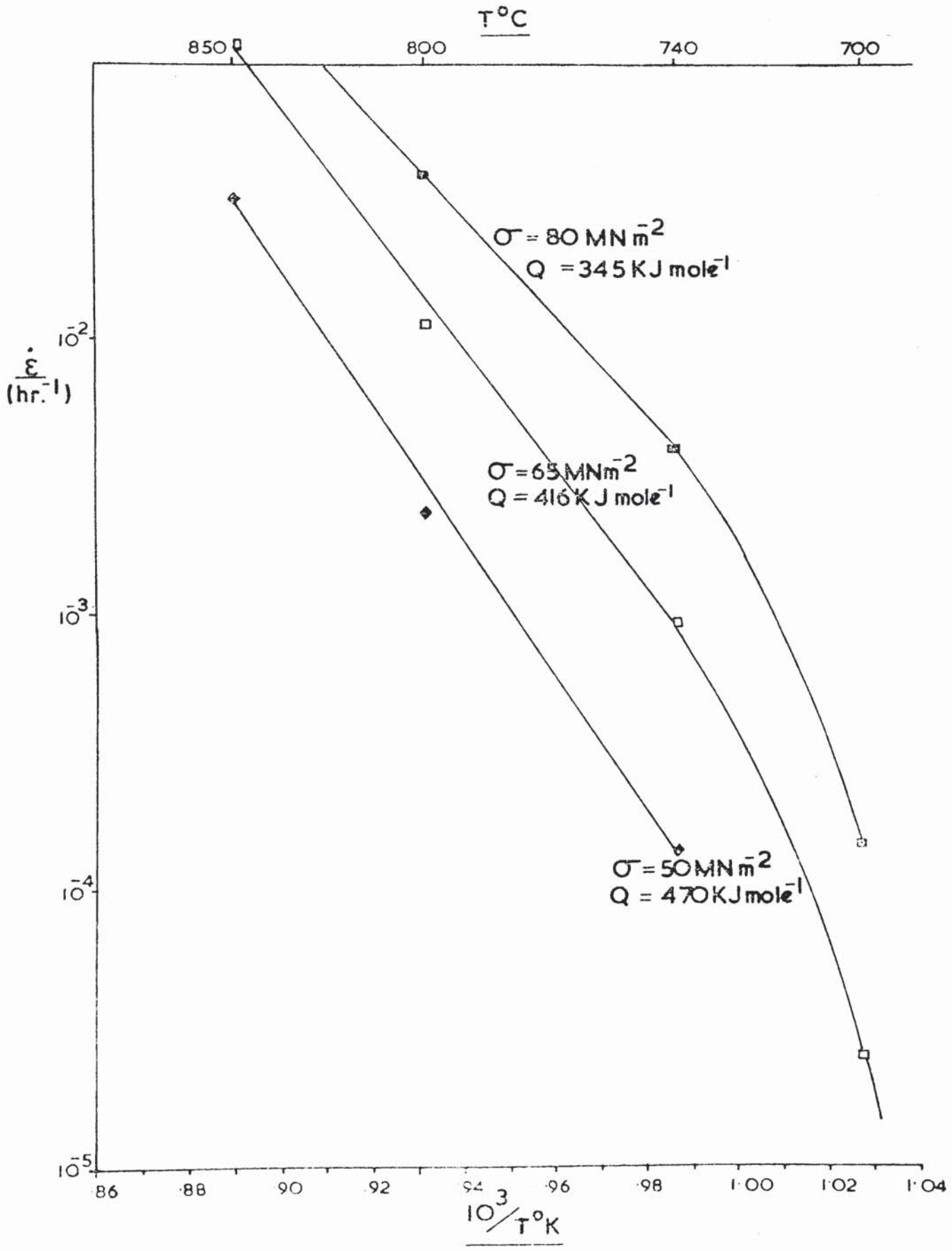

FIG. 33 Arrhenius plot of secondary creep rates to calculate creep activation energy

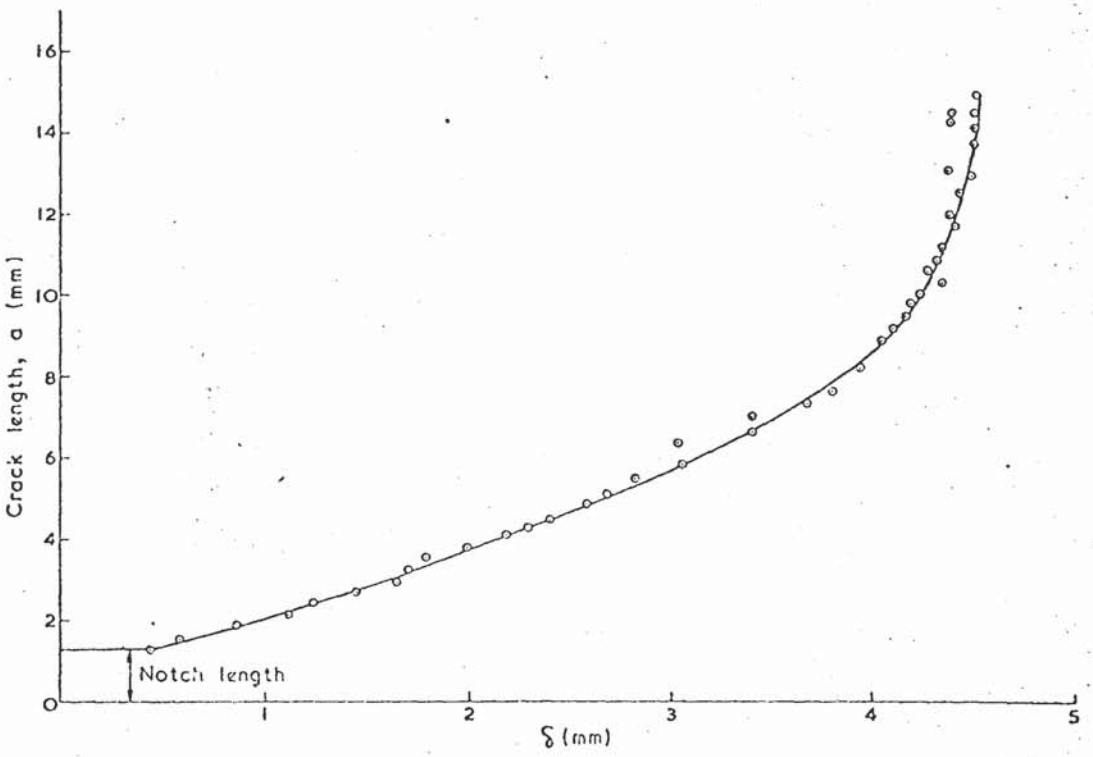

FIG 34 Variation of crack length (a) with COD (δ)

failure time increased (Figs. 35 and 36) in a similar way to the elongation to failure of plain specimens which is shown in Fig. 37.

4. 1.4.2. Stress and Strain Distribution ahead of notches under creep conditions.

Creep stress and strain distributions ahead of notches in type 316 stainless steel have been measured experimentally using the modified Hounsfield tensometer described previously. The specimens tested were double edge notched strips which had parallel lines (approximately 0·1 mm apart) scribed across the specimen perpendicular to the stress axis, in the region of the notch. Tests were performed at 750 and 650°C. under constant cross-head displacement rates of either 1.2×10^{-5} or $1{\cdot}1 \times 10^{-4}$ m. hr^{-1}, and deformation at one of the notches was observed through the microscope and recorded by the time lapse cine camera taking one photograph every 5 minutes. The output from the load cell was recorded continuously. The scribe lines were observed to bend locally near the notch tip before crack initiation occurred and analysis of the cine film after test enabled the displacement of the lines at any time to be measured.

In each test, during primary creep the load increased, became constant once secondary creep was reached and then decreased as crack propagation from the notches occurred. Thus, the time for the onset of secondary creep, t_s, in a given test was found from the load cell record. The displacements of the scribe lines at the notch root at this time could also be found from the cine film.

Two scribe lines, one near each side of the notch, were selected and the displacements between these two lines at various r values, where r = distance from the notch tip, were measured from prints taken from the cine film. Various times between t_s and the

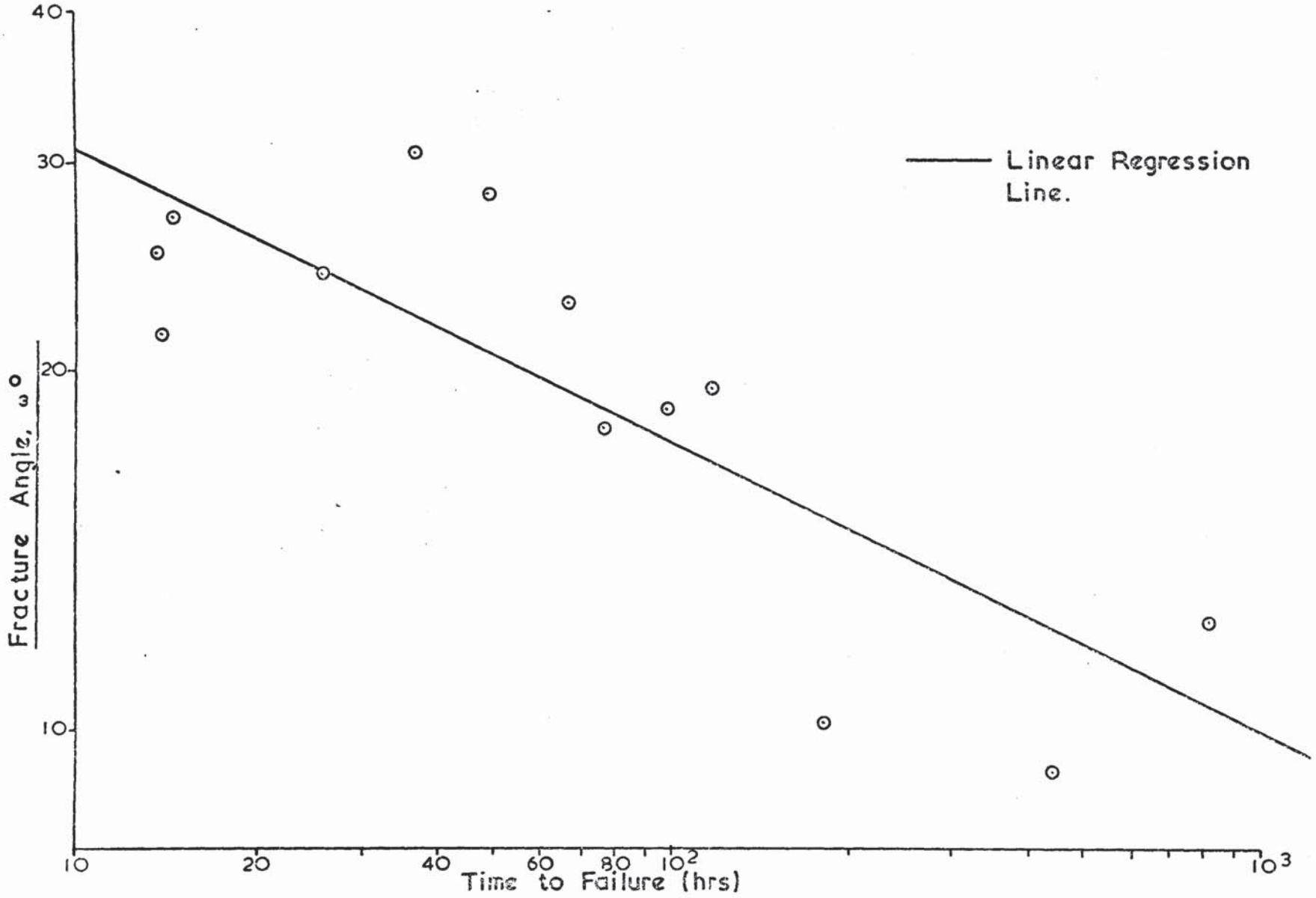

FIG. 35. Variation of Fracture Angle with Time to Failure.

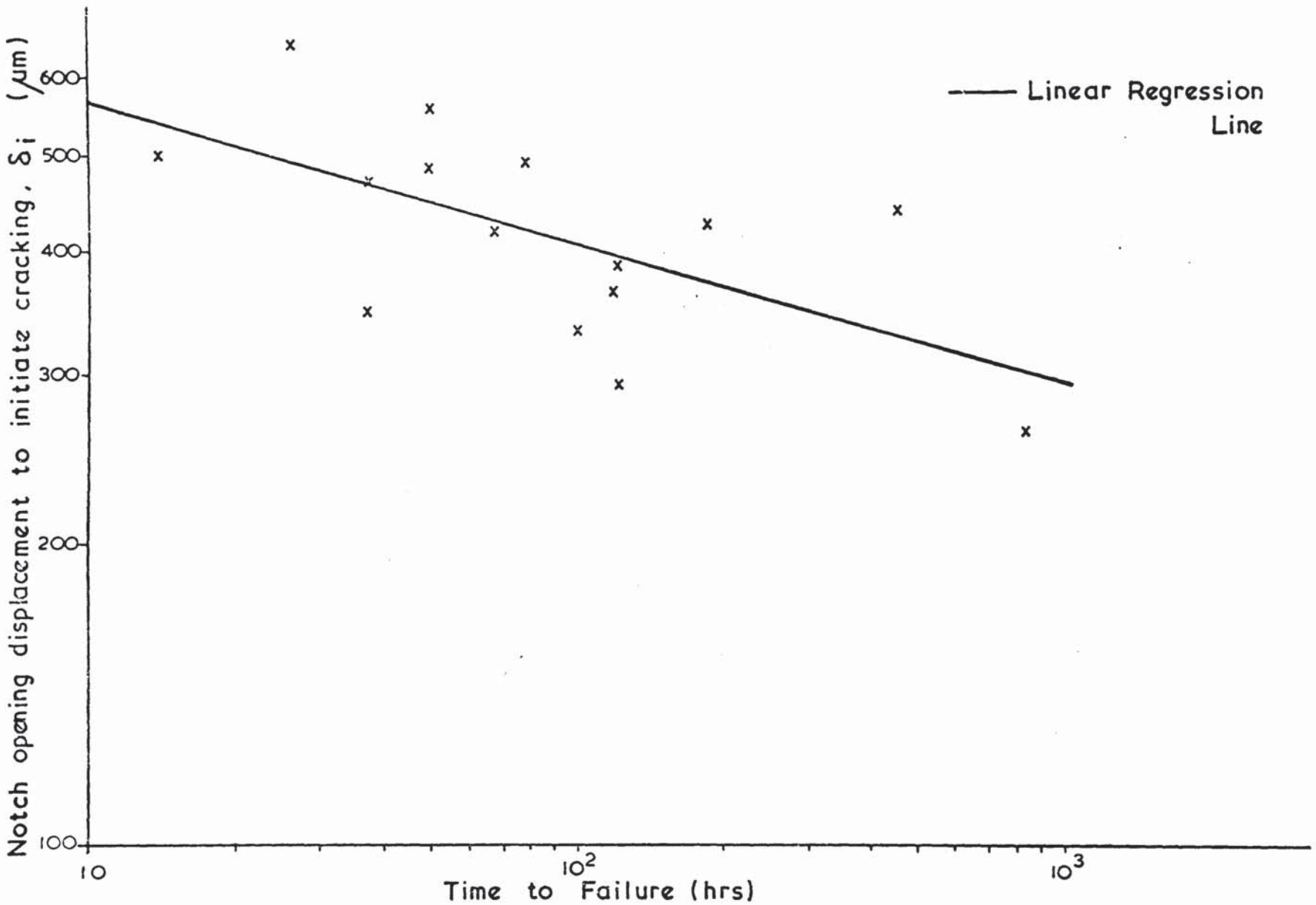

FIG. 36. Variation of δ_i with Time to Failure.

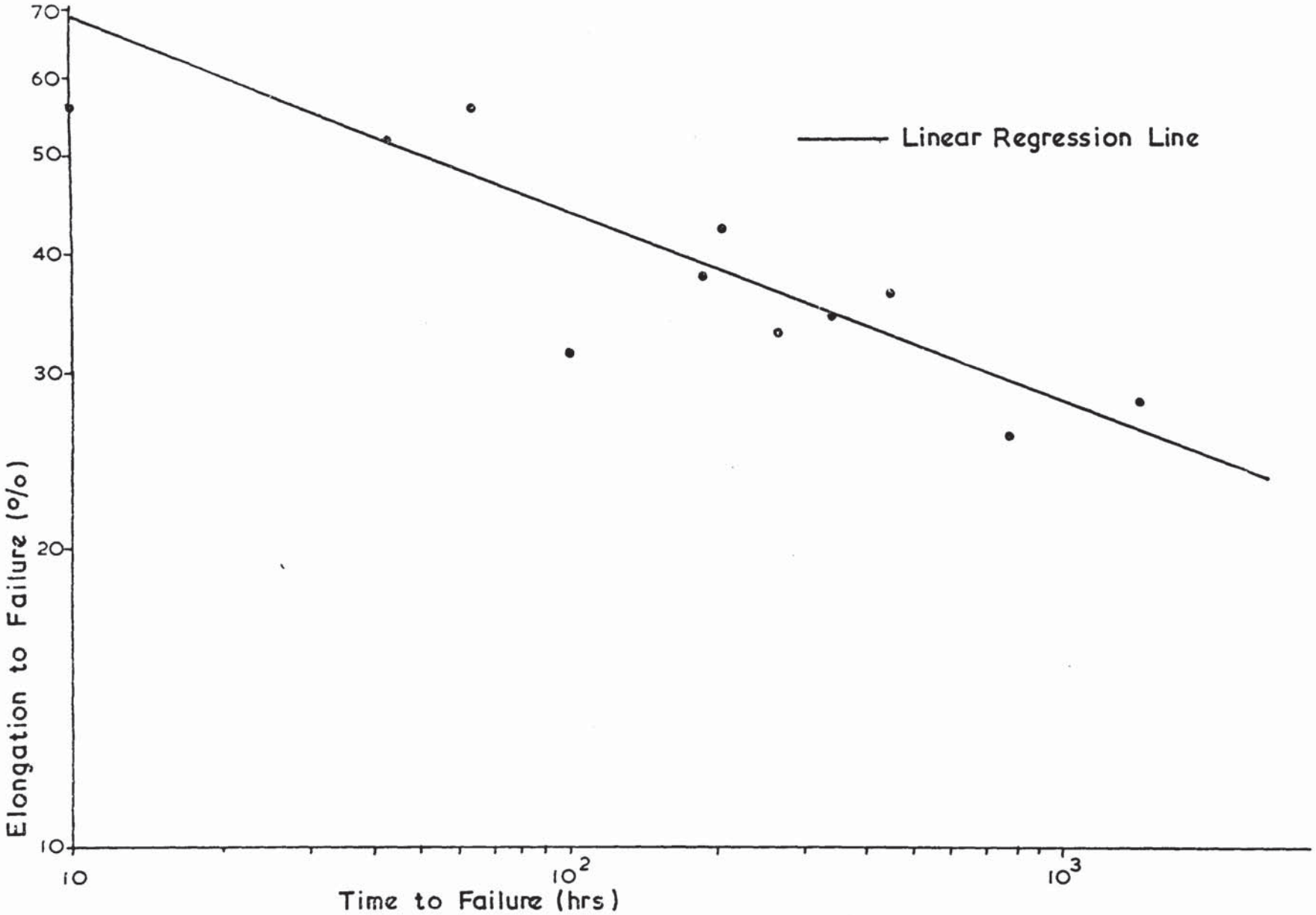

FIG. 37. Variation of Elongation to Failure with Failure Time.

time for crack initiation from the notch, t_i, were selected and at each time, the displacements between the pair of lines at the same r values were measured. Using the displacements measured at t_s as the initial "gauge lengths" at various distances from the notch, the additional displacements at the later times were found and strain and strain rate, $\dot{\varepsilon}$, values were calculated. Since the measurements were only taken once the specimen was in secondary creep, the equation $\dot{\varepsilon} = A\sigma^n$ where A and n are constants for a given temperature, was used to calculate the steady state stress, σ, acting at various distances ahead of the notch.

Fig. 38 shows the variation of strain rate with distance from the notch for the test performed at 750°C. and cross-head displacement rate of $1{\cdot}2 \times 10^{-5}$ m. hr^{-1}. Secondary creep started after about 150 hours and the strain rates at various times after this, but before crack initiation occurred, have been calculated at varying distances from the notch root. It can be seen that at times of 162·7, 182·7 and 199·2 hours, the curves coincide but at 228·5 hours the strain rates, up to about 1·5 mm from the notch, are higher. A constant strain rate region extending up to about 0·3 mm from the notch occurs and then decreases to a lower constant strain rate over the remainder of the ligament.

These three regions are also found in the other tests. The corresponding stress versus r graphs are shown in Fig. 39. It is found that the stress decreases according to $\sigma \propto r^{-s}$ after the constant stress region at the notch tip and before the nett section stress is reached. The values of s for the tests at $1{\cdot}2 \times 10^{-5}$ and $1{\cdot}1 \times 10^{-4}$ m. hr^{-1} and 750°C. are found to be 0·175 and 0·195 respectively. At 650°C. and $1{\cdot}2 \times 10^{-5}$ m. hr^{-1}, s was found to be 0·129.

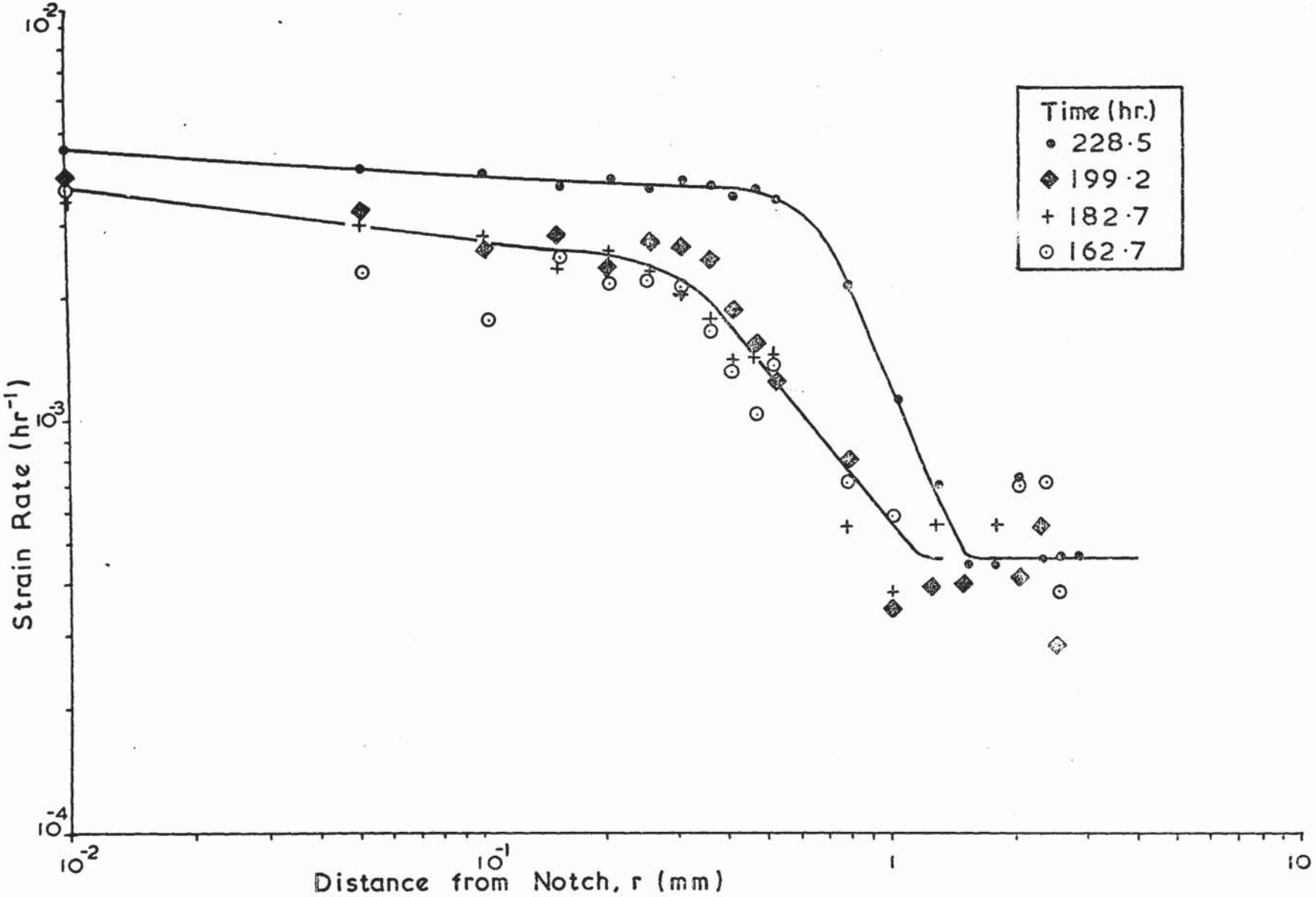

FIG. 38. Variation of Strain Rate with Distance from Notch.

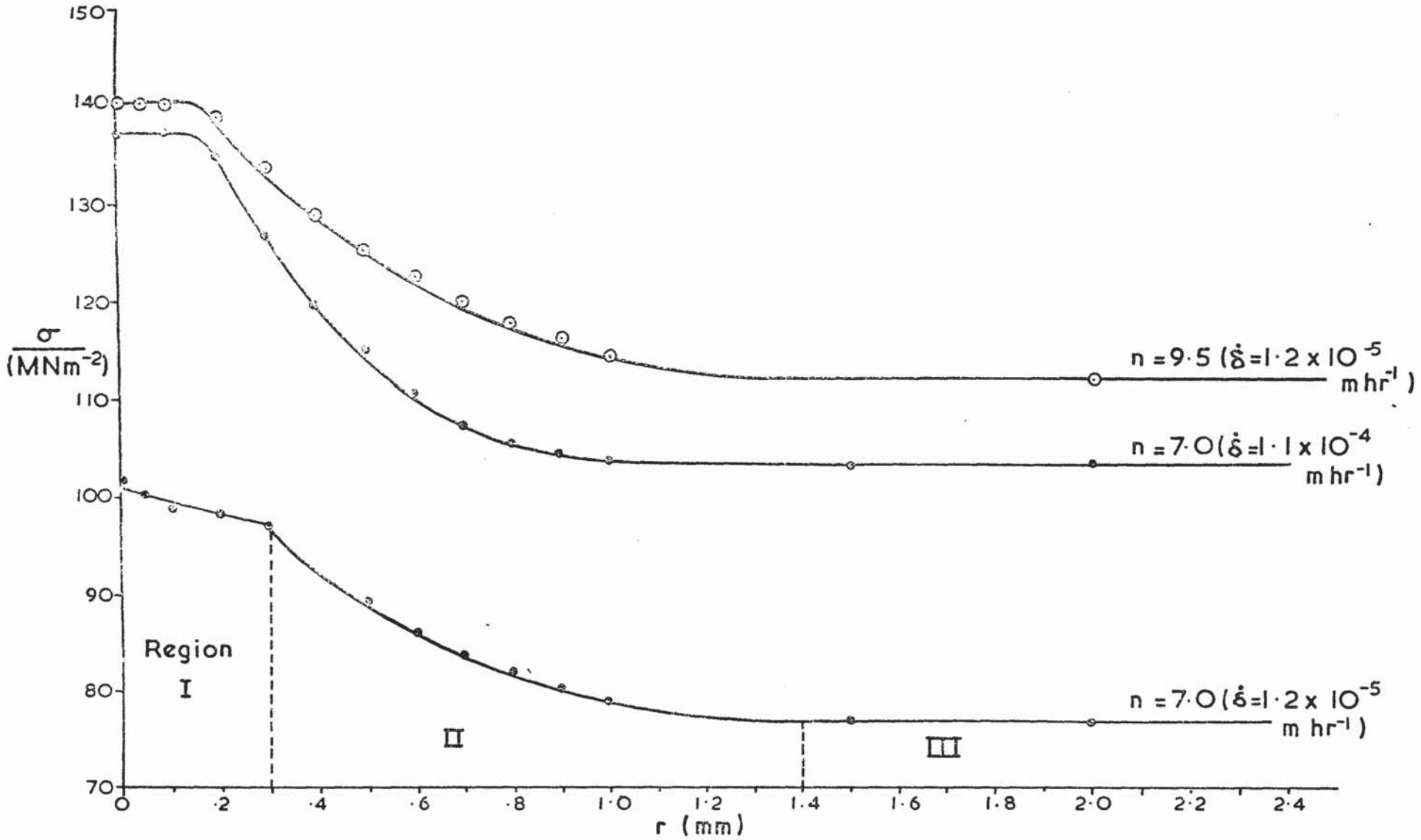

FIG. 39. Variation of Stress with Distance from Notch as a Function of n Value and Displacement Rate ($\dot{\delta}$).

4. 1.5. Microscopic aspects of crack growth from notches.

Further tests were performed at 750°C. at a cross-head displacement rate of $1{\cdot}2 \times 10^{-5}$ m. hr^{-1}, and interrupted after differing times so that the creep cracks grew to various lengths. The growth of the cracks were recorded on cine film and a typical example of the growth is shown in Fig. 40. Tests were also interrupted before macroscopic crack initiation occurred. After the required time, the tests were interrupted and the specimens were cooled under constant load conditions.

After removal from the rig, the specimens were sectioned so that the notched region could be examined metallographically. Longitudinal sections were ground and polished to a 1 μm finish and then very lightly etched in dilute aqua regia. The specimens were examined in the scanning electron microscope.

The region ahead of the notch in a specimen that had been interrupted before macroscopic cracking occurred was closely examined. It was found that extensive microscopic creep cracking had occurred. This was clearly visible up to a distance of about 120 μm ahead of the notch, as shown in Fig. 41 (a). The creep cavities were examined at higher magnification and were generally associated with grain boundary particles (Fig. 41 (b)).

Another specimen was interrupted when the creep cracks from the two notches were each about 3 mm. long (i.e. $(\frac{2a}{W}) = 0{\cdot}74$, where 2a = length of both creep cracks and notches, W = width of specimen (Fig. 42 (a)). Detailed examination showed extensive cracking ahead of the crack tip with indications that individual cavities had interlinked with each other (Fig. 42 (b)). Again association of the cavities with grain boundary particles was the usual observation (Fig. 42 (c)). The middle of the ligament, well away from either crack tip was examined and cracking was observed on a few grain boundaries.

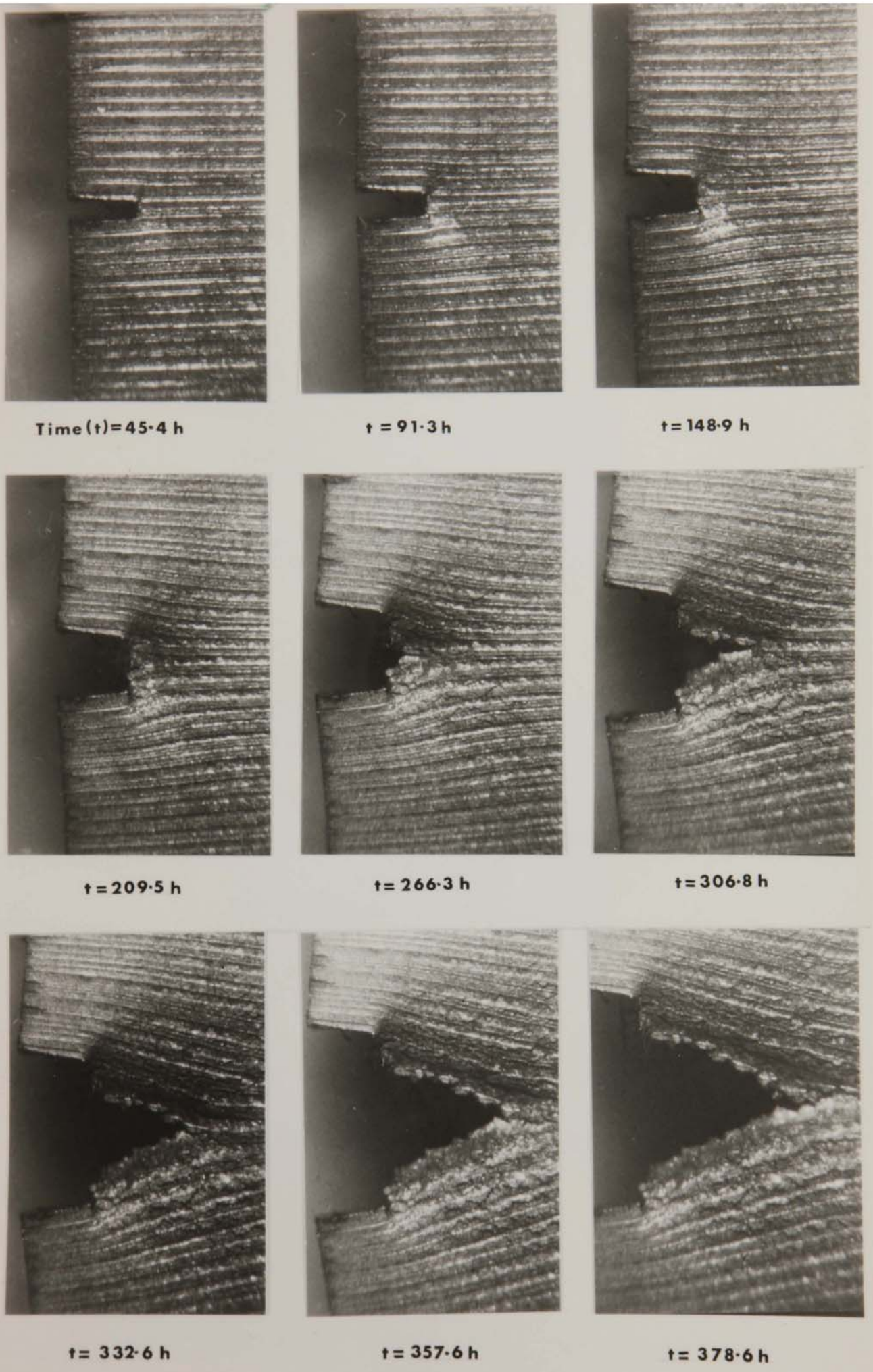

FIG. 40 Creep crack growth in type 316 steel at 650°C (Magnification ≃ 20X)
($\dot{\delta} = 1{\cdot}2 \times 10^{-5}$ m.hr.$^{-1}$)

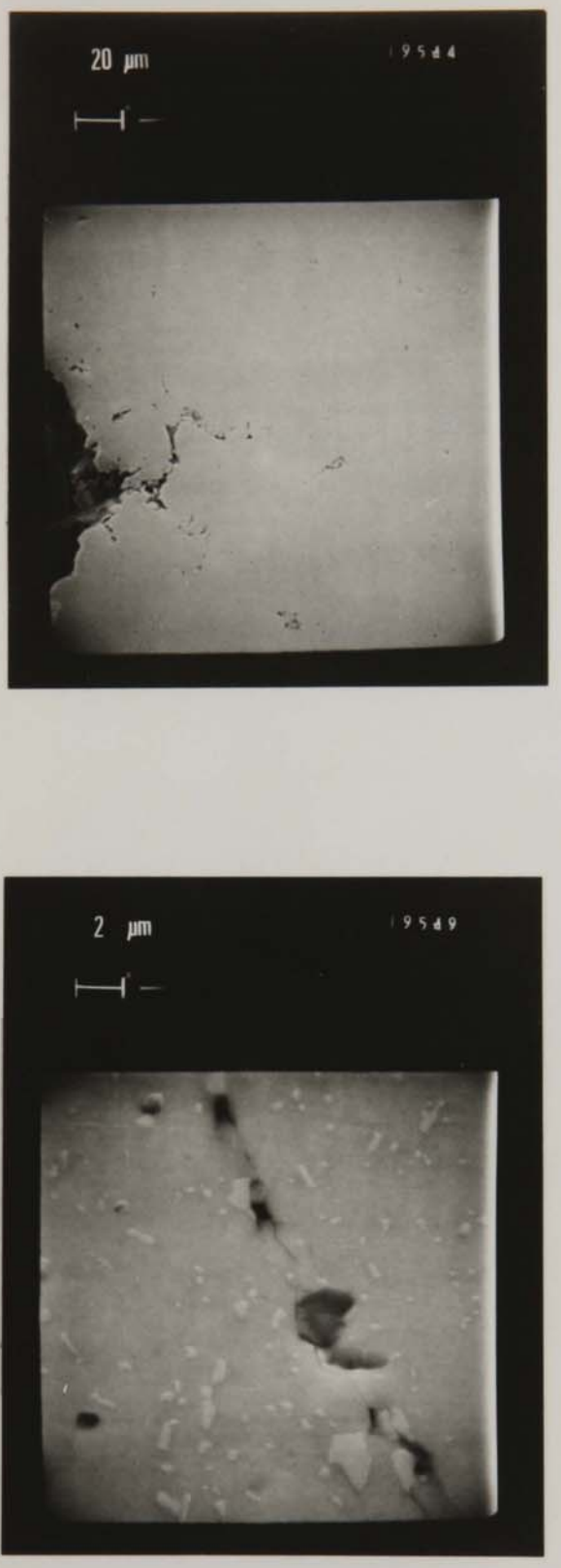

FIG 41 Creep cracking ahead of notch in type 316 steel at 750°C

(a)

(b)

Stress axis

(c)

FIG 42 Creep crack growth in type 316 steel at 750°C

A specimen interrupted after each creep crack had grown to about 1 mm (i.e. $(\frac{2a}{W}) = 0{\cdot}3$) is shown in Fig. 43 (a). Typical cavities ahead of the crack tips are shown in Fig. 43 (b). In this specimen, no sign of cracking in the middle of the ligament could be found.

(a)

(b)

Stress axis

FIG 43 Creep crack growth in type 316 steel at 750°C

4. 2. The effect of environment on creep crack growth in stainless steels

4. 2.1. The effect of iodine vapour on the creep rupture properties of M316 stainless steel.

Tensile creep rupture tests were performed on plain and double edge notched specimens of M316 stainless steel. The specimen dimensions are given in Table 6.

The specimens were stressed at 750 and 650°C. (± 1°C at each temperature) under constant loads giving the initial gross section stresses shown in Table 10, and tested following the procedure described previously. The tests were performed on notched and plain specimens at each of the gross section stresses in air, vacuum (pressure ~ 0·03 μbar) and iodine vapour (pressure ~ 0·92 μbar).

4. 2.1.1. Plain Specimens.

The results of the plain specimen tests at 80 MN m^{-2} and 750°C. are shown in Fig. 44 and it can be seen that the failure time and strain are reduced in the presence of iodine vapour compared with air and vacuum environments. The air test failed in the longest time but with intermediate ductility. These observations were confirmed by the reduction of area measurements. The other 750°C. tests at 95 and 182 MN m^{-2} showed similar features but the variation in failure time decreased with increased stress. The 650°C. tests showed similar results but with only slightly increased endurance in air compared with vacuum.

The failure times and strain parameters of the plain specimens are shown in Table 10 and Fig. 45.

Optical metallography of the crack morphology and distribution showed that specimens tested in iodine vapour contained sharp, intergranular cracks extending several grain facets from the

TABLE 10

Creep Rupture Results of Plain M316 Specimens

Temp. ($T^{o}C$)	Environ -ment	Failure Time (hrs.)	Strain (%)	Reduction of Area (%)	Strain Rate ($hr.^{-1}$)	Gross Stress (MNm^{-2})
750	I_2	307.3	29.9	35.8	6.44×10^{-4}	80
750	Air	607.5	39.2	45.8	4.10×10^{-4}	80
750	Vac	359.4	56.7	69.9	7.92×10^{-4}	80
750	I_2	98.8	27.0	38.0	2.03×10^{-3}	95
750	Air	347.8	33.7	33.0	6.44×10^{-4}	95
750	Vac	138.0	75.1	79.4	2.48×10^{-3}	95
750	I_2	0.86	32.7	53.0	2.89×10^{-1}	182
750	Air	1.47	55.0	73.4	1.90×10^{-1}	182
750	Vac	1.21	49.5	66.0	1.94×10^{-1}	182
		1.27	55.7	78.1	2.23×10^{-1}	182
650	I_2	92.9	19.1	29.2	1.07×10^{-3}	190
650	Air	186.1	38.4	52.8	8.71×10^{-4}	190
650	Vac	167.8	48.1	71.6	1.20×10^{-3}	190
650	I_2	293.5	7.80	22.5	1.38×10^{-4}	150
650	Air	775.5	26.34	37.4	1.96×10^{-4}	150
650	Vac	771.5	43.0	71.5	3.10×10^{-4}	150

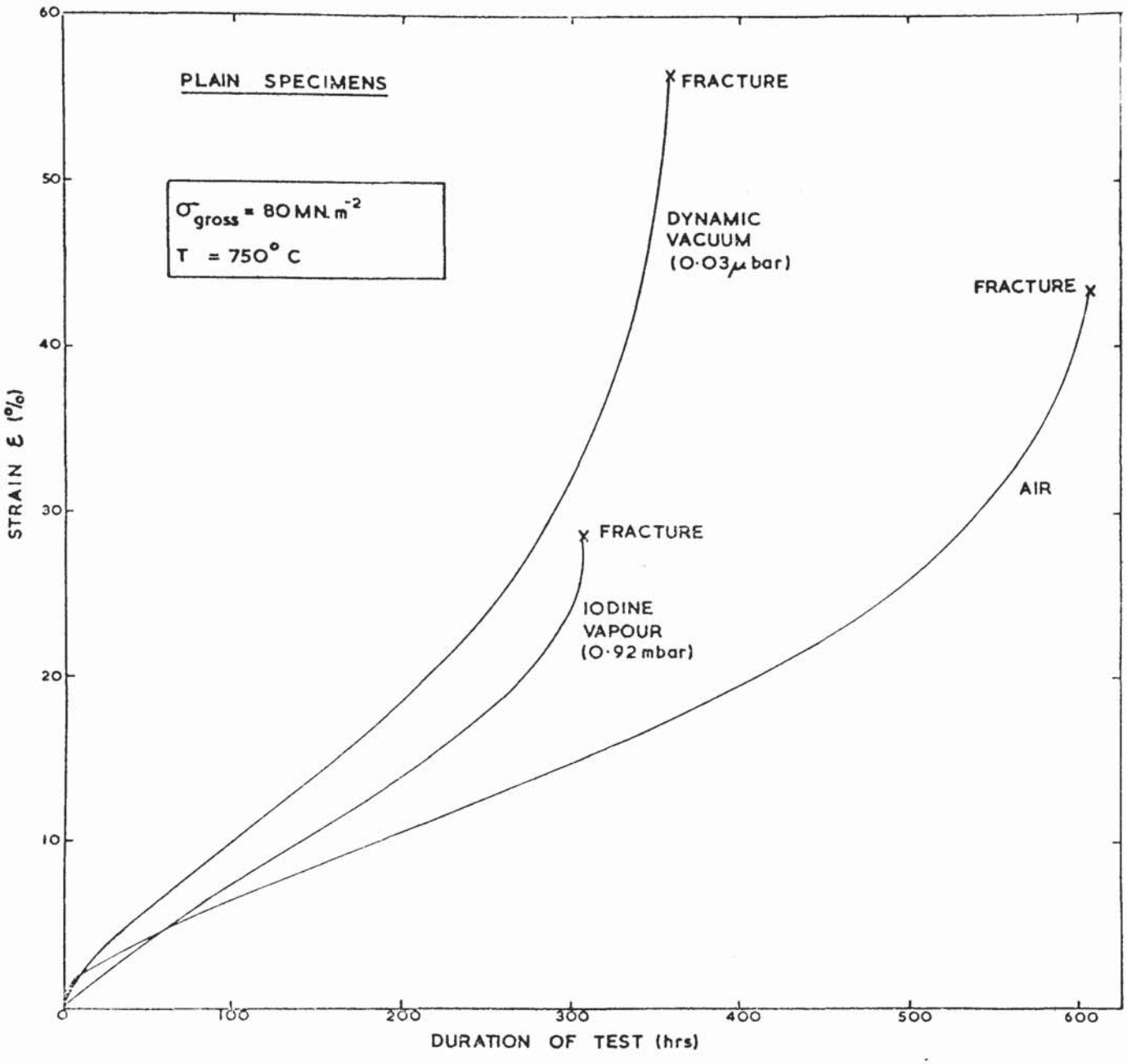

Figure 44. Overall engineering strain versus time curves for plain specimens of M316 steel tested at 80 MN m^{-2} and 750°C.

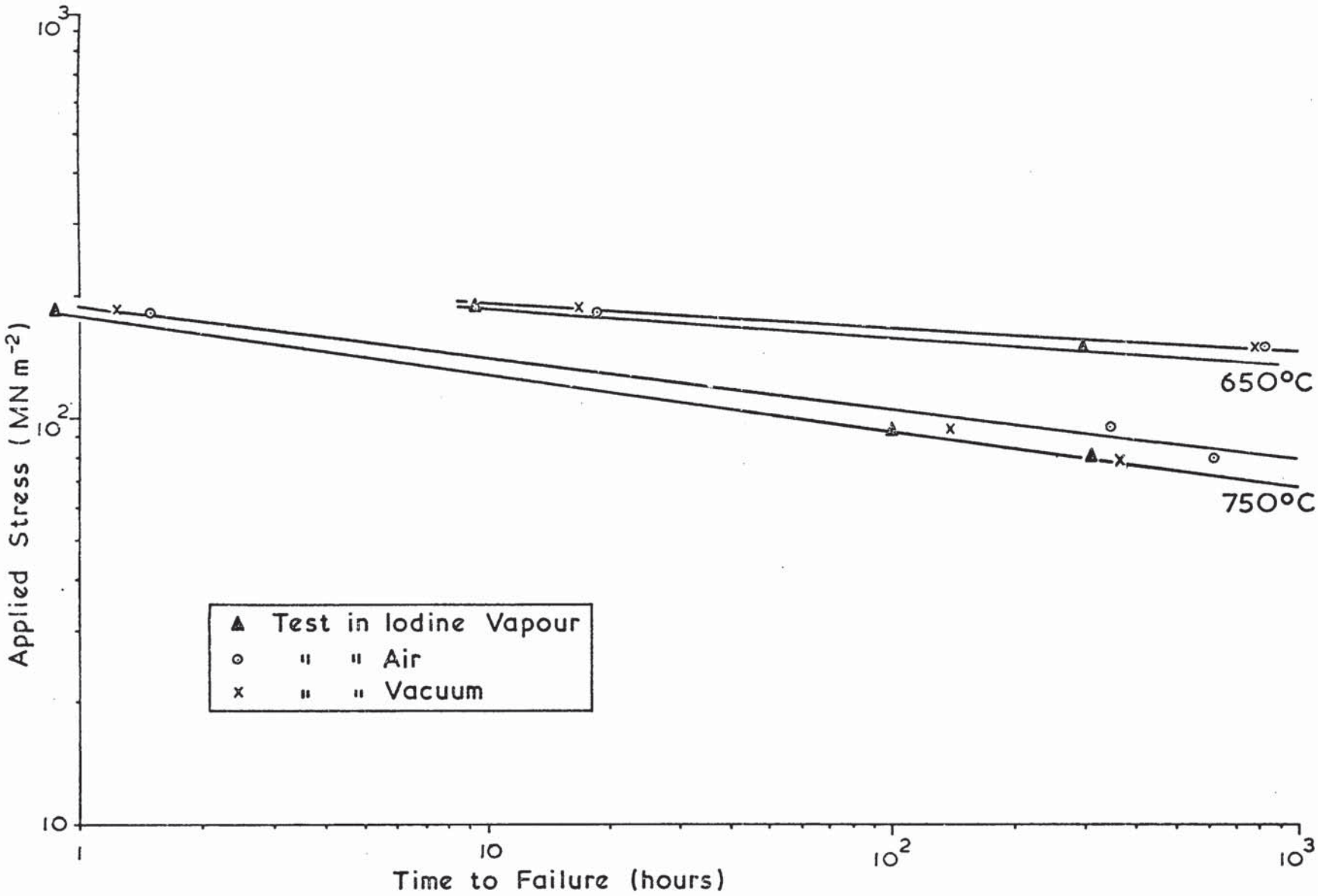

FIG. 45. Creep Rupture of Plain M316 Steel Specimens.

surface, along the whole gauge length. There was little evidence of grain deformation (Fig. 46a). The air specimens also showed cracking from the surface but most of the cracks were not as clearly intergranular as the iodine specimens and some transgranular cracking was observed (Fig. 46b). The vacuum specimens showed little evidence of surface cracking with only a few rounded grain boundary cavities distributed throughout the gauge length (Fig. 46c). Scanning electron micrographs of the fracture surfaces at 750°C. showed similar behaviour. The iodine specimens exhibited extensive regions of intergranular fracture extending inwards from the surface and a transgranular region towards the centre where final failure occurred (Fig. 47a). In the air specimens, oxidation products tended to mask some of the surface features but the fracture mode appeared to be mixed trans and intergranular (Fig. 47b). A ductile fracture occurred in the vacuum specimens evidenced by considerable necking and the presence of cusps in the necked region (Fig. 47c).

4. 2.1.2. Notched Specimens.

The results of the tests at 750 and 650°C. are shown in Table 11.

The results of the notched specimen tests at 80 MN m^{-2} and 750°C. are shown in Fig. 48 and again the failure time and overall extension of the iodine specimen were reduced compared with the air and vacuum tests. The amount of reduction in failure time by the iodine vapour decreased with increasing stress level (Fig. 49).

The notch opening displacement to initiate cracking (δ_i) at each stress level and temperature is plotted against initial nett section stress in Fig. 50. At 750°C., the embrittling effect of iodine vapour reduced δ_i in the 80 and 95 MN m^{-2} tests in contrast with the specimens tested in vacuum which gave the largest displacement at both stress levels. The intermediate values for the air specimens

a

b

c

FIG 46 Surface cracks in gauge length of specimens tested in (a) iodine vapour (b) air (c) vacuum at 80MNm^{-2} and 750°C Stress axis horizontal

Magnification X 200

a

b

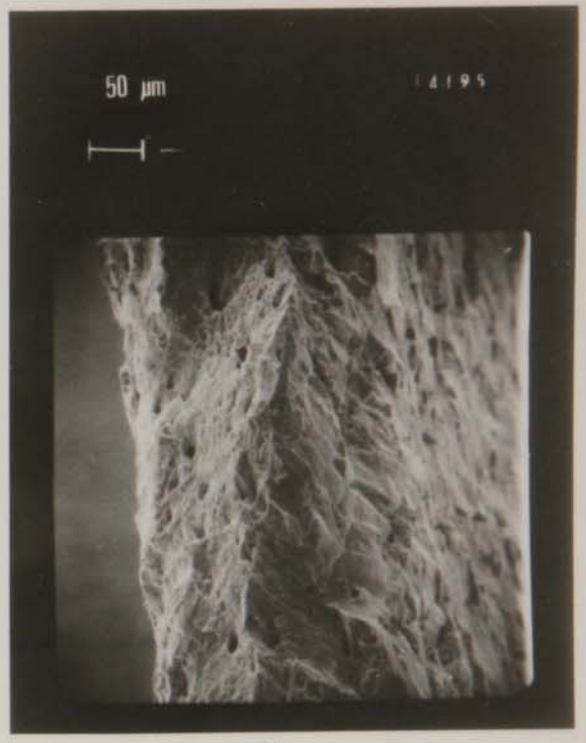

c

FIG 47 Scanning electron micrographs of fracture surfaces after (a) iodine vapour (b) air (c) vacuum tests at $80 MN m^{-2}$ and $750^{\circ}C$.

TABLE 11

Results of Notched M316 Stainless Steel Specimens

Temp (^{o}C)	Gross-section Stress (MNm^{-2})	Nett-section Stress (MNm^{-2})	Failure Time (hrs.)	Environment
750	80	96	57.4	I_2
750	80	98	136.1	Air
750	80	98	119.8	
750	80	98	142.2	Vac
750	95	112	33.6	I_2
750	95	114	49.1	Air
750	95	115	50.8	Vac
750	95	115	60.6	
750	182	219	0.24	I_2
750	182	218	0.32	Air
750	182	217	0.31	Vac
650	190	227	14.3	I_2
650	190	226	36.8	Air
650	190	227	31.9	Vac
650	150	192	62.3	I_2
650	150	194	136.5	Air
650	150	196	143.1	
650	150	194	147.7	Vac

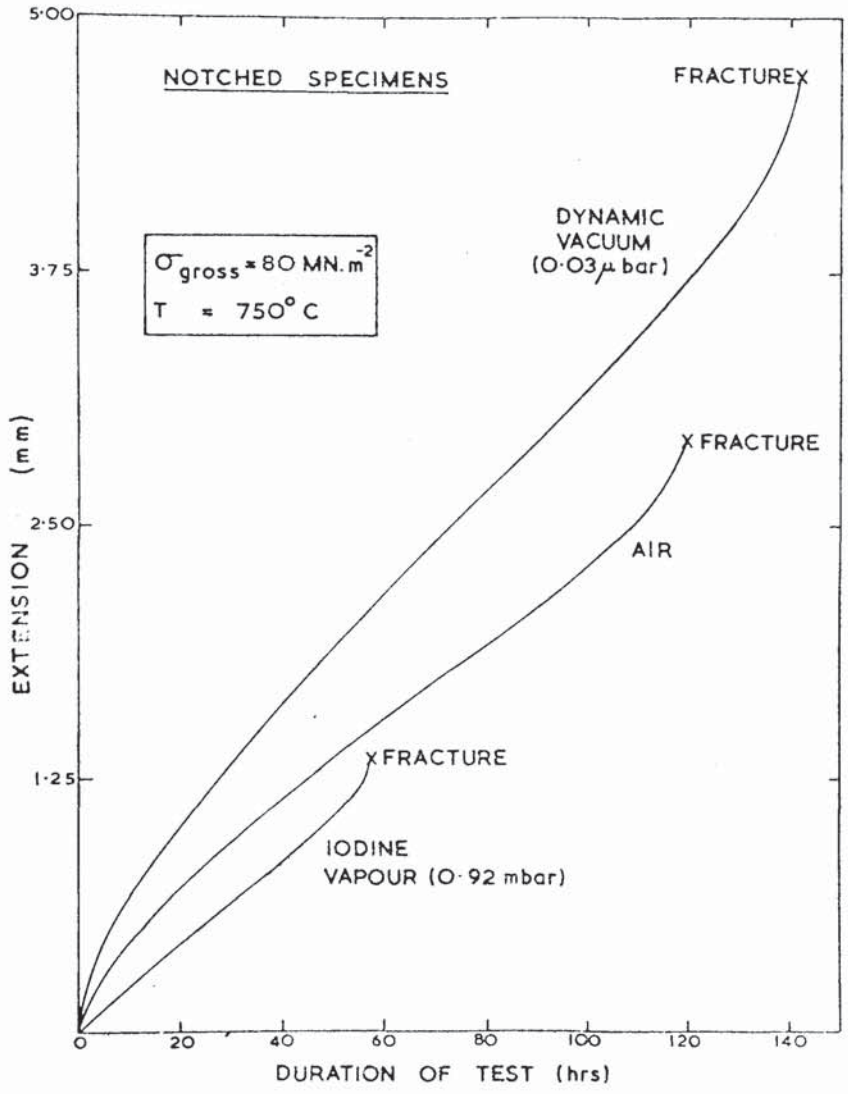

igure **48**. Overall elongation versus time curves for notched specimens of M316 steel tested at 80 MN m^{-2} and 750°C.

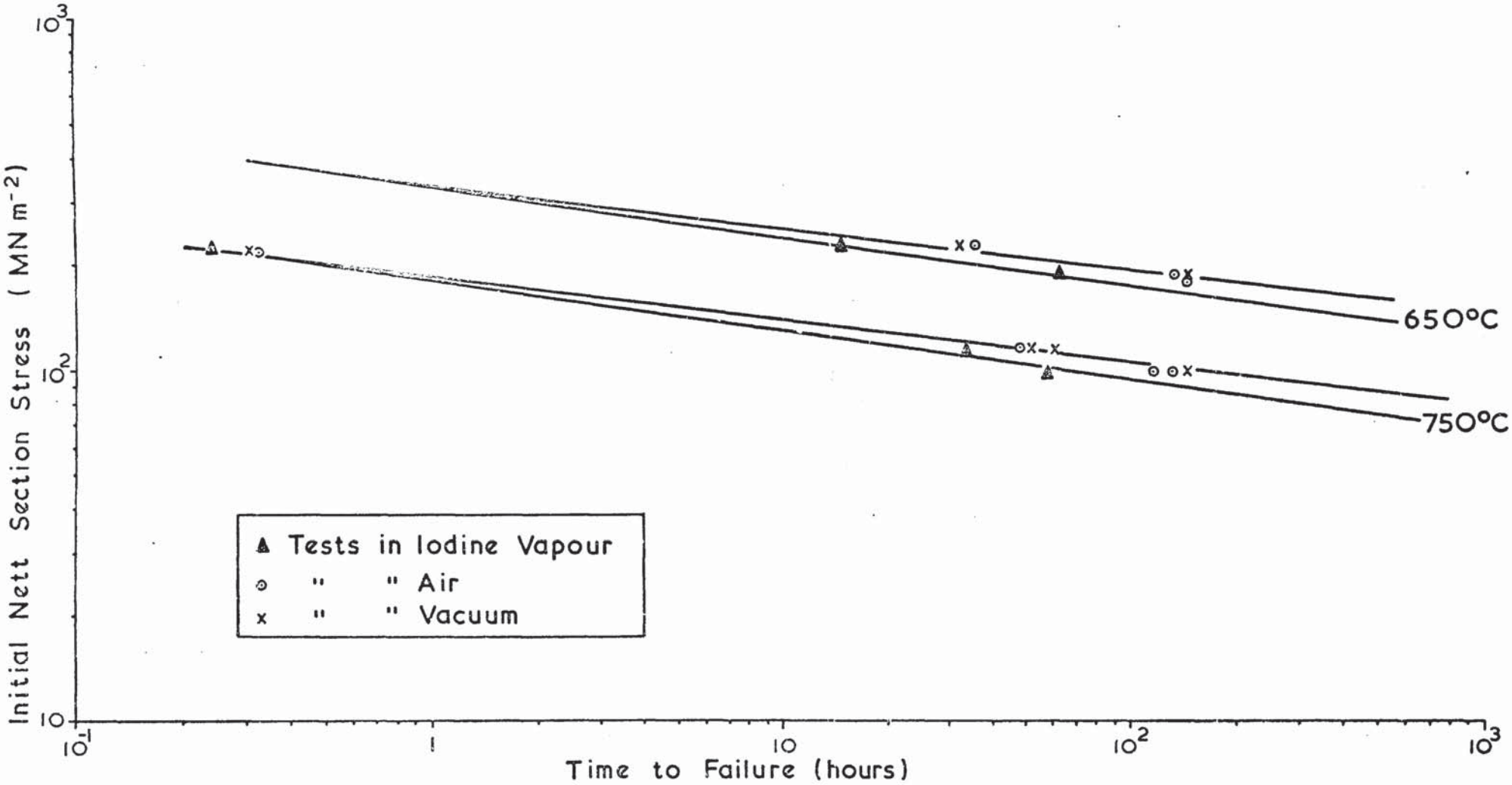

FIG. 49. Creep Rupture of Notched M316 Steel Specimens.

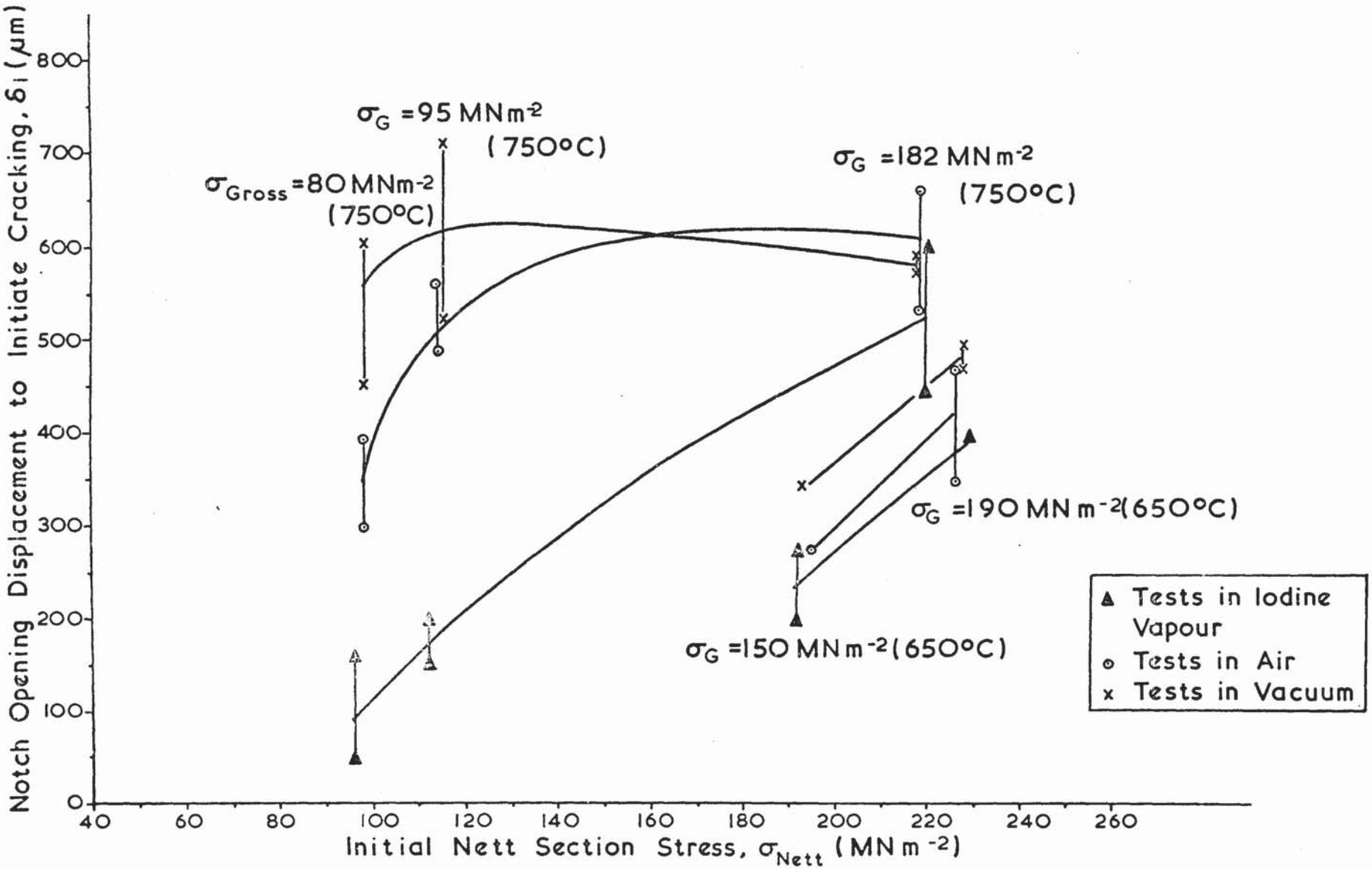

FIG. 50. Variation in δ_i with Initial Nett Section Stress at 650 and 750°C.

indicate a more marked reduction of the initiation displacement in the longer term 80 MN m^{-2} tests. A similar variation is shown in Fig. 51 where the times for crack initiation from the notch (t_i) are plotted against the initial nett section stresses. The 182 MN m^{-2} tests showed little effect of environment on δ_i and t_i. The iodine vapour also reduced δ_i and t_i at 650°C. but the reduction was less marked than at 750°C. for similar failure times. The reduction in δ_i also decreased with increasing stress.

The creep crack propagation rates were calculated and have been plotted against the crack opening displacement rates (obtained from the notch region extension method) in Figs. 52-56 for the various stresses at both temperatures; a linear relationship is found in each case. At 750°C., the 80 MN m^{-2} tests indicate that crack propagation in the specimen exposed to iodine vapour occurred with least ductility and, for a given crack opening displacement rate, was faster than the air and vacuum specimens by factors of about 1·5 and 2·2 respectively. However, in the 95 MN m^{-2} tests, the propagation rates in iodine vapour fell within the 95% confidence limits of the vacuum test, indicating that the iodine had little effect on the propagation rate. Crack propagation in air was about a factor of 1·6 faster than in vacuum at 95 MN m^{-2}. At 182 MN m^{-2} environmental effects on crack propagation rates were negligible.

At 650°C., iodine vapour had little effect on crack propagation rates for given rates of crack opening displacement. Crack propagation rates in air were about a factor of 1·7 faster than in vacuum at 190 MN m^{-2} and 650°C. At 150 MN m^{-2}, any enhancement of crack propagation rates in air was slight. At this stress the crack propagation rates in vacuum were higher than the iodine vapour by up to a factor of 5.

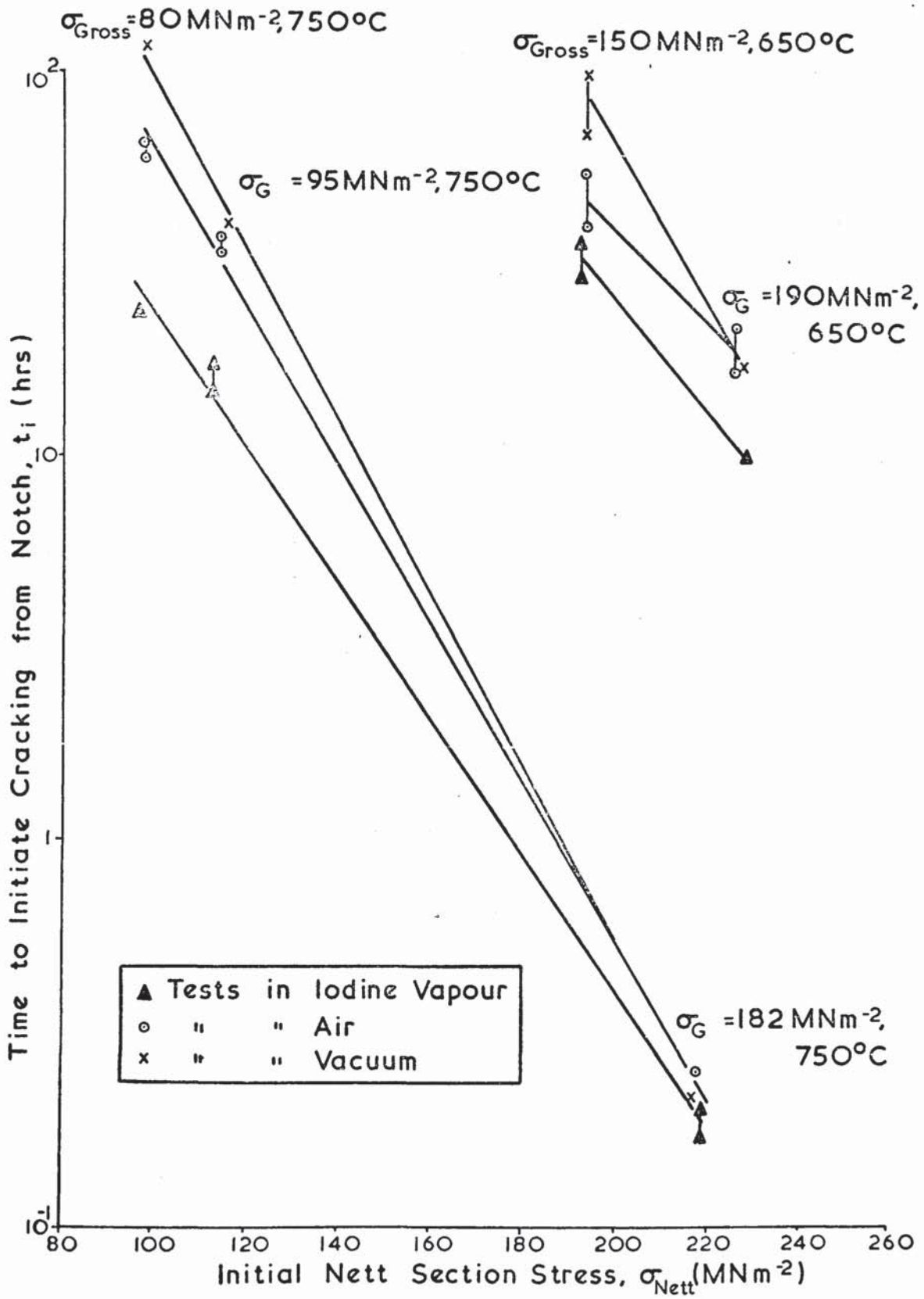

FIG. 51. Variation of Time for Crack Initiation with Initial Nett Section Stress in M316 Steel.

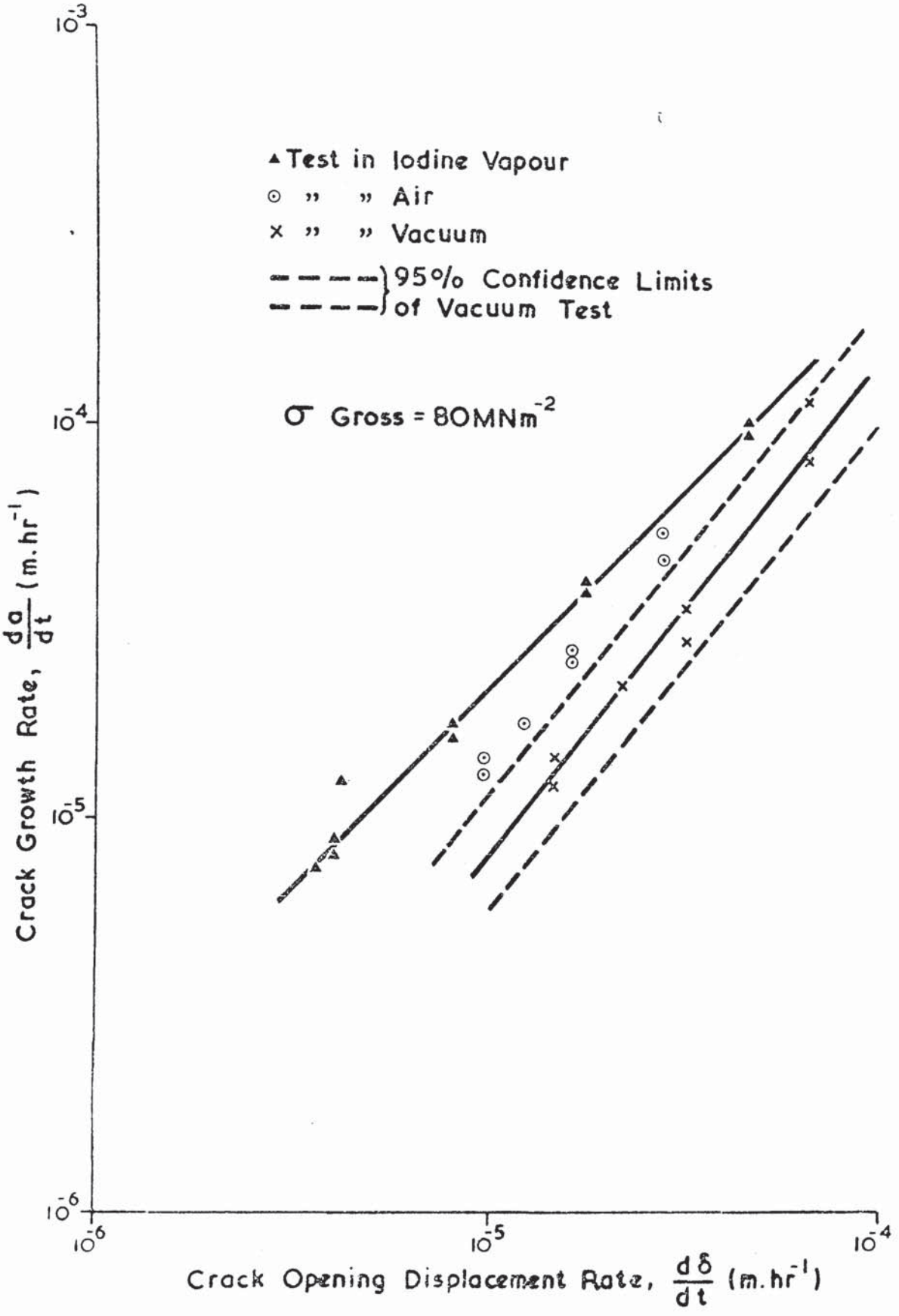

Figure 52 Crack growth rate versus crack opening displacement rate for M316 steel specimens tested at 80 MN m^{-2} and 750°C.

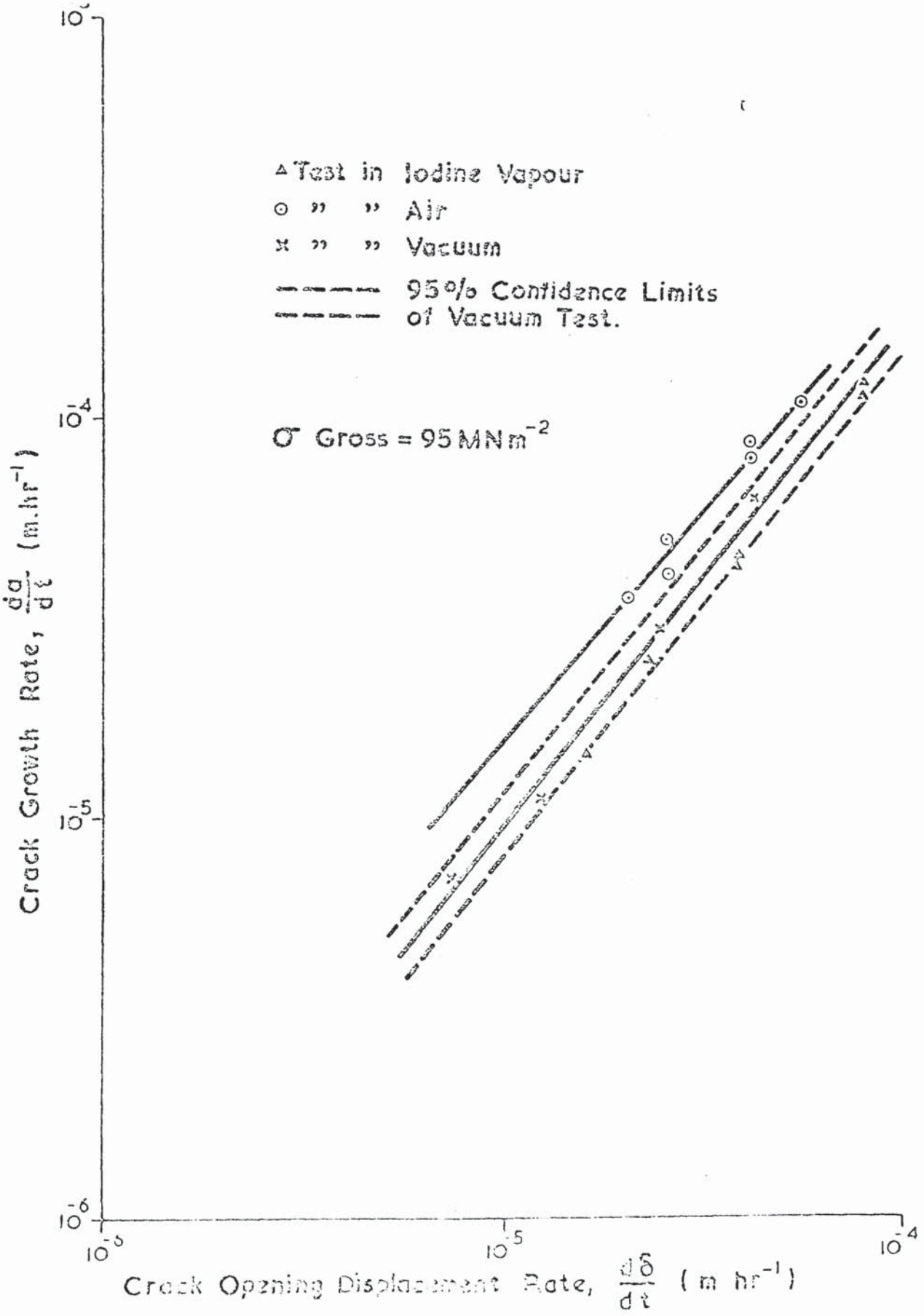

Figure 53. Crack growth rate versus crack opening displacement rate for M316 steel specimens tested at 95 MN m^{-2} and 550°C.

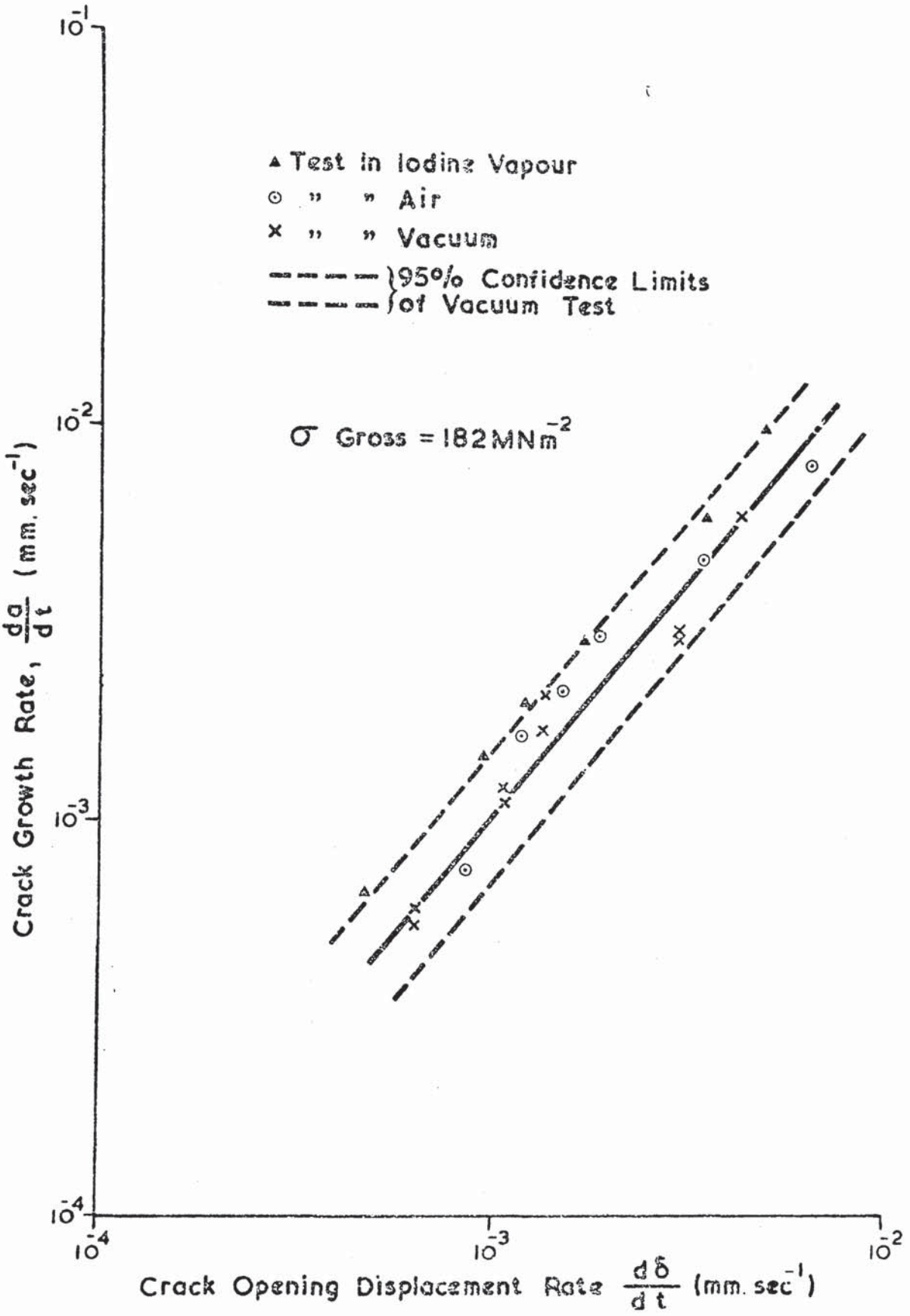

Figure 54. Crack growth rate versus crack opening displacement rate for M316 steel specimens tested at 182 MN m^{-2} and 750°C.

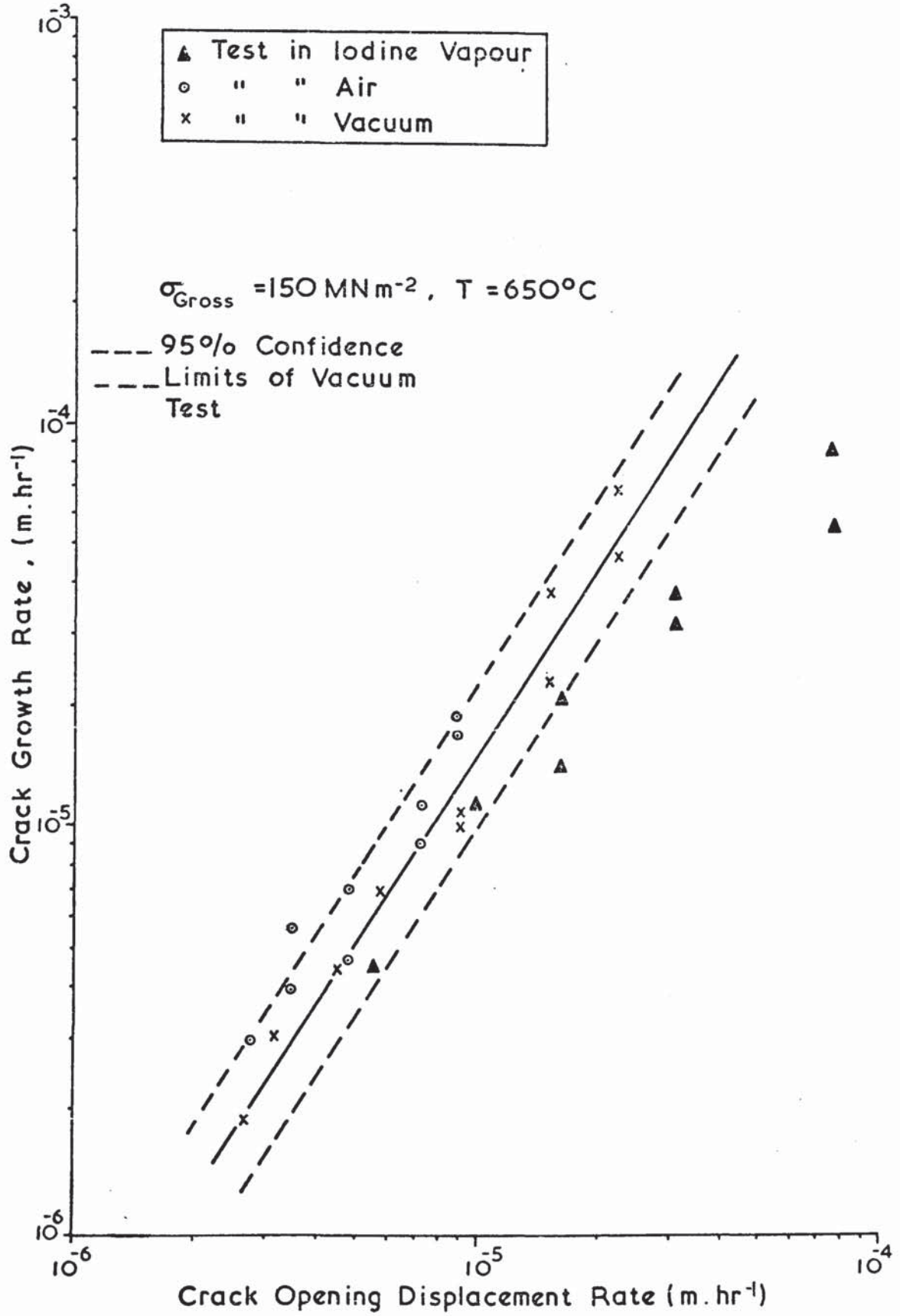

FIG. 55. Crack Growth Rate versus Crack Opening Displacement Rate for M316 Steel Specimens Tested at 150 MNm^{-2} and 650°C.

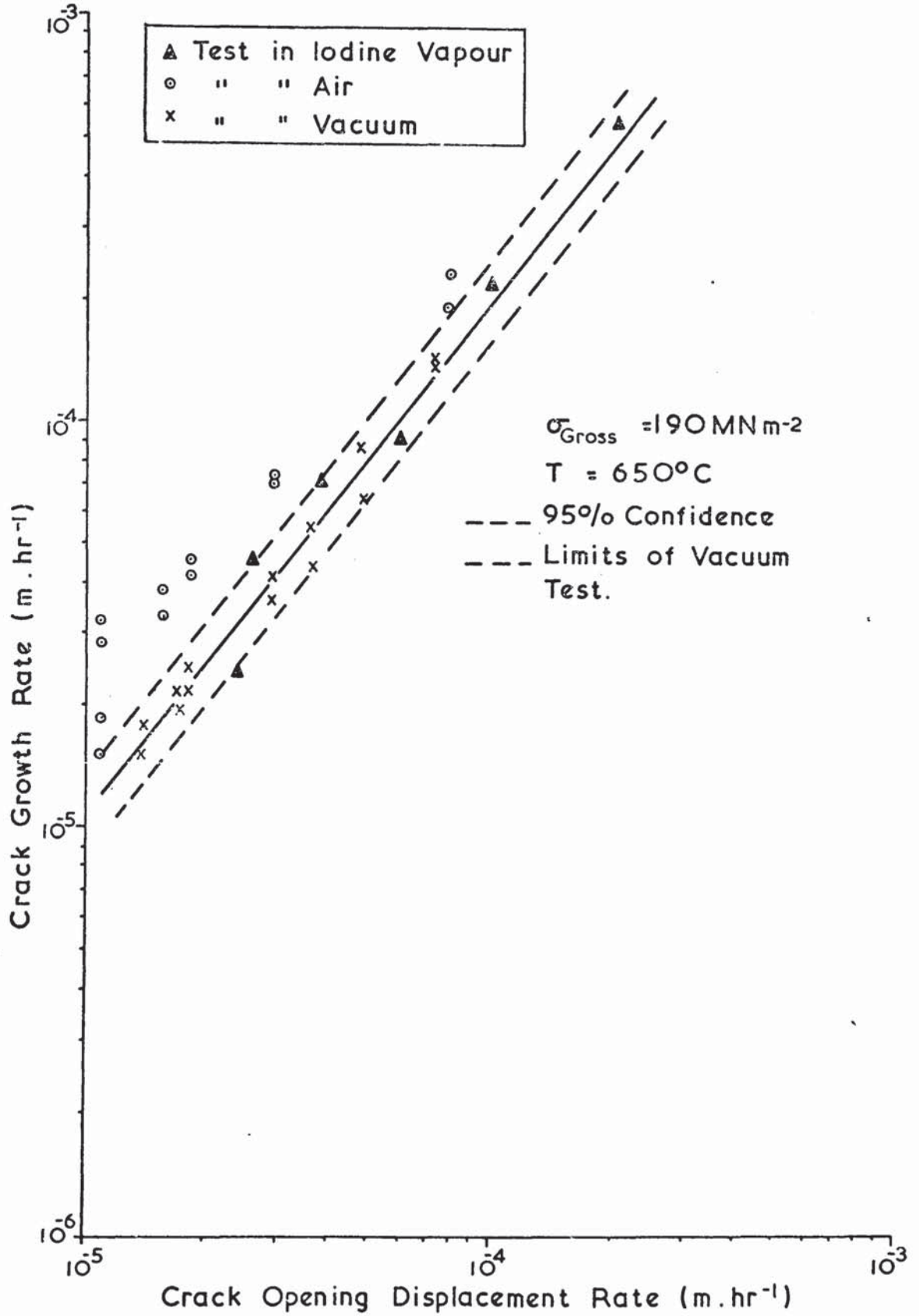

FIG. 56. Crack Growth Rate versus Crack Opening Displacement Rate for M316 Steel Specimens Tested at 190 MNm^{-2} at 650°C.

4. 2.2. The effect of neutron irradiation on the creep rupture properties of 20Cr/25Ni/Nb stainless steel.

Tensile creep rupture tests have been performed on plain and double edge notched specimens of irradiated and unirradiated primary recrystallised 20Cr/25Ni/Nb stainless steel. The specimens for irradiation were prepared from one batch of steel but there was insufficient material for all the unirradiated control specimens, so it was necessary to manufacture some of these specimens from another batch of 20Cr/25Ni/Nb steel. The analyses of the two batches are given in Table 4 and the specimen dimensions in Table 6. Thus, absolute comparisons between the irradiated specimens of batch 1 and unirradiated specimens of batch 2 are not possible but trends in the creep rupture behaviour of the irradiated and unirradiated specimens can be compared.

The specimens were irradiated at 40°C. to doses of $6 - 7 \times 10^{19}$ thermal neutrons/cm^2, $2 - 3 \times 10^{19}$ fast neutrons/cm^2 in the Herald Reactor.

The tests were performed in vacuum (0·03 μbar) at 750°C. under constant load conditions using the apparatus described previously. All specimens were left for 24 hours at 750°C. before the load was applied.

4. 2.2.1. Plain specimens

The results of the plain specimens are shown in Figs. 57 and 58. Also included in these figures are data obtained by Hitchcock (to be published) on irradiated and unirradiated specimens of batch 1 steel. For comparison, some other unirradiated 20Cr/25Ni/Nb data from different batches are also shown (Nicholson, unpublished work).

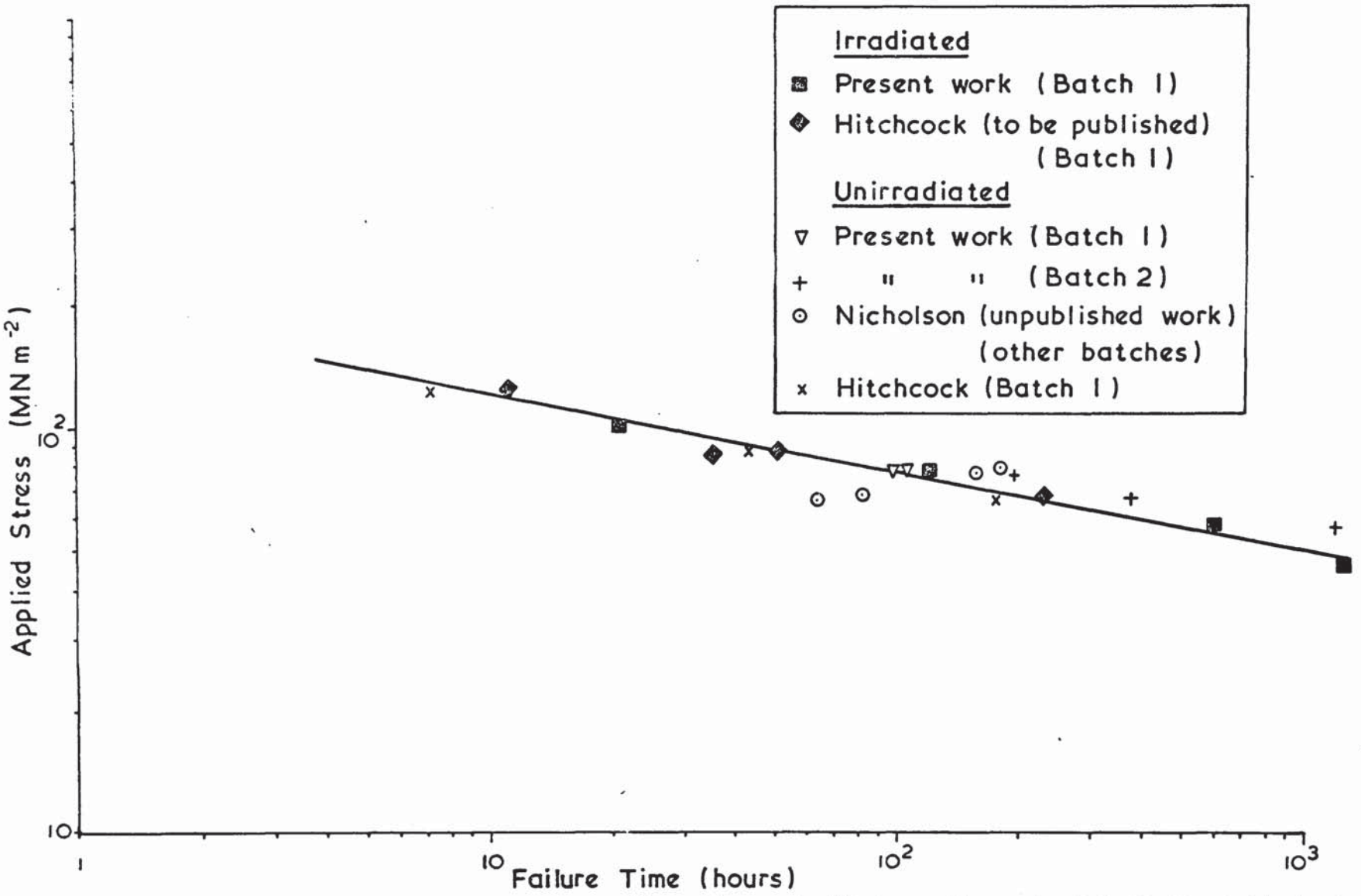

FIG. 57. Creep Rupture of Irradiated and Unirradiated 20Cr/25Ni/Nb Steel.

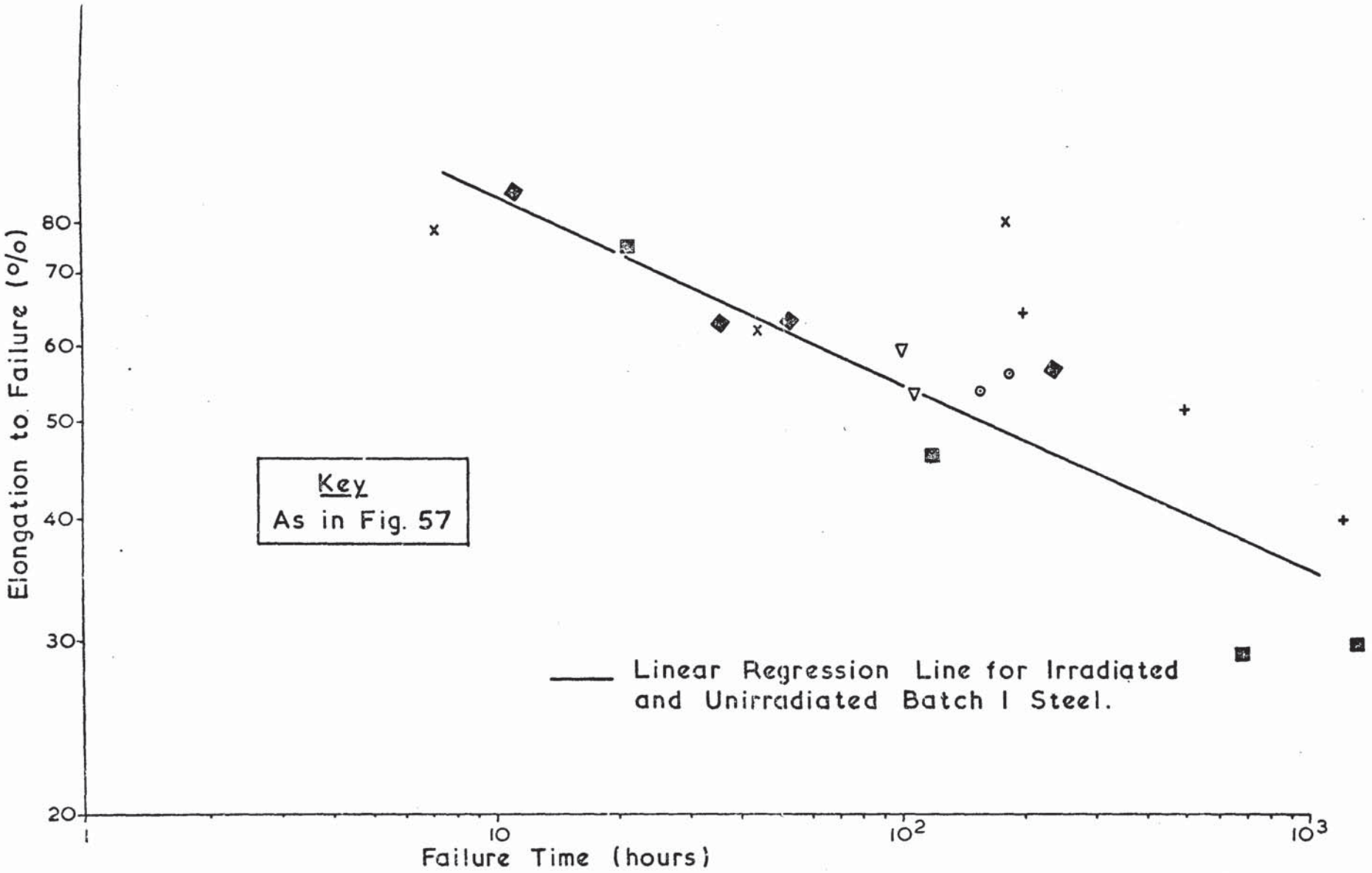

FIG. 58. Variation of Elongation to Failure with Failure Time in Irradiated and Unirradiated 20Cr/25Ni/Nb Steel.

When the irradiated and unirradiated batch 1 specimen results are compared, it can be seen that contrary to previous investigations, the effects of irradiation are negligible. Indeed all the irradiated specimens failed with ductilities greater than about 30% and for failure in less than 100 hours, the ductility was greater than about 60%. Boron autoradiographs were produced of the batch 1 steel and are shown in Fig. 59. It can be seen that the boron was evenly distributed with no segregation to grain boundaries. A few boron-rich particles showed up.

The endurance and ductility of the batch 2 specimens for a given stress are up to factors of 2 and 1·5 respectively greater than the irradiated and unirradiated batch 1 specimens. However, this is within the batch to batch scatter observed in many materials. The batch 2 specimen results show that the ductility decreases with increasing time, as observed in the batch 1 material.

4. 2.2.2. Notched Specimens.

Fig. 60 shows the results of the irradiated batch 1 steel and the unirradiated batch 2 steel specimens. As observed with the plain specimens, the endurances of the notched batch 2 specimens are about a factor of 2 greater than the batch 1 specimens, reflecting the batch to batch scatter.

Crack initiation displacements, δ_i, and propagation rates have been measured by the NRE method. Fig. 61 shows that δ_i for a given initial nett section stress is greater in the batch 2 material, but both batches show decreasing δ_i values with decreasing stress. When the crack propagation rates are compared (Fig. 62), no significant differences in behaviour can be detected and the irradiated crack growth data fall within the 95% confidence limits of the unirradiated specimens, which can be described by the equation:-

X130

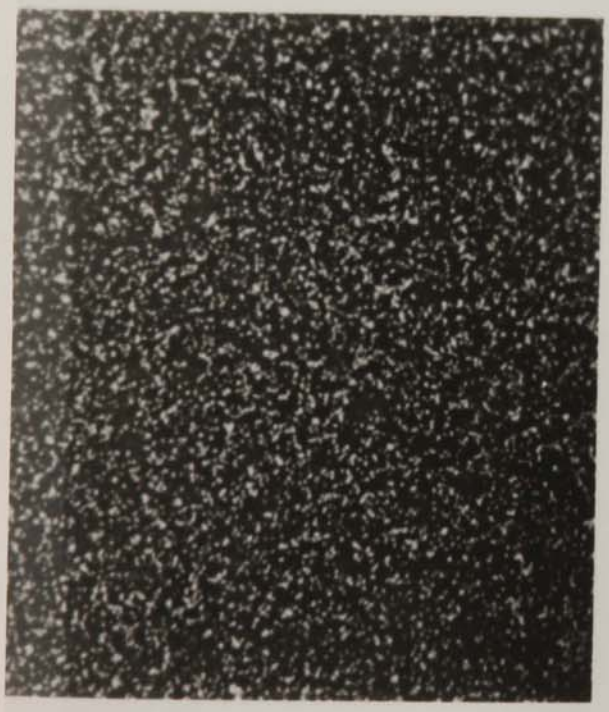

X500

FIG 59 Boron autoradiographs of primary recrystallised 20Cr/25Ni/Nb stainless steel

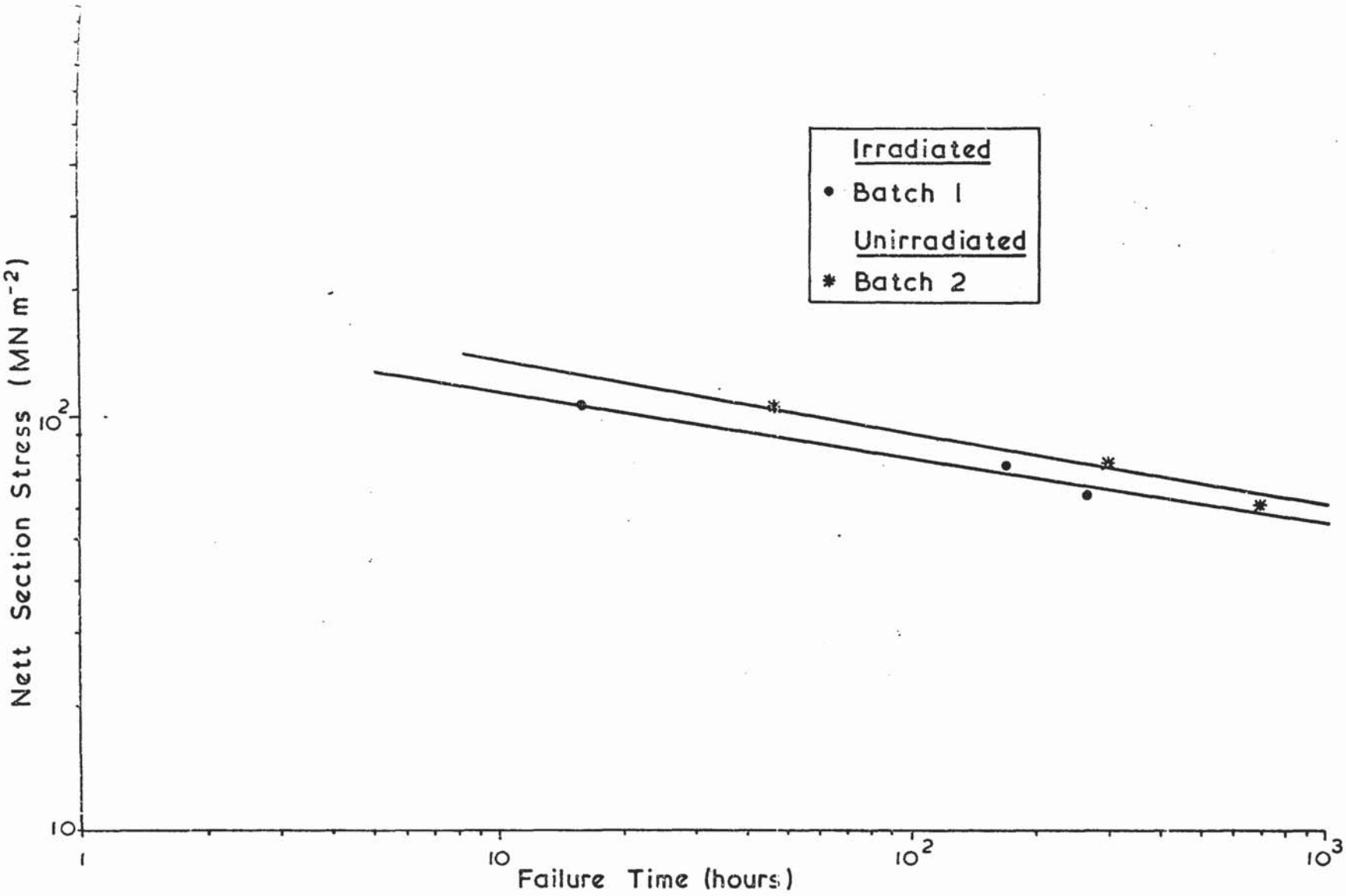

FIG. 60. Creep Rupture of Notched Specimens of Irradiated and Unirradiated 20Cr/25Ni/Nb Steel.

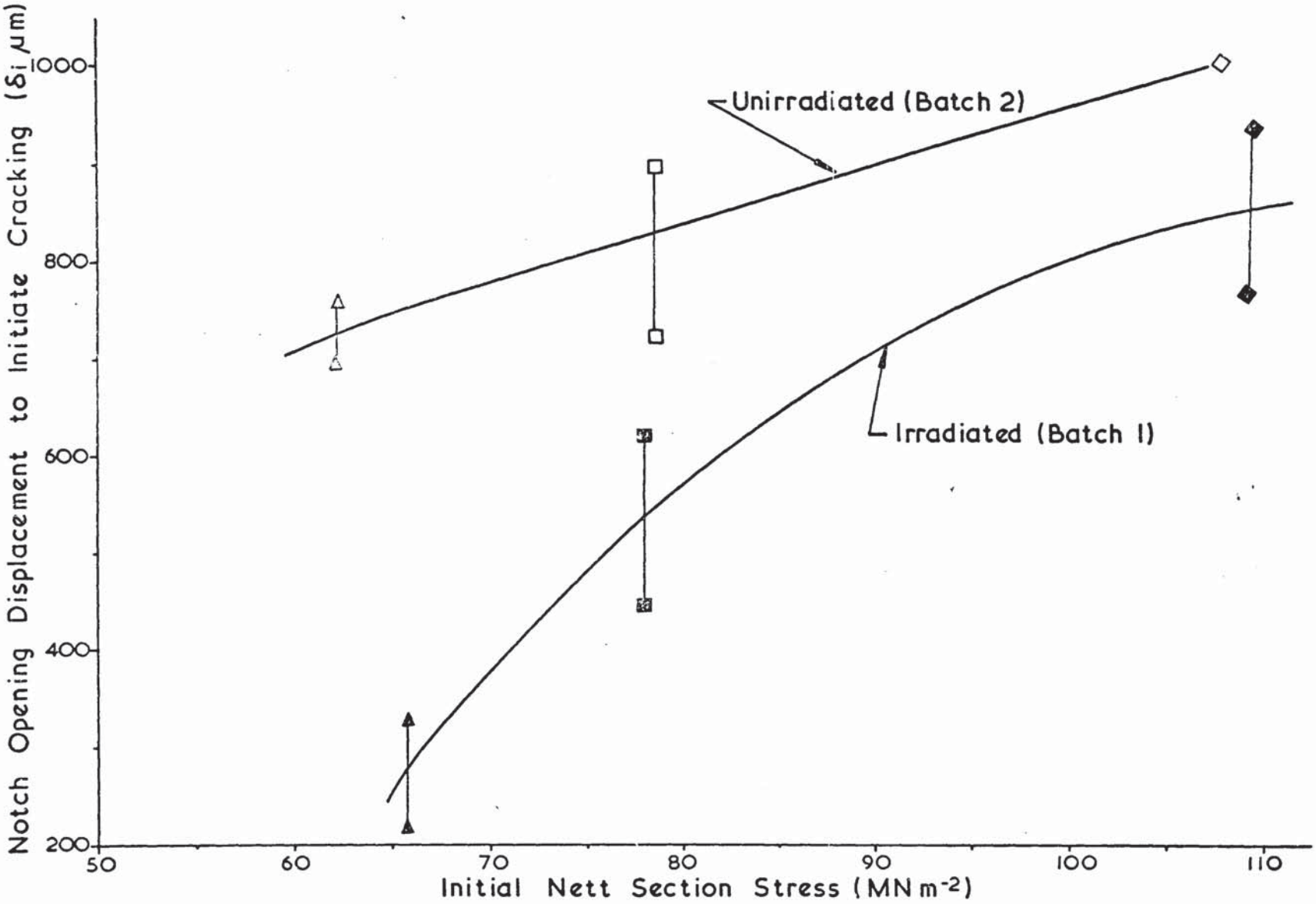

FIG. 61. Variation of δ_i with Initial Nett Section Stress.

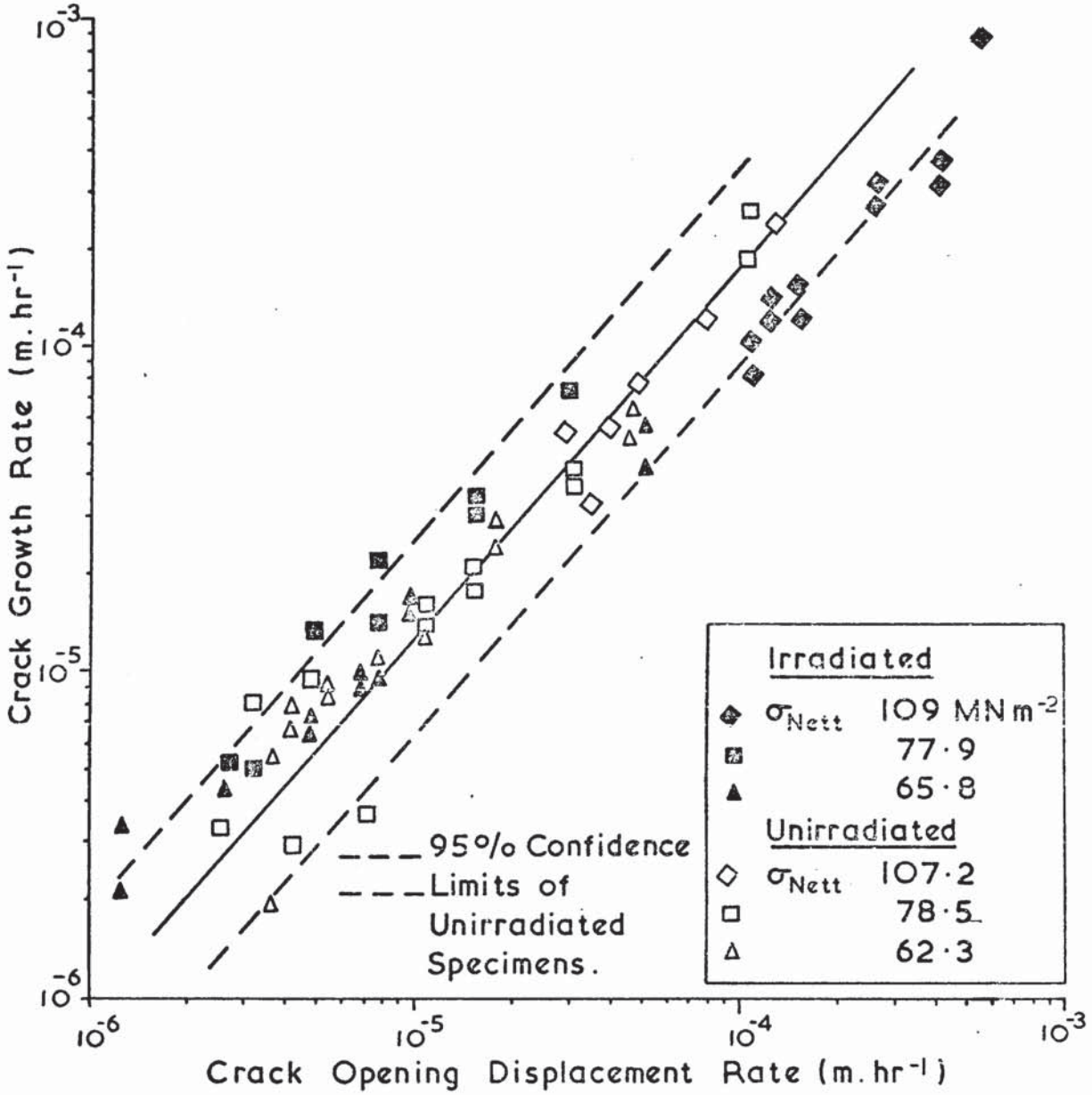

FIG. 62. Variation of Crack Growth Rate with Crack Opening Displacement Rate in Irradiated and Unirradiated 20 Cr/25 Ni/Nb Steel.

$$\dot{a} = 6 \cdot 81 \, \dot{\delta}^{1 \cdot 1}$$

The fracture surfaces of the irradiated and unirradiated specimens were examined in the scanning electron microscope and examples are shown in Fig. 63. It can be seen that ductile transgranular fracture occurred in both the irradiated and unirradiated specimens at high stresses with considerable necking in the thickness direction. (Figs. 63 (a) and (b)). At lower stresses, the fracture mode was mainly intergranular as shown in Figs. 63 (c) and (d).

(a) Irradiated, $\sigma_{Nett} = 109{\cdot}1 MNm^{-2}$

(b) Unirradiated, $\sigma_{Nett} = 107{\cdot}2 MNm^{-2}$

(c) Irradiated, $\sigma_{Nett} = 65{\cdot}8 MNm^{-2}$

(d) Unirradiated, $\sigma_{Nett} = 62{\cdot}3 MNm^{-2}$

FIG 63 Scanning electron micrographs of fracture surfaces of notched specimens of irradiated and unirradiated 20Cr/25Ni/Nb steel tested at 750°C

CHAPTER 5.

DISCUSSION

5.1. Creep Crack Growth in AISI type 316 stainless steel.

5.1.1. Criteria controlling creep crack growth.

In tests on SEN and NCH specimens of type 316 stainless steel at 740°C., it was found that for a given stress intensity factor, K_I, the crack growth rates were different in the two types of specimen (Fig. 25). If a real link existed between K_I and creep crack growth rate, then for a given K_I, the measured growth rate would have been independent of geometry.

Qualitatively, it can be imagined that the elastically determined stresses at the instant of applying the constant load will tend to be relaxed by creep. Thus the rate and extent to which the stresses relax prior to rupture will determine the applicability of LEFM. The initial state of stress given by LEFM is given by equation (4). Clearly the elastically determined stress is very large where r is small and thus a locally high creep rate will modify the stress field. The rate of relaxation of this stress field is calculated in Appendix 1. An expression for the time taken for the stress to relax from the elastically determined level to a lower level is derived. This equation is then applied to the A.I.S.I. type 316 stainless steel specimens at 740°C and it is found that the time for the local stress to relax from the high elastically determined level to 1·5 times the nett section stress is only about 60 seconds in a creep test lasting many hours. Clearly, this stress relaxation makes the K-distribution of stress, predicted by LEFM, inapplicable. The experimentally measured stress distribution mentioned previously confirms this and will be discussed later.

It has been found that the nett section stress is a successful criterion for creep crack growth and the different curves

in Fig. 25 can be shown to be quantitatively consistent with the hypothesis that the nett section stress is the controlling parameter. A crack is imagined to propagate across a SEN and a NCH specimen, both subjected to load L, and thus at each crack length K_I and nett section stress can be calculated. K_I values are calculated for the SEN and NCH specimens using equations (32) and(33a and b) respectively. Nett section stresses are calculated by the equation, $\sigma_{Nett} = \frac{L}{B\ (W-a)}$, where B = 1 unit for both specimens and W = 20 units for the NCH specimens and 10 units for the SEN specimens. Fig. 64 shows the relationship between K_I and σ_{Nett}, both divided by load L, as the crack is imagined to propagate across the SEN and NCH specimens. The curves of the two specimen geometries are quite distinct and their different slopes can be related to the difference between the curves in Fig. 25 since, from equation (34),

$$\Delta\sigma_{Nett} = \frac{\Delta\dot{a}}{p N \sigma_{Nett}^{p-1}}$$

so that,

$$\frac{\Delta\ (\sigma_{Nett}/_L)}{\Delta\ (K_I/L)} = \frac{1}{p N \sigma_{Nett}^{n-1}} \frac{\Delta\dot{a}}{\Delta K_I}$$

or, at the same σ_{Nett} in SEN and NCH specimens:

$$\frac{\left.\dfrac{\Delta\ (\sigma_{Nett}/_L)}{\Delta\ (K_I/_L)}\right)_{NCH}}{\left.\dfrac{\Delta\ (\sigma_{Nett}/_L)}{\Delta\ (K_I/_L)}\right)_{SEN}} = \frac{\left.\dfrac{\Delta\dot{a}}{\Delta K_I}\right)_{NCH}}{\left.\dfrac{\Delta\dot{a}}{\Delta K_I}\right)_{SEN}} \qquad (36)$$

From Fig. 25, the right hand side of equation (36) is about 6 (taking slopes where $\dot{a}$ and hence σ_{Nett} are the same). From Fig. 64, the left hand is also about 6 (again taking positions having

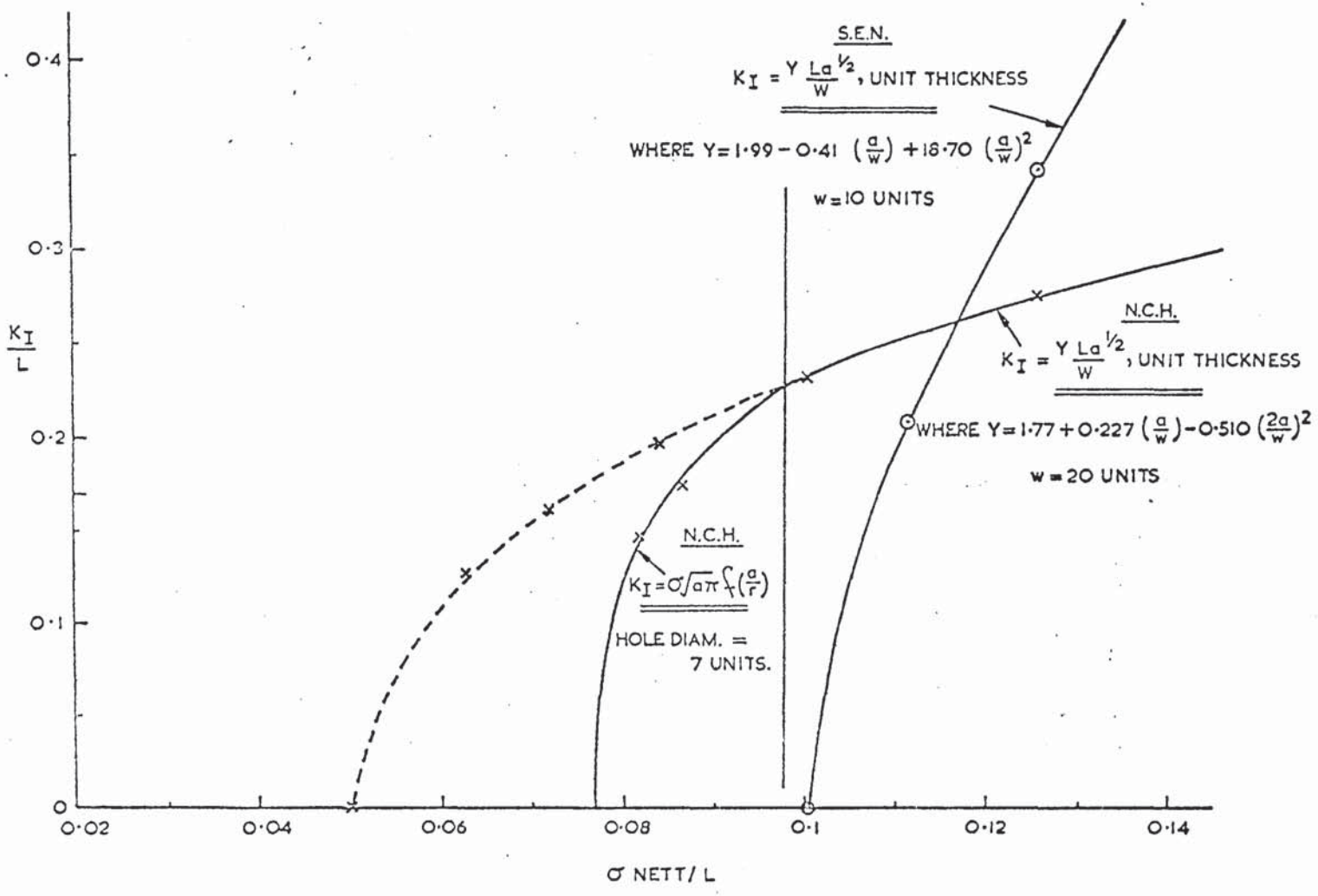

FIG 64 Variation in stress intensity factor, K_I, with nett section stress, σ_{Nett}, both divided by load L, for SEN and NCH specimens.

the same σ_{Nett}). These figures show that the results support the σ_{Nett} hypothesis even when they are plotted, as in Fig. 25, against K_I.

The applicability of equation (34) over the temperature range 600 to 850°C. for 316 stainless steel is demonstrated in Fig. 27. Table 9 indicates that p (equation (34)) and n (equation (15)) are equal. Equation (34) may now be written:

$$\frac{da}{dt} = \frac{N}{A} \dot{\epsilon} \qquad (37)$$

The displacement rate, $\dot{\delta}$, and the strain rate, $\dot{\epsilon}$, are related thus:

$$\dot{\delta} = l_o \dot{\epsilon} \qquad (38)$$

where l_o is the "gauge length" of the straining material. Substituting $\dot{\epsilon}$ from equation (38) into equation (37) gives:

$$\frac{da}{dt} = \frac{N}{A} \cdot \frac{1}{l_o} \cdot \frac{d\delta}{dt} \qquad (39)$$

Creep crack growth rates are therefore determined by the ligament displacement rates. This is because after the relaxation, the residual stress concentration at the crack tip ensures that the local strain rate is greater than the strain rate in the rest of the ligament, which is subjected to the nett section stress. However, across the notch region of specimens where bending moments are negligible, the displacement rate is constant. Accordingly, the "gauge length" at the crack tip is smaller than across the ligament and thus a localisation of strain occurs at the crack tip. This strain localisation, resulting from the crack tip stress and strain rate, causes further crack propagation to occur once a critical local strain has been exceeded. Therefore, creep crack propagation is governed by the crack tip strain and the displacement needed to achieve this strain is determined by the

degree of stress relaxation at the crack tip. Creep crack growth rates are therefore a function of the displacement rates at the crack tip and in the ligament, as has been found experimentally.

Further evidence which lends support to this conclusion is provided by the calculated activation energies in the temperature range 740 - 850°C. for the 316 stainless steel specimens. Apparent activation energies for crack growth of 352 - 372 $KJmole^{-1}$ are close to the apparent activation energies for creep of 345 - 416 $KJ\ mole^{-1}$ for stresses between 80 - 65 $MN\ m^{-2}$. The variation of these apparent activation energies with stress is thought to be a consequence of the temperature dependence of the crack growth and creep exponents (p and n respectively) illustrated in Fig. 29. A similar effect has been noted for the variation of creep activation energies in 20Cr/25Ni/Nb stainless steel by McLauchlin (1972).

The increase in apparent activation energy for temperatures below 740°C. needs further investigation to establish whether there is a change in rate controlling process. This possibility arises from the work of Mazza and Willoughby (1966) who found the creep activation energy at 600°C. to be 523 $KJ\ mole^{-1}$ and suggested that at this temperature creep occurred by cross-slip rather than by the dislocation climb mechanism observed by Garofalo et al (1963) at higher temperatures. The climb mechanism may have been suppressed by fine precipitates on the dislocations at 600°C., as has also been observed by Barnby (1965). However, further work on the mechanisms is needed before any definite conclusions can be reached.

When degeneration of the initial crack tip stress field occurs in creep, the nett section stress (in some cases incorporating an allowance for a bending component) should be generally usable to make predictions of creep crack growth rates. Indeed the reference stress (Williams and Price (1974)) or the equivalent stress (Haigh (1973)) are equal to the nett section stress for crack geometries

that do not include a bending component, as is the case for the NCH and double edge notched specimens tested here. The SEN specimens were long in order to reduce the rotation. Some limitations should be borne in mind, however. An incubation period before crack growth started was observed in the tests, so that equation (34) by itself would tend to underestimate the life of a structure. Another limitation is when creep modifies the stress applied to the crack as it would if this were generated by temperature differences, for example, or residual stresses. These situations are essentially "strain-controlled" and it may be more straightforward to adopt a strain-based crack growth parameter in place of σ_{Nett} such as the crack opening displacement (COD).

Wells and McBride (1967) have measured the COD(δ) during creep crack growth and commented that the deformations and δ in components might be satisfactorily correlated under creep conditions by application of general yielding stress analysis. In a study of creep rupture under the wedging action of oxide (Formby (1972)), the relationship between wedging displacement (i.e. δ) and crack growth has been investigated. The results indicate an approximately linear variation of crack length with δ after an initiation displacement required to start the cracking. This linear variation is consistent with a suggestion by McClintock (1968) that the angle (ω) developed at the tip of a propagating crack between the fractured surfaces is a characteristic of ductility. Thus,

$$a = \frac{1}{\omega} (\delta - \delta_i) \qquad (40)$$

where a is the crack length and δ_i is the COD to initiate cracking and thus allows the incubation period to be incorporated simply into the calculation. Measurements of δ and a on the type 316 stainless steel specimens show a similar relationship to apply for part of the specimen width (Fig. 34). Equation (40), therefore, allows the amount

of cracking to be calculated if δ and ω are known. Also differentiating this equation with respect to time, gives a linear relationship between crack growth rate and displacement rate as was found for equation (39). It can thus be seen that equation(39) and (40) are compatible.

5. 1.2. Macroscopic aspects of crack growth.

5. 1.2.1. Crack initation and propagation.

The occurrence of an initiation displacement and an approximately constant fracture angle have been established in the 316 steel specimens and δ_i and ω have been measured (Figs. 35 and 36). The fact that ω and δ_i are reproductibly measurable indicates that certain minimum displacements must be achieved for crack initiation and propagation.

Since crack growth rates are a function of ligament displacement rates, the observed constant fracture angle can be simply explained.

Since $\omega = \dfrac{\Delta\delta/\Delta t}{\Delta a/\Delta t}$ where $\Delta\delta$ is the increase in COD in time Δt and Δa is the increase in crack length in time Δt, substitution for $\dot{\delta}$ and $\dot{a}$ gives $\omega = \dfrac{l_o A \sigma_{Nett}^{n}}{N \sigma_{Nett}^{p}}$. Thus, when $n = p$,

$$\omega = \frac{l_o A}{N} = \text{constant.} \qquad (41)$$

If $n > p$, ω will not be constant but will increase with increasing crack length to give the fracture profile shown in Fig. 65 (a). If $n < p$, ω will decrease with crack length giving the profile shown in Fig. 65 (b).

For a given specimen size, equation (41) shows that changes in ω with varying stress and failure time, will produce a change in the value of N. This stress dependence of N is not very marked in Fig. 26 but when the scatter in the data is considered, N can change by at least a factor of five between the upper and lower limits of the scatter bands. The measured changes in ω are within this scatter, thus

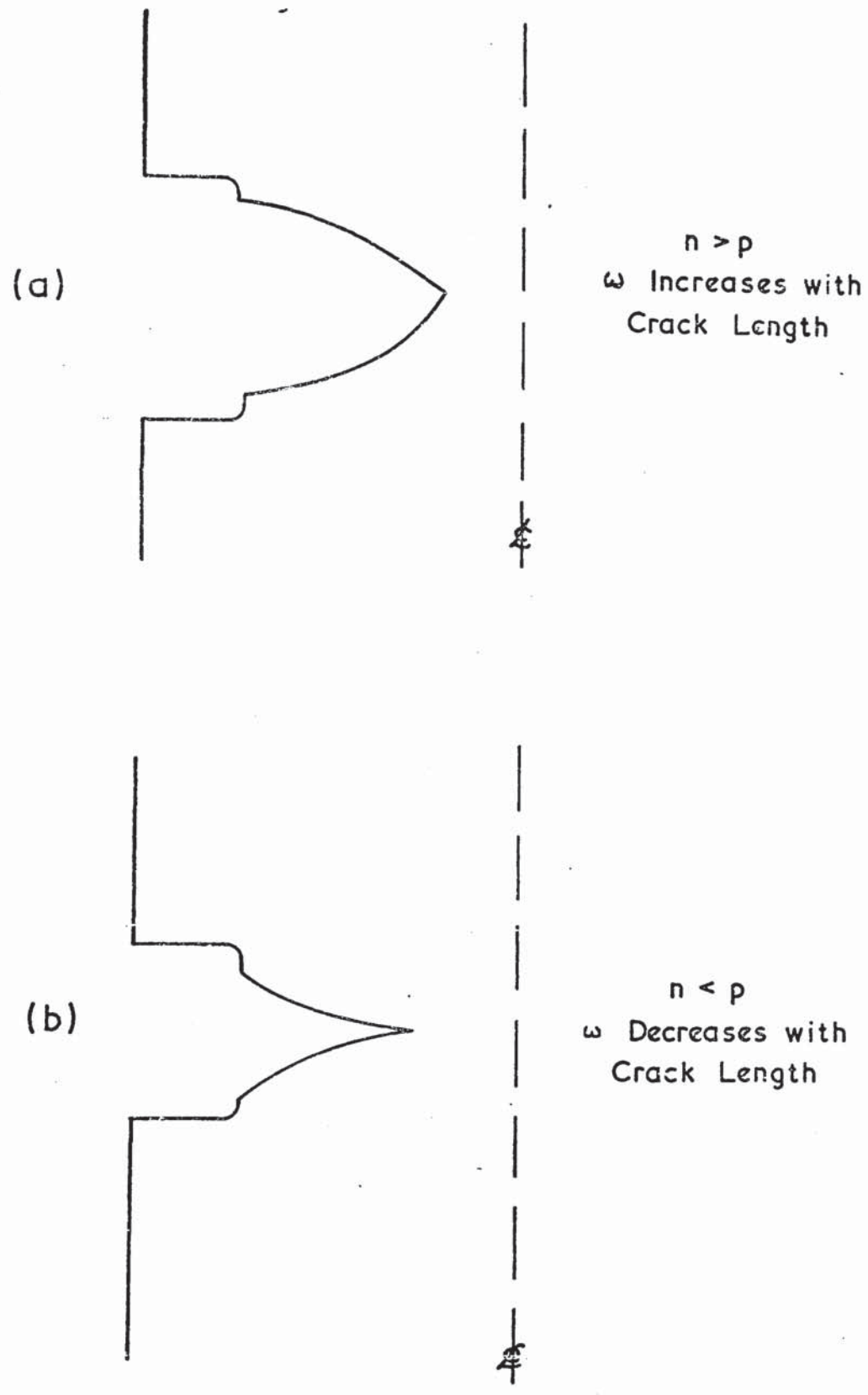

FIG. 65. The Effect of n and p Values on the Fracture Angle (ω).

accounting for the apparent lack of a stress dependence of N.

Since ω and δ_i are both in different ways measures of the ductility of the material, it would be expected that they would vary with time in a similar manner to the ductility of plain specimens. It is generally found that the elongation to failure of plain specimens, ϵ_f, decreases with increasing time as the contribution to the overall elongation from grain boundary deformation processes increases. Fig. 37 shows the decrease in ϵ_f with time for the 316 stainless steel specimens tested here and Figs. 35 and 36 confirm the concomitant decrease in δ_i and ω.

Neither ω nor δ_i are parameters which are commonly measured in creep rupture tests, particularly in long term tests. What information there is refers to the elongation to rupture of plain specimens. The relationships between δ_i and ϵ_f, and ω and ϵ_f can be utilised to calculate values of δ_i and ω relevant to service conditions, i.e. times of test up to 30 years, and thus by using equation (40), the amount of creep cracking can be deduced. Therefore, for given failure times Fig. 66 enables ω and δ_i to be related empirically to ϵ_f. The graphs in Fig. **66** have been interpolated between the origin and the short term data points and can be used to convert existing very long term ϵ_f data to δ_i and ω values. For example ϵ_f in 10^5 hours can be as low as 10% (Trueman et al (1966)) and this would give ω equal to $2{\cdot}5^{\circ}$ and δ_i equal to 136 μm.

5. 1.2.2. Stress and strain distribution ahead of notches under creep conditions.

The lack of correlation between creep crack growth rates and K_I is a consequence of the stress redistribution that occurs at the notch tip, as previously described. The experimentally measured stress distributions confirm this, showing that the stress does not vary as $r^{-\frac{1}{2}}$ (where r = distance ahead of notch) as would be predicted

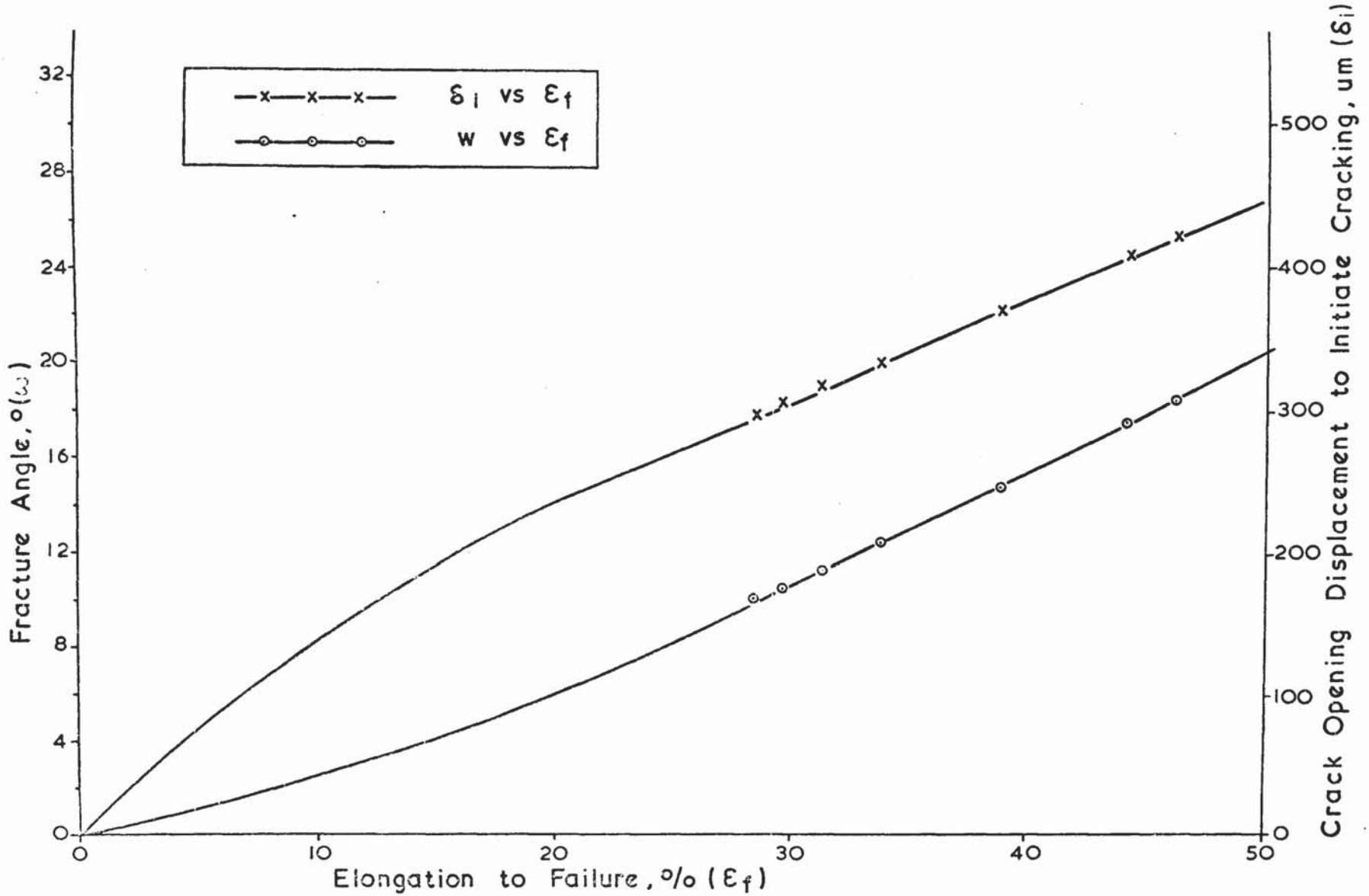

FIG. 66. Empirical Relationship between Fracture Angle (ω), COD (δ_i) and Elongation to Failure (ε_f).

by LEFM. The stress distribution can be divided into three regions (Fig. 39).

In region II, it is found that the stress, σ, is proportional to r^{-s} and s is determined by the stress exponent, n, in the secondary creep equation, such that as n increases, s decreases consistent with the suggestions of Barnby (1974) and Williams and Price (1974). Barnby used an elastic analogy suggested by Hoff (1954) to evaluate the stress distribution. Hoff showed that the stresses in an elastic solution are the same as those in the creep solution and the elastic deformations are numerically equal to the creep rates in the creep problem. Barnby calculated the stress distribution ahead of a crack in a material deforming according to the non-linear elastic law:-

$$\epsilon \alpha \sigma^{n}$$

The creep analogue is therefore the steady state creep equation (equation (15)). The calculated creep stress distribution varied as $\sigma \alpha r^{-\frac{1}{2n}}$.

Rice and Rosengren (1968) considered the stress distribution ahead of a crack in a power law hardening material, i.e. $\epsilon \alpha \sigma^{1/d}$, for d between 1 and 0, and found the stress distribution in this material to vary as $\sigma \alpha r^{-\frac{d}{d+1}}$. The creep analogue of the power law hardening material is the steady state creep equation if $\frac{1}{d}$ equals n. Therefore, the creep stress distribution becomes $\sigma \alpha r^{-\frac{1}{n+1}}$ (a result confirmed by Goodall and Chubb (1974) using finite element computer analysis to calculate the crack tip stresses during creep). The exponent values calculated experimentally are compared with the theoretical results in Table I2. Values of R, where R is the length of Region I, are also included. Fig. 67 compares the various stress distributions with the experimental results and it can be seen that the Rice and Rosengren model is closer to the experimentally determined values.

TABLE 12

Comparison of Values of s and R found by Experiment and Calculation

Temp. (^{o}C)	Displacement Rate ($m.hr^{-1}$)	s (Experiment)	n	$s = \frac{1}{n+1}$	$s = \frac{1}{2n}$	R (Experiment) (mm)	R (Calculated) (mm)
750	1.2×10^{-5}	0.175	7.0	0.125	0.071	0.3	0.35
	1.1×10^{-4}	0.195				0.15	0.25
650	1.2×10^{-5}	0.129	9.5	0.096	0.052	0.15	0.23

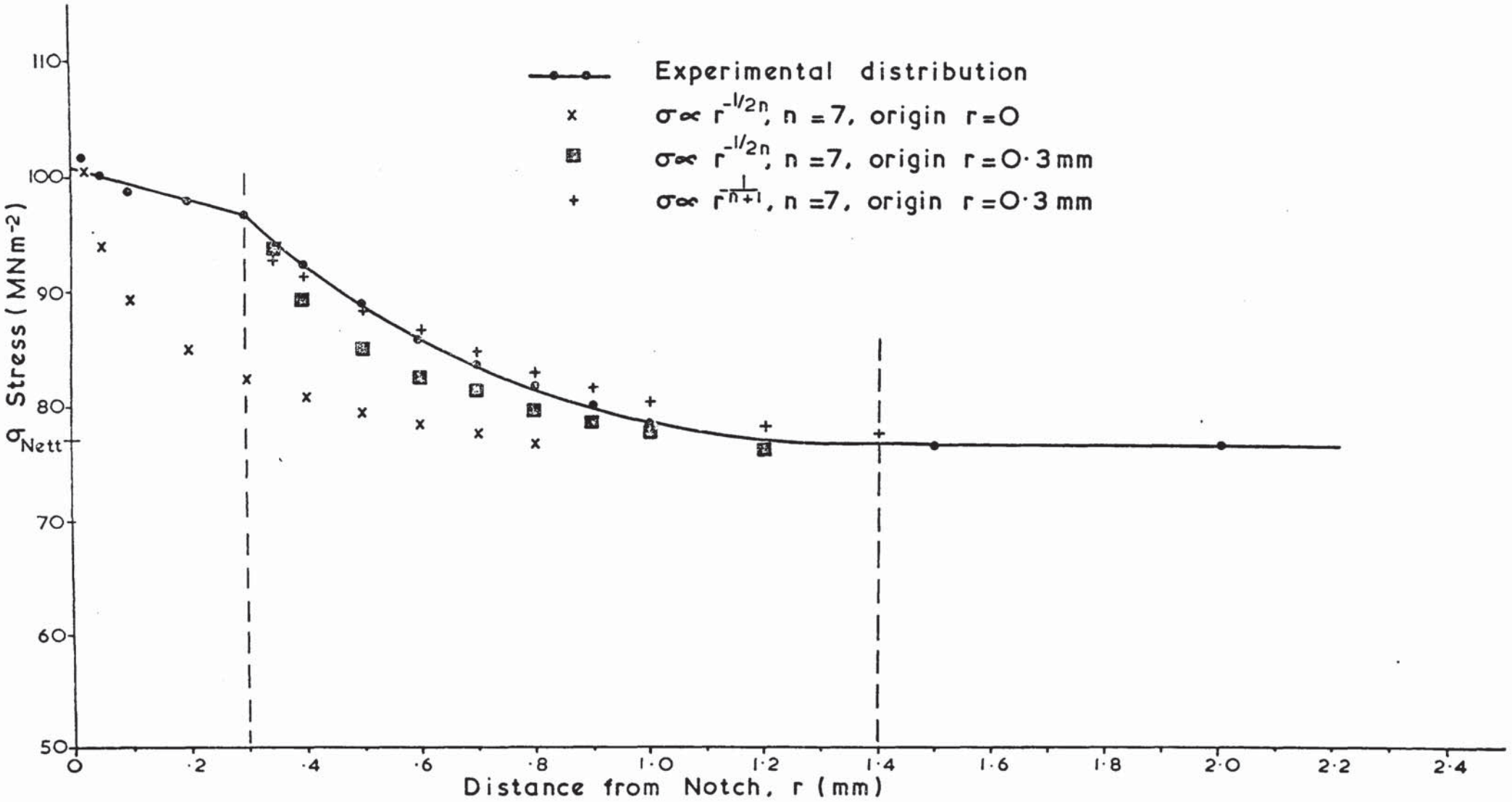

FIG. 67. Comparison between Experimental Stress Distribution and Theoretical Models.

In region I, the strain rate and stress are constant. However, Fig. 38 shows that at a time of 228·5 hours, the strain rate at a given r value within this region is greater than the strain rate at the earlier times that were considered. Macroscopic crack initiation was observed at about 230 hours, so that the increased strain rates at 228·5 hours suggest that this region was in tertiary creep.

For tests conducted on similar specimens at ambient temperatures, the stress level near the notch tip would be the flow stress but under creep conditons where the plastic zone extends across the whole ligament in the 316 steel specimens, it is difficult to define a time independent flow stress. Thus, the stress in region I will be determined by the applied displacement rate and by the local strain rate.

The length of region I can be calculated as follows. In the absence of a constant stress region, the stresses in region I would vary as found in region II, i.e. $\sigma = F\, r^{-s}$, where F is a constant determined by the applied stress and temperature. However, at r_I the stress equals the maximum crack tip stress (determined by the displacement rate) as shown in Fig. 39. Therefore, to maintain the load carrying capacity, a constant stress region of length R ($> r_I$) is produced. At r_I, the total area under the curve is:-

$$\int_0^{r_I} F\, r^{-s}\, dr = \left[\frac{F\, r^{1-s}}{1-s} \right]_0^{r_I}$$

$$= \frac{F\, r_I^{1-s}}{1-s}$$

After relaxation to the constant stress level, the area under the curve = $\sigma_I\, R$

To a first approximation, $\dfrac{F r_I^{1-s}}{1-s} = \sigma_I\, R$

$$\therefore \quad R = \left(\frac{1}{\sigma_I}\right) \quad \frac{Fr_I^{1-s}}{1-s}$$

Now $$\sigma_I = \left(\frac{\dot{\varepsilon}}{A}\right)^{1/n}$$

$$\therefore R = \left(\frac{\dot{\varepsilon}}{A}\right)^{-1/n} \quad \frac{F\, r_I^{1-s}}{1-s} \qquad (42)$$

From equation (42), if the crack tip strain rate increases, $\left(\frac{\dot{\varepsilon}}{A}\right)^{-1/n}$ and $\frac{r_I^{1-s}}{1-s}$ decrease and F will increase with a nett result that R will decrease with increasing strain rate as has been found experimentally. The values of R have been calculated from the data obtained from the tests at displacement rates of $1{\cdot}2 \times 10^{-5}$ and $1{\cdot}1 \times 10^{-4}$ m. hr^{-1} and the values of R are compared with the experimentally measured values in Table I2. It can be seen that within the accuracy of the experiments the values compare favourably and confirm that as the displacement rate increases, the length of the constant stress region decreases.

In region III, the stress is the nett section stress which for these tests is determined by the applied displacement rate.

5. 1.3. Microscopic aspects of crack growth.

As the load increases during primary creep, the stress at the notch root increases and consequently the strain rate is varying within region I. This is indicated by the local bending of the scribe lines near the root and produces a strain gradient before the onset of secondary creep. Once secondary creep is reached and constant strain rate conditions apply, the strain gradient within Region I is maintained at this level. The occurrence of this strain gradient is shown when the notch root region is closely examined using a scanning electron microscope. It is observed that microscopic creep cavities extend a distance of about 120 μm. from the notch root. The morphology and distribution of these cavities suggest that the presence of a notch in these specimens

localises the deformation and hence the cavitation but the actual mechanisms involved in the crack nucleation and growth will be as observed in the plain specimen tests.

The cavities in the 316 steel are generally associated with grain boundary particles of $M_{23}C_6$. The model proposed by Harris (1965) for cavity nucleation by grain boundary sliding causing stress concentrations at non-wetting particles will be inapplicable since it is known that $M_{23}C_6$ particles are strongly adherent (Kegg (1971)). Also since the particles are not fractured the specific model proposed by Smith and Barnby (1967) that the cavities are nucleated by the particles being cracked as a result of dislocation pile-up mechanisms, is also ruled out. However, a similar mechanism to the Smith and Barnby model can be envisaged in which dislocation pile-ups at particles cause particle/grain boundary interface decohesion rather than particle fracture. This model was used by Fleck et al (1975) to explain the observation of cavities associated with uncracked particles in a copper-based alloy. In the Smith and Barnby model, the stress concentration at the particle is determined by the length of the dislocation pile-up in the boundary plane which is determined by the inter-particle spacing. Fleck et al suggested that the length of dislocation pile-up was not restricted to the interparticle spacing and suggested an additional pile-up in the matrix of length, l_{matrix}, and inclined at an angle θ to the grain boundary. Thus, the effective length of pile-up becomes:-

$$l_p = l_{g.b.} + l_{matrix} \cos \theta$$

where $l_{g.b.}$ is the length of the pile-up in the plane of the boundary.

Uncertainties in the value of the fracture surface energy and the effective length of pile-up prevent quantitative assessment of this model for the 316 steel at 750°C. However, the observations suggest

that such a nucleation mechanism may be operating.

The shape and orientation of the cracks to the stress axis suggest that growth occurs by deformation processes involving grain boundary sliding.

As the macroscopic crack grows across the ligament, the material well removed from the crack tip is straining in the manner described previously, and cumulative creep damage can result in microscopic crack nucleation and growth at points distant from the crack tip. Examples of these cracks have been observed at 750°C. when the macrocracks were about 74% of the ligament width, and thus considerable ligament straining had occurred. Also since the macrocrack is growing into regions of progressively more damaged material, the amount of micro-cracking ahead of the main crack increases with increasing crack length.

5. 2. The effect of environment on creep crack growth in stainless steels.

5. 2.1. The effect of iodine vapour on the creep rupture properties of M316 stainless steel.

Iodine vapour embrittles M316 stainless steel reducing failure strain by at least a factor of 2 and the failure time by 1·3 compared with vacuum data at 750°C. and by factors of at least 2·5 and 1·7 respectively for the tests at 650°C. The embrittlement of 20Cr/25Ni/Nb stainless steel by iodine vapour observed by Lobb and Jones (1973) was attributed to the effect of a selective corrosion process forming small surface grain boundary cracks in all parts of the specimen. In the stressed gauge length, these cracks propagated into the specimen reducing the cross-sectional area. Similarly in the M316 steel, examination of the unstressed heads of the iodine exposed specimens revealed some intergranular penetration of about 10 μm, while in the gauge length extensive intergranular cracking was found at both temperatures (Fig 46 (a)). Final failure occurred in a more ductile transgranular manner when the load-bearing area had reduced and the stress had increased to the level necessary for rapid shear.

Lobb and Jones (1973) suggested that iodide formation ($Fe I_2$, $Ni I_2$ and $Cr I_2$) occurs on exposure of 20Cr/25Ni/Nb steel to iodine vapour. Of these iodides $Cr I_2$ has the highest formation energy and is formed preferentially on the steel surface. They observed chromium depletion in grain boundary regions which implies that chromium is being preferentially removed from the metal to form iodide. At sites such as grain boundaries, where the chromium is rapidly replenished by diffusion from the interior, attack proceeds with the formation of an intergranular iodide penetration. This penetration locally reduces the cross-sectional area and can propagate as a grain

boundary crack under the local stress. It is felt that such a mechanism can form a basis for the explanation of the embrittlement observed here.

The results at 750°C. show increased endurance for the plain specimens tested in air compared with those in vacuum together with a reduction in the failure strain and secondary creep rate; it is thought that this is due to nitriding and/or oxidation of the steel. At 650°C. similar effects are observed but the increased endurance in air is much smaller than at 750°C.

5. 2.1.2. Crack Initiation.

Figs. 50 and 51 show the marked effect that corrosive environments have on crack initiation from the notches. For example, the initiation displacement δ_i is reduced by a factor of about 5 in iodine vapour compared with vacuum in the 80 MN m^{-2} tests at 750°C. but by a factor of 3·4 in the 95 MN m^{-2} tests. Similarly, the reduction in δ_i (and t_i) in air compared with vacuum is less in the 95 MN m^{-2} tests, indicating that iodine attack and the possible nitriding/oxidation processes are stress and time dependent. At 182 MN m^{-2} there is no reduction in δ_i by environment.

At 650°C., the results show similar trends. In the tests at 150 MN m^{-2}, δ_i is reduced by iodine compared with vacuum and air but only by factors of 1·5 and 1·2 respectively. t_i is also reduced by the iodine vapour at 150 and 190 MN m^{-2} compared with air and vacuum but at 190 MN m^{-2}, the difference in t_i between air and vacuum tests is negligible.

These results suggest the existence of a threshold stress above which there is insufficient time for environmental embrittlement to occur, but below which embrittlement occurs, becoming more severe as the stress is reduced. However, the present data are insufficient to permit precise threshold stresses to be specified.

5. 2.1.3. Crack Propagation

The results indicate a decreasing effect of environment on crack propagation as the initial applied stress is increased. Even at the lowest stress (80 MN m^{-2}) at 750°C. the main environmental effect is on crack initiation. Nevertheless certain conclusions can be drawn from the crack growth results and these are discussed below with particular reference to the 80 MN m^{-2} tests at 750°C.

For the crack to grow from length a to (a + δa) (where a > the initial notch length), some critical crack tip strain, ε_c, corresponding to some critical displacement, δ_c, must be reached. The time taken to reach this displacement will be determined by the crack opening displacement rate and, when general yielding occurs, this is controlled by the displacement rate in the ligament as discussed previously. This suggestion is confirmed by the linear relationships shown in Figure 52. For a given displacement rate the growth rate is highest in the specimen exposed to iodine vapour indicating that δ_c has been reduced by chemical attack. Such enhanced crack growth can be expressed:-

$$\dot{a} = \dot{a}_m + \dot{a}_E \qquad (43)$$

where $\dot{a}_m$ is the crack growth rate determined by the material properties in an inert environment and $\dot{a}_E$ is the additional growth rate from the reduction in crack tip ductility by the aggressive environment.

It is known that crack growth rate in a non-aggressive environment is controlled by crack opening displacement rate ($\dot{\delta}$) (equation(39)) so that $\dot{a}_m = B\dot{\delta}^y$, where the constant B is a measure of the ductility associated with crack propagation and y has a value of 0·8 to 1·4(from the previous work and Robson (1972), Soo (1974), Haigh (1974)). If $\dot{a}_E$ is also determined by $\dot{\delta}$, then equation (43) could be written:-

$$\dot{a} = B\dot{\delta}^y + C\dot{\delta}^x \qquad (44)$$

The values of the constants and exponents for the range of $\dot{\delta}$ shown in Figure 52 are summarised for each environment in Table 13. Since the crack growth rates (for a given $\dot{\delta}$) in the three environments are in the order $\dot{a}(I_2$ vapour) > $\dot{a}$(air) > $\dot{a}$(vacuum) then, $\delta_c(I_2$ vapour) < δ_c (air) < δc (vacuum).

For a given environment, changes in δ_c as the crack propagates are shown by the values of the exponents x and y. Where environmental effects are negligible (i.e. in vacuum tests where $\dot{a}_E$ is zero), δ_c is determined by material properties alone. If y > 1 (see Table 13), δ_c (vacuum) decreases as the crack propagates and thus the fracture angle, ω, decreases as shown in Fig. 65 (b). This behaviour may result from the cumulative damage process in the uncracked ligament where the crack is growing into progressively more strained material: the necessary additional displacement at the crack tip decreases with increasing crack length.

The values of y are compared at both temperatures and each stress in Table 14. It is found that as the stress increases, the value of y approaches unity, suggesting that the cumulative damage is becoming less at the high stress levels. Indeed at 650°C. and a stress of 150 MN m^{-2} the high y value gives crack growth rates in the vacuum tests faster than in the iodine tests for a range of $\dot{\delta}$

Where marked environmental effects occur δ_c is reduced. As the crack propagates, changes in δ_c (environment) are shown by the value of the exponent x. For x > 1, embrittlement increases and δ_c(environment) decreases with increasing $\dot{\delta}$. Therefore, the crack propagates faster for a given $\dot{\delta}$. For x < 1, environmental embrittlement decreases with increasing $\dot{\delta}$ so that δ_c (environment) increases until it is equal to δ_c (vacuum), i.e. δ_c is now material determined with no environmental effects.

Iodine embrittlement at the crack tip is thought to be

TABLE 13

Values* of the Crack Growth Parameters in Equation (44) for 80 MN m^{-2} Tests at 750°C

ENVIRONMENT	B	y	C	x
Vacuum	16.4	1.3	0	0
Air	16.4	1.3	3.6	1.1
Iodine Vapour	16.4	1.3	0.08	0.8

*Quoted for $\dot{a}$ and $\dot{\delta}$ in $m.hr^{-1}$.

TABLE 14

Variation in y with Stress

Temperature (°C)	Gross-section Stress (MNm^{-2})	Initial Nett-Section Stress (MNm^{-2})	t_f (hrs.)	y
750	80	98	142.2	1.3
750	95	112	50.8	1.25
750	182	218	0.31	1.19
650	150	194	147.7	1.55
650	190	227	31.9	1.27

time dependent so that as the crack growth rates increase, the embrittlement should be relatively less effective (i.e. $x < 1$). This conclusion is supported in the range of crack growth rates considered here, although for this series of tests, the environments have much more effect on crack initiation than propagation.

The crack growth rates have not been related to nett section stress since difficulties arise in the calculation of the stress due to large changes in the specimen thickness as the crack propagates in the vacuum and iodine vapour specimens. This is because in the vacuum tests, extensive necking occurs, which for a given crack length will mean that the actual nett section stress is greater than if no reduction in thickness had occurred. Similarly for the iodine tests, intergranular penetration in the thickness direction due to iodide formation will reduce the effective thickness, again causing an increase in nett section stress for a given crack length.

5. 2.2. The effect of neutron irradiation on the creep rupture properties of 20Cr/25Ni/Nb stainless steel.

The results of the irradiated and unirradiated 20Cr/25Ni/Nb steel specimens at 750°C. show that the effects of irradiation are negligible, which is contrary to the general observation in austenitic steels that irradiation causes embrittlement at this temperature. The embrittlement is thought to arise from the transmutation of B^{10} within the steel to helium.

The initial natural boron content of the irradiated steel tested here was 9 ppm by weight, so that the B^{10} content would have been approximately 9 atoms per million. This would produce about 2 atoms per million of helium after irradiation to a dose of 7×10^{19} n/cm^2 (Howarth (1974)). Broomfield et al (1968) suggested that a helium content of 0·15 atoms per million was required to significantly reduce the 750°C. tensile ductility of 20Cr/25Ni/Nb stainless steel. Waddington and Lofthouse (1969) have shown in solution treated unstabilised 20Cr/25Ni stainless steel that irradiation to a dose of 5×10^{19} thermal neutrons/cm^2 at 40°C. produced significant embrittlement. They suggested that the irradiation did not markedly effect wedge crack nucleation but accelerated the rate of propagation.

Although the boron content and irradiation dose should have been sufficient to produce enough helium to cause embrittlement, no such effect was observed in these specimens. The boron distribution was not investigated by the previous authors and clearly, the helium bubble distribution must be important in determining the degree of embrittlement. Williams et al (1975) have shown in type 316 stainless steel that heat treatment can have a marked effect on the boron distribution. They studied the boron distribution as a function of solution treatment temperature (900 to 1300°C.) and cooling rate (either 50 or 500°C/second). They showed that increasing boron segregation to grain boundaries occurred

during slower cooling from higher solution treatment temperatures. No segregation was observed in specimens cooled at 500°C/second (i.e. quenched in water at 0°C.) irrespective of the solution treatment temperature. The boron autoradiographs of the primary recrystallised 20Cr/25Ni/Nb steel showed no segregation to grain boundaries, consistent with the observations of Williams et al. in type 316 steel. Therefore, during irradiation helium will be produced by transmutation of B^{10} throughout the sample, reducing the helium concentration at the grain boundaries. Transmission electron microscopy of the irradiated 20Cr/25Ni/Nb steel failed to reveal any features that could be positively identified as bubbles, suggesting that the bubbles must be less than 10 Å in diameter. The helium formed in the matrix may diffuse as single atoms or small bubbles to grain boundaries or may be trapped by intragranular precipitates and thus prevented from reaching the boundaries. In 20Cr/25Ni/Nb, the association of bubbles with intragranular NbC and M_6C precipitates has been observed by Broomfield et al (1972). Therefore, by avoiding boron segregation to the grain boundaries, the helium available at the boundaries will be reduced.

Another factor which will reduce the effect of the helium bubbles is the small grain size of the primary recrystallised steel. The grain boundary surface area is accordingly increased, further reducing the grain boundary helium concentration. Martin and Weir (1966) have found that reducing the grain size decreased the irradiation embrittlement in type 304 stainless steel.

Accordingly, by a combination of a uniform boron distribution and small grain size, the irradiation embrittlement in primary recrystallised 20Cr/25Ni/Nb steel has become negligible.

CONCLUSIONS

1. In tests on SEN and NCH specimens of A.I.S.I. type 316 stainless steel at 740°C., it is found that the stress intensity factors to produce a particular crack growth rate are different in the two types of specimen, showing that LEFM does not apply.

2. Creep crack growth rates, $\dot{a}$, in both specimen geometries correlate well with the nett section stress, σ_{Nett}, so that this parameter can be used in predicting growth rates, using the equation $\dot{a} = N \sigma_{Nett}^{p}$.

3. The effect of creep relaxation, which reduces the high elastically determined stresses, is considered and it is shown that after a very short period of time, the LEFM stress distribution becomes inapplicable.

4. The possibility of using a strain-based criterion for creep crack growth, such as COD, δ, or the angle made between the fracture surfaces (the fracture angle, ω) is considered and the use of the equation $a = \frac{1}{\omega} (\delta - \delta_i)$, where δ_i is the displacement required to initiate cracking, is found to have advantages.

5. In tests on double edge notched specimens of type 316 stainless steel, it is found that creep crack growth rates correlate with nett section stress over the temperature range 600 to 850°C.

6. The stress exponent, n, in the creep equation $\dot{\epsilon} = A \sigma^{n}$ is found to be equal to exponent p between 600 and 850°C.

7. The equations $\dot{a} = N \sigma_{Nett}^{p}$ and $a = \frac{1}{\omega} (\delta - \delta_i)$ are shown to be compatible.

8. The strains in the specimens resulting from the crack tip stress redistribution are considered and together with the

experimental evidence show that creep crack growth is governed by ligament displacements and ultimately by displacements at the crack tip.

9. Apparent activation energies for creep and creep crack propagation have been measured in the temperature range 740 to 850°C. and stresses between 80 and 65 MN m^{-2}. The values are found to be 345-416 and 352-372 KJ $mole^{-1}$ respectively, suggesting that dislocation climb mechanisms could be rate controlling in the crack propagation process.

10. Below 740°C., large increases in the apparent activation energies are indicated which may arise from a change in dislocation mechanism. Further work is required to identify the rate controlling processes at these temperatures.

11. It is observed in each test on type 316 steel that certain minimum displacements must be achieved for crack initiation and propagation. For crack initiation from a notch, a displacement δ_i is required. A measure of the displacement associated with propagation is the fracture angle, ω, and ω is found to remain about constant over a range of crack lengths. Since ω and δ_i are both in different ways measures of ductility, it is found that they vary with time in a similar manner to the ductility of plain specimens, ε_f.

12. Empirical relationships have been established between ε_f, δ_i and ω, and can be used to convert existing long term measurements of ε_f to ω and δ_i.

13. The variation of stress/strain rate with distance ahead of a notch under creep conditions has been measured and is found to show three regions. The extent of the regions and stress and strain rate within them are determined by the applied displacement rate and temperature.

14. Microscopic cracking is observed ahead of notches and macroscopic creep cracks in type 316 steel at 750°C. The cavities are generally associated with grain boundary precipitates. It is thought that cavity nucleation occurs by dislocation pile-ups causing matrix-precipitate decohesion and subsequent growth occurs by grain boundary sliding.

15. Creep rupture tests on plain specimens of M316 steel at 650 and 750°C. and various applied stresses show that the failure times and strains are reduced in the presence of iodine vapour, compared with vacuum and air environments. The air tests failed in the longest times but with intermediate ductility.

16. Optical metallography revealed extensive inter-granular surface nucleated cracking in the iodine exposed specimens and a selective corrosion process is thought to cause the embrittlement.

17. For notched specimens of M316 steel, the iodine vapour has much more effect on crack initiation than propagation. The environmental effects become less marked as the duration of test is reduced. The crack propagation results indicate that growth is controlled by crack tip and ligament displacements in all environments.

18. The effect of neutron irradiation on the creep rupture properties of primary recrystallised 20Cr/25Ni/Nb steel at 750°C. has been found to be negligible. It is thought that a combination of a uniform boron distribution and small grain size causes sufficiently low helium bubble concentrations on the grain boundaries to have negligible effects on the creep rupture properties.

ACKNOWLEDGEMENTS

I should like to express my thanks to Dr. J.T. Barnby and Dr. C.L. Formby for their supervision and constructive comments during the course of this work and to Dr. R.B. Jones and Dr. R.C. Lobb and many other colleagues for valuable discussion. My thanks are also due to Mrs. I. Carling for typing the thesis.

The work was carried out at the Berkeley Nuclear Laboratories of the Central Electricity Generating Board and I wish to thank Dr. B Edmondson, the Director, and Dr. B.C. Masters, Head of Fuel and Core Division, for providing the facilities.

APPENDIX

Calculation of the time required to relax the crack tip stresses.

Initially, the local stress (σ_{local}) at the tip of the geometrical stress concentration is much larger than the nominal applied stresses (σ_{na}). Creep relaxation occurs to limit the local stress such that the rate of decrease of elastic strain equals the rate of increase of plastic strain,

$$\text{i.e. } \dot{\varepsilon}_{plastic} = -\dot{\varepsilon}_{elastic} \qquad \text{(A1)}$$

Substituting the secondary creep equation ($\dot{\varepsilon} = A\sigma^n$ where A and n are constants) for $\dot{\varepsilon}_{plastic}$ in equation (A1) gives:-

$$A\sigma^n_{local} = -\frac{1}{E}\left(\frac{d\sigma_{local}}{dt}\right) \qquad \text{(A2)}$$

At the instant the stress is applied

$$\sigma_{local} = M\sigma_{na}$$

where M is the local elastic stress concentration factor, equal to 3 for a circular hole, for example.

Thus re-arranging and integrating Eqn. (A.2). the relationship

$$t = -\frac{1}{AE}\int_{M\sigma_{na}}^{\sigma_{local}} \frac{d\sigma_{local}}{\sigma^n_{local}}$$

$$= \frac{1}{AE(1-n)}\left[(M\sigma_{na})^{1-n} - \sigma^{1-n}_{local}\right] \qquad \text{(A3)}$$

is obtained. To evaluate t in conditions relevant to the experimental work, let t equal the time to reach σ_{local} = 1·5 x the nominal applied net section stress for A.I.S.I. type 316 stainless steel at 740°C. By taking

$$E = 1{\cdot}93 \times 10^{5} \text{ MN m}^{-2}$$

$$A = 3 \times 10^{-17} \text{ hr}^{-1} (\text{MN. m}^{-2})^{-7}$$

$$n = 7$$

then from Eqn. (A.3)

$$t = \frac{\frac{1}{(1{\cdot}5)^6} - \frac{1}{M^6}}{6AE\sigma_{na\,(net)}^{6}}$$

For any $M > 2$, the M^{-6} term is negligible and therefore t is independent of the magnitude of the stress concentration. This means that the calculated time of relaxation applies over the whole of the stress field close to the crack. In particular when

$$\sigma_{na(net)} = 73 \text{ MN m}^{-2}$$

$$t_{(M>2)} = \frac{1}{68{\cdot}4\ AE\sigma_{na(net)}^{6}} \text{ hr.}$$

$$= 0{\cdot}017 \text{ hr.}$$

$$= 60 \text{ seconds.}$$

This is an upper bound solution since the secondary creep equation represents the lowest creep rate during a test at constant stress.

REFERENCES

J.M. Adamson and J.W. Martin, J.I.S.I. 210(1972)271

M.F. Ashby and R.Raj, Proc. Conf. "The Mechanisms and Physics of Fracture", Cambridge, 1975.

K.Q. Bagley, A.S. Fraser and M.A. Cillies, 1974, unpublished work.

G.R. Bainbridge, U.K.A.E.A. Report TRG 1925(R), 1970.

R.W. Baluffi and L.L. Seigle, Acta Met 3 (1955) 170.

R.W. Baluffi and L.L. Seigle, Acta Met 5 (1957) 449.

J.T. Barnby, J.I.S.I. 203(1965)392.

J.T. Barnby, Eng. Fract. Mech. 6 (1974) 627.

W. Batey and K.Q. Bagley, J. Brit. Nucl. Energy Soc. 13 (1974) 49.

B.A. Bilby, A.H. Cottrell and K.H. Swinden, Proc. Roy. Soc. A272 (1963) 304.

I.R. Birss and W.E. Ellis, Proc. BNES Conference "Voids formed by irradiation of reactor materials", Reading, 1971.

E.E. Bloom, Proc. BNES Conference "Irradiation embrittlement and creep in fuel cladding and core components", London, 1972.

E.E. Bloom and J.O. Stiegler, A.S.T.M. Spec. Tech. Pub. 484, 1970.

E.E. Bloom and J.R. Weir,A.S.T.M. Spc. Tech. Pub. 457, 1968.

R.C. Boettner and W.D. Robertson, Trans. AIME 221 (1961) 613.

G.H. Broomfield, D.R. Harries and A.C. Roberts, J.I.S.I. 203 (1965) 502.

G.H. Broomfield, J. Gravenor, J. Moffat and E.E.C. Hutchins, Proc. BNES Conf. "Irradiation embrittlement and creep in fuel cladding and core components", London, 1972.

W.F. Brown Jnr. and G. Sachs, N.A.C.A. Tech. Note 2433, 1951.

W.F. Brown Jnr., M.H. Jones and D.P. Newman, A.S.T.M. Spec. Tech. Pub. 128, 1952.

W.F. Brown Jnr. and J.E. Srawley, A.S.T.M. Spec. Tech. Pub. 410, 1966.

R.J. Bucci, P.C. Paris, J.D. Landes and J.R. Rice, A.S.T.M. Spec. Tech. Pub. 514, 1972.

B.J.Cane and G.W. Greenwood, Met. Sci. J. 9(1975) 55.

H.C. Chang and N.J. Grant, Trans AIME 206 (1956) 544.

F.J. Clauss, "Engineer's Guide to High Temperature Materials", Addison-Wesley Publishing Co. 1969.

G.J. Cocks and D.M.R. Taplin, Metallurgia 75 (1967) 229.

A.H. Cottrell, I.S.I. Symposium "Structural processes in creep", London, 1961.

A.H. Cottrell, I.S.I. Spec. Report 69 (1961) 281.

B. Cox and J.C. Wood, to be published (1975).

C. Crussard, J.Plateau and G. Henry, Proc. Joint Int. Conf. on Creep, London, 1963.

C.K.L. Davies, P.W. Davies and B. Wilshire, Phil Mag 12 (1965) 827.

P.W. Davies and R. Dutton, Acta Met 14 (1966) 1138.

P.W. Davies, K.R. Williams and B. Wilshire, Phil Mag 18 (1968) 197.

P.W. Davies and K.R. Williams, (a)Met. Sci. J. 3 (1969) 48. (b)Met. Sci. J. 3 (1969) 220.

P.W. Davies and B. Wilshire, I.S.I. Symposium "Structural processes in creep", London, 1961.

P.W. Davies and B. Wilshire, Phil Mag 11 (1965) 189.

E.A. Davis and M.J. Manjoine, A.S.T.M. Spec. Tech. Pub. 128, 1952.

F. Dobes, Scripta Met 7 (1973) 1231.

F. Dobes and J. Cadek, Scripta Met 4 (1970) 1005.

B.F. Dyson, Proc. Confer. on "Grain Boundaries", Montreal, 1973.

B.F. Dyson, Proc. Joint Meeting "Prediction of Life of High Temperature Components", London, 1975.

B.F. Dyson and D.E. Henn, J. Microscopy 97 (1973) 165.

B.F. Dyson and D. McLean, Met. Sci. J 6 (1972) 220.

B.F. Dyson and M.J. Rodgers, Met. Sci J 8 (1974) 261.

R. Eborall, Proc. Symposium on "Creep and Fracture of Metals at High Temperature", Teddington, 1954.

R. Eborall, I.S.I. Symposium "Structural processes in creep", London, 1961.

J.D. Elen, W. Van Witzenburg, M.J. de Vries and A. Glas Proc. BNES Conference "Irradiation embrittlement and creep in fuel cladding and core components," London, 1972.

E.G. Ellison and D. Walton, Proc. Int. Conf. on "Creep and Fatigue in elevated temperature applications," Philiadephia, 1973.

H.E. Evans&J.S. Waddington, Phil Mag 20 (1969) 1075.

D.J.F. Ewing and C.E. Richards, C.E.G.B. Report RD/L/N237/72, 1972.

R.G. Fleck, C.J. Beevers and D.M.R. Taplin, Met. Sci. J 9(1975) 49

R.G. Fleck, D.M.R. Taplin and C.J. Beevers, Acta Met 23 (1975) 415

C.L. Formby, 1972, Unpublished work.

F. Garofalo, Proc. A.S.T.M. (1959)957.

F. Garofalo, O. Richmond, W.F. Domis and F.Von Gemminghen, Proc. Joint Int. Conf. on creep, London, 1963.

F. Garofalo, "Fundamentals of Creep and Creep Rupture in Metals", MacMillan, New York, 1965.

A Garlick, Proc. BNES Conference "Effect of Environment on material properties in Nuclear Systems", London, 1971.

A. Garlick, Proc. Int. Conference "Physical Metallurgy of Reactor Fuel Elements" Berkeley, 1973.

A. Garlick and P.D. Wolfenden, J. Nucl. Mat 41 (1971) 274.

R.C. Gifkins, Acta Met. 4 (1956) 98.

R.C. Gifkins, Proc. Conference on Fracture, Tewkesbury, 1965.

D.M. Gilbey and S. Pearson, Royal Aircraft Establishment Tech. Report 66402 (1966).

A. Gittins, Met. Sci. J 1 (1967) 214.

A. Gittins and H.D. Williams, Phil. Mag 16 (1967) 142.

R.M. Goldhoff, Proc. Joint Int. Conf. on Creep, London, 1963.

H.J. Goldschmidt, J.I.S.I. 209 (1971) 900.

I.W. Goodall and E.J. Chubb, C.E.G.B. Report RD/B/N3227, 1974.

J.N. Greenwood, J.I.S.I. 171 (1952) 380.

J.N. Greenwood, D.R. Miller and J.W. Suiter, Acta Met 2 (1954) 150.

G.W. Greenwood, Proc. Int. Conf. on the Strength of Metals and Alloys, Cambridge, 1973.

G.W. Greenwood, Phil. Mag. 19 (1969) 423.

J.R. Haigh, C.E.G.B. Report RD/L/R 1833, 1973.

J.R. Haigh, C.E.G.B. Report RD/L/N118/74, 1974.

D.K. Hanink and H.R. Voorhees, J. Basic Eng. 84 (1962) 233.

D.R. Harries, J. Brit. Nucl. Energy Soc. 5 (1966) 74.

D.R. Harries and A.C. Roberts, A.S.T.M. Spec. Tech. Pub. 426, 1967.

J.E. Harris, Trans AIME 233 (1965) 1509.

J.E. Harris, Met. Sci. J 7 (1973) 1.

J.E. Harris, C.E.G.B. Report RD/B/N 3412, 1975.

J.E. Harris, M.D. Tucker and G.W. Greenwood, C.E.G.B. Report RD/B/N 2873, 1973.

C.B. Harrison and G.N. Sandor, Eng. Fract. Mech. 3 (1971) 403.

P.T. Heald, G.M. Spink and P.J. Worthington, Mat. Sci. and Eng. 10 (1972) 129.

T. Healey, A. Brown and M.V. Speight, Proc. Int. conf. on "Physical Metallurgy of Reactor Fuel Elements", Berkeley, 1973.

C. Herring, J. Appl. Phys. 21 (1950) 437.

J. Hill, Atom 2 (1975) 219.

D.A. Hilton and J.H. Robins, J.I.S.I. 211 (1973) 440.

J.J. Holmes, A.J. Lovell and R.L. Fish, A.S.T.M. Spec. Tech. Pub 529, 1973.

N. Howarth, C.E.G.B. Report RD/B/N 2911, 1974.

D. Hull and D.E. Rimmer, Phil Mag 4 (1959) 673.

E.D. Hyam and G. Sumner, IAEA Symposium on "Irradiation Damage of Beryllium", Venice, 1962.

J. Intrater and E.S. Machlin, Acta Met 7 (1959) 140.

G.R. Irwin, J. Appl. Phys 24 (1957) 361.

G.R. Irwin, Appl. Mat. Res. 3 (1964) 65.

Y. Ishida and D. McLean, Met. Sci. J. 1 (1967) 171.

L.A. James, Int. J. Fract. Mech. 8 (1972) 347.

C.H.M. Jenkins, Proc. symposium on "Creep and Fracture of Metals at High Temperature", Teddington, 1954.

C.H.M. Jenkins, J. Inst. Met. 70 (1944) 57.

T. Johanneson and A. Tholen, J. Inst. Met. 97 (1969) 243.

T. Johanneson and A. Tholen, Met. Sci. J. 6 (1972) 189.

C.E. Johnson and C.E. Crouthamel, J. Nucl. Mat 34 (1970) 101.

C.E. Johnson, C.E. Crouthamel, H. Chen and P. Blackburn, Trans. Amer. Nucl. Soc. 12 (1969) 564.

M. Kangilaski, J.S. Perrin and R.A. Wullaert, A.S.T.M. Spec. Tech. Pub. 457, 1969.

G.R. Kegg, C.E.G.B. Report RD/L/M331, 1971.

J.L. Kenyon, G.A. Webster, J.C. Radon and C.E. Turner, Int. Conf. on "Creep and Fatigue in elevated temperature applications",Philadelphia, 1973.

B. King, Proc. Joint Meeting "Prediction of Life of High Temperature Components", London, 1975.

G. Knowles, C.E.G.B. Report RD/B/ M2419, 1973.

D. Kramer, K.R. Garr, A.G. Pard and C.G. Rhodes, Proc. BNES Conference "Irradiation embrittlement and creep in final cladding and core components", London, 1972.

V.V.P. Kutumbarao and P. Rama Rao, Scripta Met 7 (1973) 1003.

J.D. Landes and J.A. Begley, A.S.T.M. Spec. Tch. Pub. 560, 1974.

J.C.M.Li, J. Aust. Inst. Metals 8 (1963) 206.

R.C. Lobb and R.B. Jones, Proc. Int. Conf. on "Physical Metallurgy of Reactor Fuel Elements", Berkeley, 1973.

E.S. Machlin, Trans AIME 206 (1956) 106.

M.J. Manjoine, J. Basic Eng. 84 (1962) 220.

M.J. Manjoine, Proc. Joint Int. Conf. on Creep, London, 1963.

W.R. Martin and J.R. Weir, J. Nucl. Mat. 18 (1966) 167.

W.R. Martin, J.R. Weir, R.E. McDonald and J.C. Franklin, Nature 208 (1965) 73.

J.A. Mazza and G. Willoughby, J.I.S.I. 204 (1966) 718.

I. R. McLauchlin, Proc. Conf. on "Creep of Steel and High Temperature Materials", Sheffield, 1972.

I.R. McLauchlin, C.E.G.B. Report RD/B/N 3441, 1975.

D. McLean, J. Inst. Metals 85 (1956-57) 468.

D. McLean, "Grain Boundaries in Metals", Oxford University Press, London, 1957.

D. McLean, J. Aust. Inst. of Metals, 8 (1963) 45.

F. McLintock, Int. J. Fract. Mech. 4 (1968) 101.

F.R.N. Nabarro, Proc. Conf. on Strength of Solids, Physical Soc. of London, 1948.

G.J. Neate, C.E.G.B. Report SSD MID/R. 12/74, 1975.

G.J. Neate and M.J. Siverns, Proc. Int. Conf. on "Creep and Fatigue in Elevated Temperature Applications", Philadelphia, 1973.

N.G. Needham and G.W. Greenwood, Met. Sci. J 9 (1975) 258.

K.M. Nikbin and G.A. Webster, Proc. Joint Meeting "Prediction of Life of High Temperature Components", London, 1975.

P.R. Oliver and L.A. Girifalco, Acta Met 10 (1962) 765.

P.C. Paris and G.C. Sih, A.S.T.M. Spec. Tech. Pub 381, 1964.

R. Pilkington, D. Hutchinson and C.L. Jones, Met Sci J 8 (1974) 237.

H.G. Popp and A. Cole, Proc. Air Force Conf. on "Fatigue and Fracture of Aircraft Structures and Materials", AF FDL-TR-70-144, 71, 1970.

C.E. Price, Acta Met 14 (1966) 1781.

P. Rama Rao, V.V.P. Kutumba Rao, M.C. Pandey, J.I.S.I. 211 (1973) 801.

R.T. Ratcliffe and G.W. Greenwood, Phil Mag 12 (1965) 59.

K.H. Reiff, Proc. Symposium "Radiation Damage in Reactor Materials", IAEA-SM-120/D-6, Vienna, 1969.

R. Resnick and L.L. Seigle, Acta Met 3 (1955) 605.

J.R. Rice, J. Appl. Mech 35 (1968) 379.

J.R. Rice and G.F. Rosengren, 16 (1968) 1.

P.J. Ring, M.J. Busboon and C.N. Spalaris, Proc. BNES Conference "Irradiation embrittlement and creep in fuel cladding and core components", London, 1972.

I.H. Robins, Ph.D Thesis for presentation to Univ. of Aston, 1974.

K. Robson, Proc. conf. on Properties of Heat Resisting Steels, Dusseldorf, 1972.

H.S. Rosenbaum, Electrohem Tech 4 (1966) 153.

A. Rukweid, Met. Trans 3 (1972) 3009 .

J. M. Silcock, R.W. Rookes and J. Barford, J.I.S.I. 204 (1966) 623.

M.J. Siverns and A.T. Price, Nature 228 (1970) 760.

M.J. Siverns and A.T. Price, Int. J. Fract. 9 (1973) 199.

R.P. Skelton, Met. Sci. J 9 (1975) 92.

J. Skinner and A.W.P. Newbigging, Proc. BNES Conf. on "Nuclear Fuel Performance", London, 1973.

E. Smith and J.T. Barnby, (a) Met. Sci J. 1 (1967) 56.
(b) Met. Sci J. 1 (1967) 1.

R. Soderberg, Proc. 2nd. Int. Conf. on Fracture, Brighton, 1969.

J. Soo, C.E.G.B. Report RD/L/N 182/74, 1974.

J.J. Spark, Scripta Met 3 (1969) 747.

M.V. Speight and W. Beere, Met. Sci J 9 (1975) 190.

M.V. Speight and J.E. Harris, Met. Sci J 1 (1967) 83.

J.E. Spruiell, J.A. Scott, C.S. Ary and R.L. Hardin, Met. Trans 4 (1973) 1533.

A.A.S. Steinar, Nucl. Engin. and Design 21 (1972) 237.

J.O. Stiegler, K. Farrell, B.T.M. Loh and H.E. McCoy, Trans ASM 3 (1967) 60.

J.O. Stiegler and J.R. Weir, A.S.M. Seminar "Ductility", 1967.

A.N. Stroh, Proc. Roy. Soc. A 233 (1954) 404.

R. Sumerling and E.D. Hyam, "The Metallurgy of Beryllium", Inst. of Metals Monograph No. 28, 1961.

S. Taira and R. Ohtani, Proc. Conf. on "Creep and Fatigue in Elevated Temperature Applications", Philadelphia, 1973.

D.M.R. Taplin and L.J. Barker, Acta Met 14 (1966) 1527.

D.M.R. Taplin and R.C. Gifkins, Acta Met 15 (1967) 1967.

D.V. Thornton, Proc. Int. Conf. on "Properties of Creep Resistant Steels", Dusseldorf, 1972.

C.E. Turner and G.A. Webster, Int. J. Fracture 10 (1974) 455.

P.K. Venkiteswaran, M.W.A. Bright and D.M.R. Taplin, Mat. Sci and Engin. 11 (1973) 255.

F.H. Vitovec, J. Mat. Sci 7 (1972) 615.

H.R. Voorhees, J.W. Freeman and J.A. Herzog, J. Basic Engin. 84 (1962) 207.

J.S. Waddington and K. Lofthouse, J. Nucl. Mat 22 (1967) 205.

J.S. Waddington and J.A. Williams, Acta Met 15 (1967) 1563.

G.K. Walker and H.E. Evans, Met. Sci J 4 (1970) 155.

C.W. Weaver, J. Inst. Metals 88 (1959-60) 296.

G.A. Webster, Proc. Conf. on "The Mechanics and Physics of Fracture", Cambridge, 1975.

J. Weertman, Scripta Met 7 (1973) 1129.

B. Weiss and R. Stickler, Met. Trans 3 (1972) 851.

A.A. Wells, Proc. of Symposium on Crack Propagation, Cranfield, 1 (1961) 210.

A.A. Wells and F.H. McBride , Can. Met. Quart 6 (1967) 347.

H.M. Westergaard, J. Appl. Mech A (1939) 149.

J.A. Williams, Phil Mag 15 (1967) 1289.

J.A. Williams, Proc. Conf. on "The Mechanics and Physics of Fracture", Cambridge, 1975.

J.A. Williams, C.E.G.B. Report RD/L/N 107/23, 1973.

J.A. Williams and A.T. Price, C.E.G.B. Report RD/M/R 205, 1974.

T.M. Williams, D.R. Harries and J. Furnival, J.I.S.I. 210 (1972) 351.

T.M. Williams, A.M. Stoneham and D.R. Harries, U.K.A.E.A. report AERE - R7989, 1975.

R.N. Wilson, Proc. Conf. on "Practical Implications of Fracture Mechanisms", Newcastle, 1973.

A.L. Wingrove and D.M.R. Taplin, J. Mat. Sci 4 (1969) 789.

J.C. Wood, J. Nucl. Mat. 45 (1973) 105.

J.C. Wood, Nucl. Tech. 23 (1974) 63.

D.A. Woodford, Met. Sci J 3 (1969) 234.

C.Zener, "Fracturing of Metals", ASM, Cleveland, 1948.